LIGHT-ASSISTED 3D PRINTING OF CONTINUOUS CARBON FIBER REINFORCED THERMOSET COMPOSITES

A Dissertation
Submitted to the Graduate Faculty
of the
North Dakota State University
of Agriculture and Applied Science

By

Md Zahirul Islam

In Partial Fulfillment of the Requirements
for the Degree of
DOCTOR OF PHILOSOPHY

Major Department:
Mechanical Engineering

December 2023

Fargo, North Dakota

North Dakota State University
Graduate School

Title

LIGHT-ASSISTED 3D PRINTING OF CONTINUOUS CARBON FIBER REINFORCED THERMOSET COMPOSITES

By

Md Zahirul Islam

The Supervisory Committee certifies that this ***disquisition proposal*** complies with North Dakota State University's regulations and meets the accepted standards for the degree of

DOCTOR OF PHILOSOPHY

SUPERVISORY COMMITTEE:

Chad A. Ulven
Chair

Alan Kallmeyer

Dean C. Webster

Ravi Kiran Yellavajjala

Lokesh Narayanan

Approved:

March 26, 2024
Date

Chad A. Ulven
Department Chair

ABSTRACT

Polymer 3D printing has become an emerging manufacturing technique, due to its design flexibility, however its application to produce structural components is still limited due to the poor mechanical strength and thermal stability of most 3D printed parts. Because of the superior mechanical strength of carbon fiber, 3D printing of continuous carbon fiber reinforced thermoset composites have recently been studied overcome this barrier of mechanical strength and thermal stability. Light- curing based 3D printing of continuous carbon fiber shows a promising potential, however this process also has limitations in making custom object due to fiber loop creation as the nozzle turns at the corner of the object. This study aimed to develop algorithms for light-assisted 3D printing, focusing on custom object fabrication using low-viscosity urethane acrylate and epoxy-acrylate based resins. A novel approach, laser cutting incorporated 3D printing of continuous carbon fiber reinforced thermoset composites, is presented for custom object manufacturing. Furthermore, algorithms were developed to enable the printing of various shapes, including rectangles, triangles, circles, hexagons, and grid structures. A modified algorithm was also introduced and demonstrated to simplify the printing of scalable truss structures. These proposed 3D printing technologies successfully demonstrated the manufacturing of custom objects having comparable mechanical and thermal strength with similar composites manufactured by conventional manufacturing process. Finally, this study presents an experimental approach to determine the minimum light energy required to sustain continuous fiber printing. Proper tuning of the process parameter of this proposed 3D printing technique has great potential to replace conventional manufacturing process of composites by 3D printing.

DEDICATION

To my lovely wife Zannat–E–Sadia Sarahan Jamila Rashni

TABLE OF CONTENTS

LIST OF TABLES

LIST OF FIGURES

CHAPTER 1: INTRODUCTION

Additive manufacturing, also known as 3D printing, was first developed in the 1980's. Since the first development, 3D printing has been a powerful technique showing boarder application potentials. Traditional manufacturing is a subtractive or material removing process, while additive manufacturing produces a 3D model in a layer-by-layer building process. 3D printing offers reduction in development time, material, and cost, flexibility of production, realization of complex geometries. 3D printers bring revolutions in manufacturing and prototyping. The utilization of 3D printers shows a shift from traditional prototyping to production-based applications. 3D printing is divided into several categories. Material extrusion and vat polymerization are two major categories of 3D printing technology.

Fused deposition modeling (FDM) is the most widely used and rapidly evolving material extrusion-based 3D printing technology. FDM printer used thermoplastic filament as a feedstock. A wide range of low-cost filament materials are available for FDM printers, such as: ABS, PLA, Nylon, PET, PC, PEEK, etc. FDM printing technology converts the thermoplastic filaments to semi-molten form using a heated nozzle and deposits the semi-molten filament in a layer-by-layer fashion to manufacture an object. However, the printed objects from FDM printer exhibit low mechanical strength and poor surface finish.

Stereolithography (SLA), one type of vat polymerization, is a layer-by-layer 3D printing technique widely used to manufacture composites using liquid photo-curable thermoset resins. The liquid resin material is traditionally placed in a vat. In the SLA, the building platform is submerged into liquid thermoset resin. SLA printer manufactures by selectively curing thermosetting resin using high energy ultraviolet (UV) laser irradiation. A computer control laser system scans point to point to cure specific regions of a layer. The building platform then moved by the layer height

to continue printing on the next layer. The main advantage of SLA printing process is fast and high resolution. However, the printed specimens from SLA printer exhibited poor mechanical strength.

To enhance mechanical properties, 3D printed polymeric material was reinforced by short fiber. 3D printing of short fiber reinforced composites was performed using both thermoplastic and thermoset filaments. Ning et al. [1] and Tekinalp et al. [2] performed 3D printing using filament produced by mixing ABS thermoplastic pellets and carbon fiber powders. Thereafter they studied the improvement in mechanical strength due to carbon fiber powder addition. However, the improvement was not sufficient for high performance applications.

Thermoset based polymeric materials were also 3D printed widely with short fiber reinforcement. Nashat et al. [3] reported the direct ink write based 3D printing of epoxy resin with short carbon fiber reinforcement. Griffini et al. [4] demonstrated UV light assisted 3D printing of thermoset resin with short carbon fiber reinforcement. Zhao et al. [5] showed the light assisted 3D printing of epoxy acrylate resin with short Kevlar fiber. They achieved tensile strength of 52 MPa, while cured resin was showing strength of 30 MPa. Sano et al. [6] exhibited an SLA 3D printing process for a commercial photocurable epoxy resin and short glass fiber. They achieved a strength of 22 MPa, while cured resin showed strength of 10 MPa. The addition of short fiber increases the stiffness of the part, but the strength increases is still limited as fiber pull may occur before fiber breakage.

Continuous fiber reinforcement is the ultimate solution to increase mechanical strength of fiber reinforced composites. Continuous fiber-reinforced composites have been extensively utilized across various industries, spanning from aerospace to ground transportation, for centuries. This popularity is attributed to their exceptional qualities such as high strength, stiffness, lightweight nature, thermal stability, and resistance to chemicals. Traditional manufacturing

methods rely on costly molding tools for shaping resin and fibers, making mass production essential to control expenses.

In contrast, 3D printing, well-suited for rapid prototyping and product development, enables the fabrication of continuous fiber-reinforced composites without the need for molds. This approach offers significant advantages in terms of design flexibility and cost-efficiency. As a result, researchers have taken a keen interest in 3D-printed continuous fiber composites due to their ability to provide substantial strength in specific desired directions. Extrusion based 3D printing, with in-nozzle impregnation of fibers, is the most promising fabrication technique for continuous fiber reinforced composites. Continuous carbon fiber reinforced composites are 3D printed with both thermoplastic and thermoset matrix materials.

There are two approaches to print continuous carbon fiber with thermoplastic resin matrix. The first approach is known as “In-nozzle impregnation”. 3D printing of continuous carbon fiber reinforced thermoplastic composites was performed by Matsuzaki et al. [7] using in-nozzle impregnation process. Printed specimen showed a tensile strength of 185 MPa with a fiber volume fraction of 6.6%. Moreover, Quio et al. [8] performed in-nozzle impregnation-based 3D printing of continuous fiber reinforced thermoplastic composites using PLA as matrix material.

Another approach of printing continuous fiber reinforced thermoplastic composites is based on extruding pre-impregnated fibers. A version of 3D printer using extrusion of pre-impregnated continuous fiber was commercialized by Markforged in 2014. This 3D printer utilizes carbon, glass, and aramid fiber prepreg. Caminero et al. [9] performed 3D printing of continuous fiber using Markforged printer and evaluated their interlaminar strength.

3D printing of continuous carbon fiber reinforced thermoset composites was performed successfully in various mechanisms. Hao et al.[10] reported 3D printing of continuous carbon fiber

reinforced epoxy composites. They used highly viscous epoxy resin (5000- 10000 mPas) to 3D print with continuous fiber. Continuous fiber passed through the resin pool and performed 3D print using direct ink write (DIW) printing process. In DIW printing process, print ink possesses sufficient elastic modulus to retain shapes after being deposited on the print bed. Post curing of the printed specimen was performed in a high temperature chamber. Therefore, they achieved tensile strength of 792 MPa. Moreover, this study showed 3D printing of grid, nuts, and honeycombs structure.

Effect of various print parameters on the mechanical properties of 3D printed continuous carbon fiber reinforced thermoset composites was performed by Ming et al [11]. They used solid epoxy resin as a matrix material having glass transition temperature of 75 °C. In their study, continuous carbon fiber was pre-impregnated with resin and resin impregnated fiber was deposited on the print bed through a heated print nozzle.

Furthermore, Zhang et al. [12] showed the 3D printing of continuous carbon fiber reinforced composites utilizing solid epoxy resin. The softening temperature of the resin was 79 °C. Resin impregnated fiber deposited on the print bed from a heated nozzle and the resin solidified on the print bed at room temperature. The post curing of the printed specimen was performed at elevated temperature. Thus, printed specimens exhibited the tensile strength of 825 MPa.

Xiao et al. [13] reported the 3D printing of phenol-based epoxy resin with continuous carbon fiber. They used in-nozzle impregnation of fiber and resin to perform 3D printing. Deposited resin on the print bed was cooled down rapidly using air flow. Therefore, the viscosity of the resin increases and will be able to retain shape on the print bed. Thereafter they post cured the printed specimen in a vacuum oven. Thus, they attained tensile strength of 1012 MPa with a fiber weight fraction of 53%.

Dong et al. [14] established a thermic lance assisted 3D printing process for continuous carbon fiber reinforced composites using thermosetting phenolic resin. They prepreg continuous carbon fiber with resin, employed the thermic lance at a certain temperature to adhere fibers on working platform. The optimum pre-cure temperature was found to be 260 °C. They achieved a tensile strength of around 450 MPa.

A novel extrusion-based approach was demonstrated by Xu et al. [15] to 3D print continuous carbon fiber reinforced thermoset composites. In their study, continuous carbon fiber passed through a syringe containing polyamide resin, and a piston pushed the polymer. Hence, the viscous polymer creates shear force on the continuous fiber. Thus, continuous fiber extrudes from the print head. This is a DIW printing process of continuous carbon fiber. Thus, they achieved tensile strength of 550 MPa with a fiber weight of 53%. Moreover, they showed 3D printing free standing structures using UV light curable resins.

UV light assisted 3D printing of continuous carbon fiber got significant attention as its facilities printing with low viscosity resin. DIW printing process requires critical resin preparation to obtain specific rheological properties. Abdullah et al. [16] demonstrated a UV light assisted 3D printing process for continuous carbon fiber and acrylate thermoset resin. They investigated the influence of different process parameters, such as: resin viscosity, nozzle size, printing speed, etc., on the quality and mechanical properties of the printed specimen. However, they attained a tensile strength of 55 MPa with a fiber volume fraction of 34%.

UV light assisted 3D printing process for continuous carbon fiber and thermoset resin was furthermore reported by Rahman et al [17]. They used commercially available low viscosity acrylate based thermoset resin. In-nozzle impregnation-based printing process was used to 3D print

continuous carbon fiber and low-viscosity thermoset resin. They achieved a mechanical strength of 134 MPa with a fiber volume fraction of 7%.

Furthermore, Jiang et al. [18] reported UV -assisted 3D printing of continuous carbon fiber composites using a dual cure thermoset resin. Resin was cured using both UV light and thermal energy. They achieved a tensile strength of 470 MPa with a fiber volume fraction of 30%. Furthermore, they exhibited the reshapability and reproducibility of the printed composites.

Continuous fiber-reinforced thermoset composites have garnered significant attention in the realm of additive manufacturing techniques for composites. This is primarily due to their robust intermolecular crosslinking and the polymer chain reactions occurring at the interfaces between the resin and fibers. These characteristics endow them with superiority when compared to analogous thermoplastic composites. However, most thermoset resins are liquid at room temperature, thus requiring the print ink to possess shape-retention capability, or the use of additional instant curing mechanisms, such as thermal or light-assisted methods, to enable successful 3D printing. Light-assisted 3D printing of continuous carbon fiber-reinforced (CCFR) thermoset composites have shown significant potential for producing high-performance composites using readily available, low-viscosity thermoset resins.

The main goal of this dissertation is to develop algorithms for 3D printing diverse shapes and objects using light-assisted printing processes, while ensuring that the printed items exhibit strength comparable to conventionally manufactured composites.

This section outlines the structure and content of this dissertation. Chapter 2 discusses the 3D printing of objects with internal features by incorporating laser cutting after each layer of 3D printing using urethane acrylate resin. Furthermore, this chapter includes the mechanical characterization of the printed specimens using urethane acrylate resin. A disclosure (RFT-635)

has been filed using the findings from this chapter and a manuscript for a journal publication is under preparation. Chapter 3 presents an algorithm for printing complex shapes, including rectangles, triangles, hexagons, and grid structures using low viscosity thermoset resin. This chapter also encompasses void analysis and mechanical characterization of the printed specimens with a relatively high resin content. Based on the results from this chapter, a manuscript has been prepared for submission to the journal "Progress in Additive Manufacturing", and a preprint version of these findings is already available online. Chapter 4 describes the effect of adding a rheological modifier on the mechanical properties of 3D printed CCFR thermoset composites. A manuscript has been prepared from the output of this chapter and is awaiting submission. Chapter 5 presents the 3D printing of CCFR thermoset composites with bisphenol-A epoxy acrylate (BEA) resin and their mechanical characterization. Moreover, this chapter demonstrates an optimized printing path for printing truss structures. A manuscript for journal publication is being prepared based on the outcomes of this chapter, and a full conference article for MSEC 2024 is currently under review. Chapter 6 presents the experimental approach for measuring the minimum laser power required for printing with continuous carbon fiber reinforcement and thermoset resin. This chapter also compares the laser power requirements for the urethane acrylate resin and the BEA resin. The outcome of this chapter has been published as a research article for the IMECE 2023 conference. In conclusion, this dissertation contributes to the advancement of 3D printing for CCFR thermoset composites, offering a promising path towards high-strength manufacturing of complex shapes and structures in the realm of additive manufacturing.

CHAPTER 2: INCORPORATION OF LASER CUTTER IN THE LIGHT-ASSISTED 3D PRINTING OF CONTINUOUS CARBON FIBER REINFORCED THERMOSET COMPOSITES

2.1. Introduction

Continuous carbon fiber reinforced (CCFR) thermoset composites demonstrate outstanding mechanical properties such as specific strength and specific stiffness as well as fatigue durability, thermal resistance, chemical resistance, wear resistance, and low density. They are extensively used in various industries including automotive, aircraft, medical, coatings, food, and engineering [19]. Due to the requirement of complex manufacturing equipment, such as autoclaves, and processes, conventional manufacturing of thermoset composites is expensive. Moreover, it is exceedingly difficult to change or modify the design of the mold or tooling once it has been manufactured.

Compared to conventional manufacturing processes, additive manufacturing (AM), also known as 3D printing, of fiber-reinforced composites has garnered much attention due to its design flexibility. Other advantages of additive manufacturing over conventional processes include simplifications in the production processes, cost efficiency, and reduced material consumption. In traditional manufacturing processes, creating complex geometries often requires assembling multiple parts, whereas 3D printing allows for the production of a single component [6].

Fused deposition modeling (FDM) is the most popular and widely available polymer 3D printing technique. In FDM, a heated nozzle is used to convert thermoplastic filament into a semi-molten form. The movable nozzle deposits the semi-molten material layer-by-layer as required to create a 3D object [20]. Commonly used thermoplastic filaments include ABS, PLA, PEEK, and polyamide [21]. However, the application of FDM printed parts is limited due to their poor

mechanical and thermal properties. The tensile strength of FDM 3D printed polymers is typically limited to a range of 15 - 45 MPa [22]. The melting temperature of the thermoplastic polymers used falls within the range of 150- 200˚C. In contrast, thermoset polymers are known for their improved mechanical properties and thermal stability.

Thermoset polymers are of significant importance due to their thermal stability, chemical resistance, environmental stability, and improved mechanical strength. 3D printing of thermoset polymers is achieved by curing materials layer by layer, which can be accomplished through photopolymerization or heat. Photopolymerization involves crosslinking thermoset polymers using light in the visible or ultraviolet (UV) region. This process employs photosensitive liquid resin composed of liquid monomers, oligomers, and a photo initiator [23], with these resins primarily being acrylate-based. Acrylate-based resins undergo free radical polymerization in the photopolymerization process. During this process, the photo-initiator generates radicals when exposed to light. These generated radicals then interact with electron-deficient sites to form covalent bonds between monomers and oligomers [24], [25]. These radical reactions establish a highly crosslinked network during the printing process. It is important to note that these chain-forming solidification reactions are irreversible and cannot be reverted to a liquid state.

Two very popular methods for 3D printing thermoset polymers are Stereolithography (SLA) and digital light processing (DLP). In both cases, UV laser irradiation is used to selectively cure or harden photocurable thermoset resin as needed. After completing the curing of each single layer, a working platform is raised by a single layer height. In SLA printing, a fast-moving laser is employed for curing, while in DLP, projector light is used to cure one layer at a time [5, 26] . The SLA and DLP printing processes require photosensitive resin with very low viscosity (ranging from 0.1 to 10 Pa.s). These printing processes enable high-resolution printing with a good surface

finish, but they often result in poor mechanical properties [5, 26]. The tensile strength of 3D printed thermoset polymers using these methods is typically limited to a range of 25-70 MPa [25].

To enhance the mechanical properties of light-cured thermoset polymers, numerous studies have focused on 3D printing short fiber-reinforced thermoset composites. In this approach, short or discontinuous fibers (such as glass, Kevlar, carbon) are blended with the resin to create printed objects, resulting in improved mechanical strength [4-6]. However, it is important to note that the enhancement in mechanical properties achieved through short fiber reinforcement is relatively limited when compared to continuous fiber reinforcement. Tensile strength values for short fiber reinforced thermoset composites still remain below 100 MPa [27]. Consequently, research into 3D printing continuous fiber-reinforced composites is of paramount importance.

3D printing of continuous fiber reinforced composites (CFRC) is based on a modified Fused Deposition Modeling (FDM) method, also known as Fused Filament Fabrication (FFF). In this material extrusion-based 3D printing technique, continuous fibers were drawn through a nozzle and deposited layer-by-layer to create a 3D object. In the case of thermoplastic filament, the thermoplastic filament melts within the heated nozzle. The fibers become impregnated with resin within the nozzle before being deposited on the print bed. In recent years, significant research has been reported in the literature on additive manufacturing of CCFR thermoplastic composites [7, 8, 28-31]. CCFR thermoplastic composites exhibit excellent mechanical strength. Goh et al. [32] reported a tensile strength of CCFR thermoplastic composites ranging from 570- 630 MPa for a fiber volume fraction of 41%. However, as discussed earlier, thermoplastic composites are thermally less stable compared to the thermoset composites. In the case of thermoset resin based CCFR composites, direct ink writing (DIW) based printing approach is used. A liquid-like thermoset resin is used as the print ink, and liquid-soaked fibers maintain their shape on the print

bed either due to the high elastic modulus of the print ink or through the rapid solidification of the print ink. Rapid solidification can be achieved using thermally initiated rapid frontal curable resin or light-laser irradiation. However, literature on CCFR thermoset composites is still limited.

The 3D printing of CCFR thermoset composites was initially demonstrated using the DIW printing technique with viscous epoxy resin by Hao [10]. The printed structure was self-sustaining due to the high elastic modulus of the print ink and was subsequently thermally cured after printing. Ming [11] investigated the effects of various processing parameters on the mechanical properties of these CCFR thermoset composites manufactured using DIW-based 3D printing techniques, which require resins with high viscosity to maintain structural integrity. Printing with high-viscosity liquid resin necessitates a meticulous design of the printing nozzle, with specific attention to preventing resin clogging. Furthermore, it demands a precise pumping system design to control the flow of highly viscous resin.

Recent advancements in 3D printing of CCFR thermoset composites mainly involve the use of reactive resin systems with rapid frontal polymerization. Zhang successfully 3D printed CCFR epoxy-based thermoset composites using a self-propagating in-situ frontal curing enabled reactive resin system [19]. The resulting printed structures were free-standing. Additionally, CCFR printing was demonstrated by extruding carbon fiber through the application of shear stress using a viscous thermoset resin [15]. However, it is crucial to formulate the resin correctly to ensure the rapid in-situ curing of the print ink.

Light-assisted DIW-based 3D printing of CCFR thermosets has a significant advantage as it allows for the use of resins with a wide range of viscosities. Due to the presence of auxiliary instant high-energy light-based curing, this light assisted DIW printing can work with resins having a wide range of viscosity. Light assisted curing is an efficient, cost-effective, energy-

saving, and environmentally-friendly solidification technique for polymer matrix composites [33]. 3D printing of CCFR thermoset composites using a light laser was successfully demonstrated in literatures [17, 34].

A major challenge in the continuous fiber printing process is achieving a 180° curved turn of the fibers. When printing curved lines with continuous fiber, issues such as undulation, twisting and peeling from the bed can occur in the filament, significantly deteriorating the quality of the printed product [35-37]. Consequently, when fibers need to make turns at the corners of an object, they tend to create loops at those corners, which poses difficulties in creating smooth edges for the printed objects. Furthermore, these looped fibers at the corners end up being higher than the rest of the layer and can interfere with the next print layer. Moreover, the size of the fiber bundle also impacts the printability of minimum circle radius in continuous fiber 3D printing [35]. Therefore, the corners of the printed object may become dimensionally inaccurate and uneven.

CCFR composites can also be manufactured using laminated object manufacturing (LOM). LOM is a layer-by-layer manufacturing process in which thin cross-sectional layers are sliced based on a CAD model using a CO2 laser and then adhered to the previous layer using a hot laminating roller [38-40]. Inspired by LOM, the manufacturing of CCFR thermoplastic composites was reported by Lin [41]. Prepreg composite sheets of carbon fiber were laser cut based on CAD geometry, stacked, and bonded using heat produced by collimated laser beam. In the case of thermoset composites, heat energy is not helpful for bonding one layer to another, as thermoset resins are not thermally reversible. However, the concept of laser cutting after each layer is worth considering for incorporating into the manufacturing of custom-shaped objects in CCFR thermoset additive manufacturing.

The objective of this study is to integrate the concept of laser cutter-based LOM manufacturing with light-energy assisted DIW 3D printing for CCFR thermoset composite manufacturing. This study demonstrates a hybrid manufacturing process for producing complex shapes in CCFR thermoset composites by integrating both additive and subtractive manufacturing techniques. Continuous carbon fiber layers were deposited using a light-assisted additive manufacturing technique. To achieve the desired shapes from the deposited fiber layer, CO2 laser cutting was employed to cut and subtract superficial material after each layer of additive manufacturing. Furthermore, this research involves the mechanical characterization of 3D printed composites and compares their mechanical properties with conventionally manufactured composites.

2.2. Materials and Methods

2.2.1. Fibers and resin

Teijin 3K continuous carbon fiber tow was used to 3D print. The carbon fiber strand has 3000 filaments, and each filament have average diameter of 7 µm. The linear density of the fiber is 200 tex (tex defines the weight in gram for 1000m of fiber). The density of the fiber is 1.77 g/cm^3. Tensile strength and tensile modulus of the fiber is 4100 MPa, and 240 GPa respectively. The elongation of those carbon fiber is 1.7% at break. Carbon fiber 1K filament was found to be susceptible to breaking during the printing due to tension on strand, hence 3K filament is used in this study. Moreover, 3K carbon fiber filament is helpful to obtain higher volume fraction in the printed object.

Photo-curable urethane acrylate resin, commercially known as Peo-poly Moai Tough resin, was purchased from Matter Hackers (CA, USA), and was used as a matrix material. FTIR analysis of the resin was performed to confirm the existence of urethane (-OCONH-) and acrylate groups

(CH2=CH-COO-) within the resin. This resin is designed to cure under light-irradiation of wavelength 405 nm. The density of the resin is 1.15 g/cm^3.

To overcome the limitation of single mode polymerization, a dual curing photo chemistry-based system has been applied. In this study, a photo-thermal dual curing process was implemented to obtain high performance thermosets. Free radical based photopolymerization with high curing rate can quickly happen during the printing process, and then the thermal curing reaction was performed to significantly boost the performance of obtained object. Thus hybrid (dual) curing could easily form interpenetrating networks (IPNs) [23].

Luperox P (LP), tert-butyl peroxybenzoate (98%), is a type of peroxide free-radical thermal initiator for polymerization of various monomers. 0.5% LP was mixed with urethane acrylate resin to prepare the print ink. The 3D printed specimens, with light-assistance, were post cured thermally at 180°C for 8 h to complete the polymerization reaction.

2.2.2. Printing process

Figure 1 shows the schematic diagram of the printing process. As shown in Figure 1, two light-lasers were focused as a line at each side of the printing nozzle. Laser irradiation works as a medium of instant curing for resin-soaked fiber just after being extruded on the print bed. The light-laser was focused as a line of irradiation to make the focusing of the laser simple. Shining the laser as a line reduces the effort of focusing the laser exactly at a point. The light laser used has a wavelength of 405 nm, and 800 mW power. The temperature generated by the UV light on the print surface was measured using a thermal IR camera. It was recorded to be between 36 and 38 ˚C. Furthermore, no signs of damage to the fiber or matrix material were observed because of continuous exposure to the UV laser light on the printed layer. Continuous carbon fiber strand was fed through the top of a print nozzle. As shown in Figure 1, a simple custom-made nozzle was

manufactured (through 3D printing) to feed resin and fiber simultaneously. A syringe needle was attached to the tip of the nozzle. The size of the syringe needle is 14 Gauge (inner diameter = 1.6 mm). Choosing the correct nozzle size is crucial for preventing fiber issues, such as fraying and tearing, by ensuring sufficient resin flow to properly wet-out fibers during printing [34]. No mechanical mechanism was employed to feed fibers through the nozzle. The continuous fiber are coming out of the nozzle with the movement of the print head, while the print bed was kept fixed. A hot-rolled steel plate was used as a print bed.

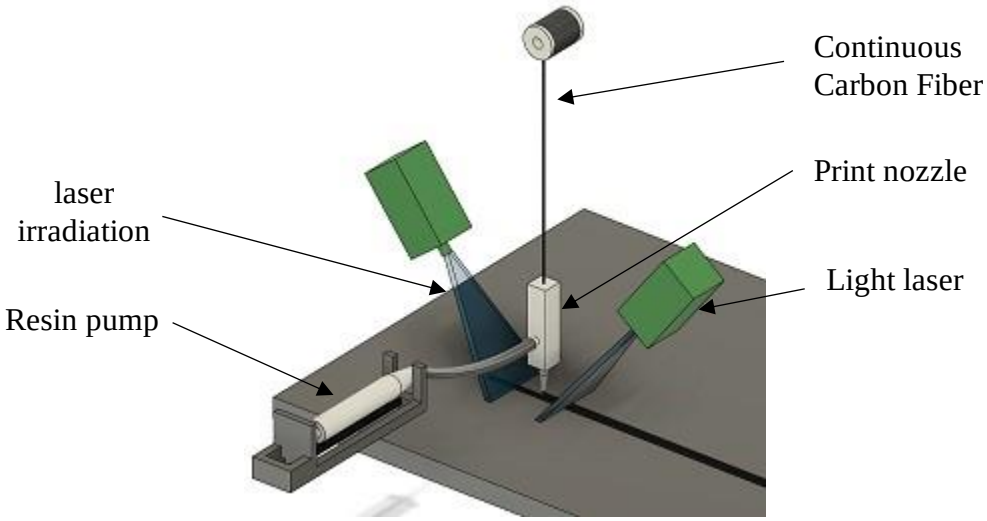

Figure 1: 3D printing process of continuous carbon fiber reinforced composites with light curable urethane acrylates resin.

A commercial FDM printer gantry was modified to develop the custom 3D printer to print CCFR thermoset composites. Repetier-Host (Hot-World GmbH & Co. KG, Germany) software was used to control the movement of print head through a required path and speed using the custom G-code generated through a MATLAB program. Printing speed (S) was set to 210 mm/min. Thermal initiator mixed commercial photosensitive thermoset resin (Peo-poly) was fed through a tube attached at the side of the print nozzle. Resin was fed at a constant flow rate during the printing using a syringe pump. The resin flow rate (F) was set to 0.121 ml/min. Printing speed (S) and

resin flow rate (F) combinedly define the amount of resin dispensed during the printing process. Therefore, a general factor is required to incorporate the effect of both parameters. Here, the ratio of resin flow rate and printing speed ($\frac{F}{S}$) is defined as a parameter to describe the amount of resin dispense per unit length of 3D printing. For current printer parameters setting, value of $\frac{F}{S}$ is 0.576 ml/m.

Fibers are being impregnated with the resin within the print nozzle. Resin impregnated fibers maintain their shape by curing just after being laid on the print bed using high energy light-laser irradiation. To prevent the resin being clogged at the tip of the nozzle by curing through light irradiation, the light-laser was focused on a certain distance from the nozzle tip. Each light-laser was focused around 10 mm away from the nozzle tip. The difference between the actual printed object and programmed printing path was equal to the distance between the nozzle and laser irradiation. The vertical gap between the nozzle tip and the print bed or the previously printed layer was set to 0.5 mm. The gap between two adjacent print lines is set as 1 mm.

2.3. Challenge of this Printing Process

The primary challenge of this printing process is the 180° turn of the fiber at the edge. While making this turn, the fiber forms a loop at the edge. Figure 2(a) shows the 3D profile of the fiber loop formation at the edge. This loop impedes the creation of the finished edge of the printed objects. Since the light-laser is focused at a specific distance from the print head, a portion of the fiber at the corner will not attach to the bed and will retracted back with the print head's motion, resulting in the formation of a fiber loop. Consequently, the height of the fiber loop at the edge will be greater than the corresponding print height in other parts of the object. Figure 2(b) shows the average layer height profile along the length, indicating greater layer height at the position of fiber loops. The 3D profile and average layer height profile of the fiber loop was measured using

3D optical profilometer (Keyence, VR series). These fiber loops at the corner can pose issues when printing adjacent fiber lines, and the increased layer height at the corner due to the fiber loop may cause problems when printing the next layer of the objects.

These issues in the printing processes were addressed by implementing CO2 laser cutting at the edge after each layer of printing. Figure 2(c) shows the schematic of the laser cutting path at the edge. Figure 2(d-f) exhibited the process of laser cutting. To enable laser cutting after each layer of printing, a hot-rolled steel plate was used as the print bed. Glass beds would melt when cutting carbon fiber with a laser cutter, and aluminum beds have a high reflective index, making them unsuitable for use with a laser cutter. As shown in Figure 2(g), the excess fibers after the laser cut were removed from the print bed using metal scraper, and then blown away using air flow. Figure 2(h) shows the smooth edges after removing excess fibers. Incorporating laser cutting after each layer allows for the production of finished and neater corners on the objects and resolves the problem of having greater fiber loop height at the corner for printing the next layer of the object (Figure 2 (b)).

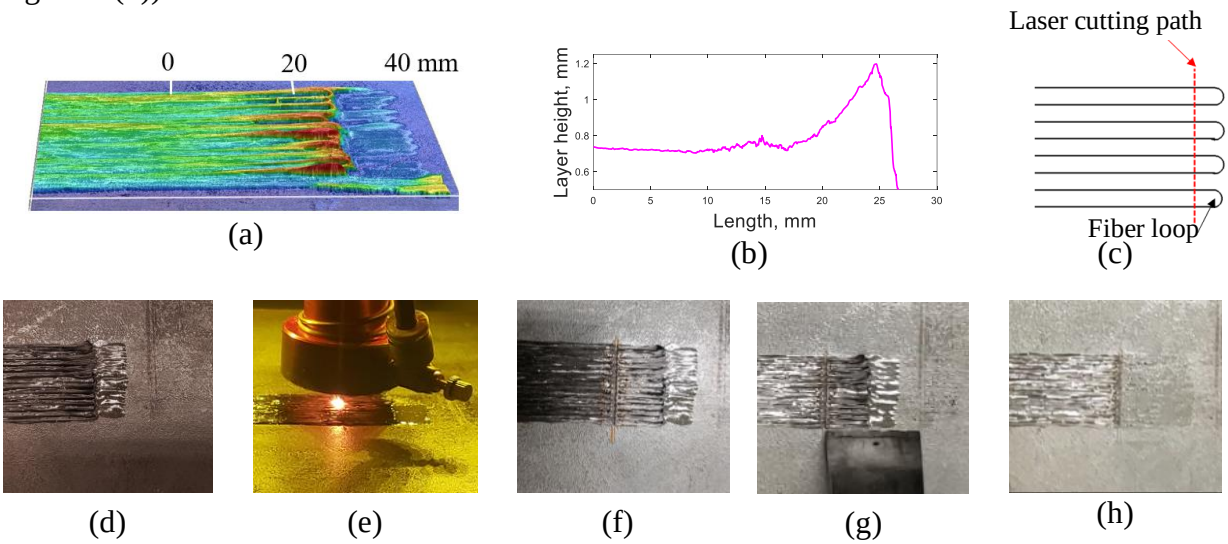

Figure 2: (a) 3D profile of fiber loops at the edge, (b) layer height profile, (c) schematic for laser cutting path, (d) printed layer with edge, (e) laser cutting, (f) layers after the laser cut, (g) removing excess fibers with scraper, (h) after removing excess fibers.

Furthermore, a flexible nozzle tip was employed, which has adequate stiffness to move the fiber along with the print head's motion while being able to bend to continue printing if the nozzle tip becomes entangled with the fiber loop. This nozzle tip's flexibility enables the printing of adjacent lines of fibers within a single layer without the nozzle becoming entangled in the fiber loop.

2.4. Printing of Custom Object

This section illustrates the custom object printing process, which integrates laser cutting after each layer of fiber printing. Figure 1 depicts the printing of a carbon fiber lay-up, while Figure 3 displays laser cutting process based on CAD design. After cutting with the laser cutter, the excess portion of the fiber lay-up was removed using a metal scraper, as depicted in Figure 2 (g) This iterative process of printing, cutting, and removing excess fibers continues until the entire object is printed. Although this demonstrated process separately performs the printing, cutting, and removing of excess fibers tasks, the study proposes the concept of an autonomous printer that performs these tasks consecutively to produce complete objects. Despite the challenges associated with machining thick conventionally manufactured carbon fiber objects [42], thick carbon fiber objects can be 3D printed by employing laser cutting after each printing layer. After laser cutting a layer, excess material can be removed from the print-bed using high-pressure air.

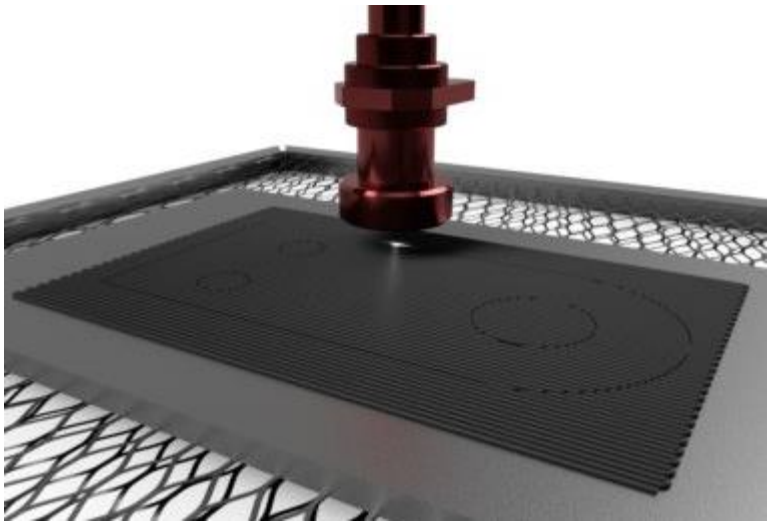

Figure 3:Schematic of laser cutting followed by printing for each subsequent fiber layer.

Figure 4 (a) displays the CAD design of the object intended for printing to demonstrate the process of printing each layer followed by laser cutting. Figure 4 (b) displays a fiber lay-up printed by the custom-made 3D printer using the process discussed in Section 2.2. After each layer was printed, a CO2 laser cutter was employed to cut the printed layer based on the CAD geometry. A 75 W universal laser cutter was operated at 40% power, and 0.3% speed to cut a single layer of 3D printed carbon fibers. Figure 4 (c-d) illustrates the fiber lay-up with 0˚ and 90˚ orientations after it was cut with the laser cutter. A rectangular boundary around the object was generated by the laser cutter to separate superficial fibers from the main object. The superficial fibers outside of the rectangular boundary were removed from the print bed using a metal scraper. The damage on the printed layer caused by the CO2 laser cutter was not spread over the entire layer because the CO2 laser cutter utilizes a highly concentrated form of energy to cut through the fiber lay-up. However, some burnout of the matrix material was observed at the edge of the cut.

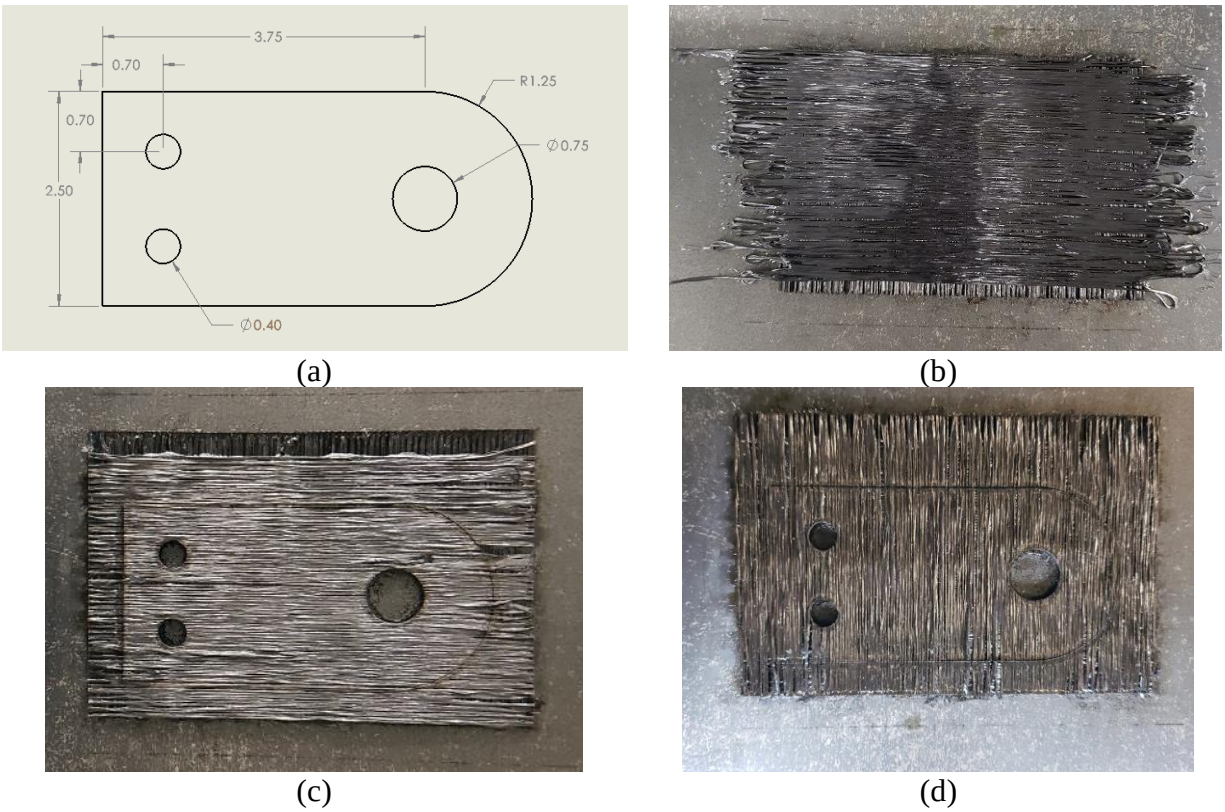

Figure 4: Manufacturing process of custom object using 3D printing incorporated with CO2 Laser cutter (a) CAD model of the object, (b) 3D printed fiber layup before laser cut (c) 0˚ fiber lay-up after laser cut (d) 90˚ fiber lay-up after laser cut.

Figure 5 (a) shows the custom object image of the nine-layer custom object after being printed. The fabricated object consist of nine bi-directional layers, and the symmetric fiber lay-up is as follows: $[(0/90)_2/0/(90/0)_2]$. Incorporating a laser cutter after each layer of printing enables the 3D printing of custom-shaped objects with smooth corners and interior features, such as holes. This hybrid manufacturing technique combines both addition and subtraction of materials; however, the percentage of material subtracted during this manufacturing technique is potentially less compared to the traditional subtractive manufacturing technique. Figure 5 (b) also shows the Micro-CT images of the printed object. The printed object has significant void content. Void content could be reduced significantly by controlling the resin flow rate during the printing process. To analyze the effect of laser cutting on the properties of printed composites, void analysis

could be conducted both near the cutting region and away from it. This has the potential to be a valuable area for future research.

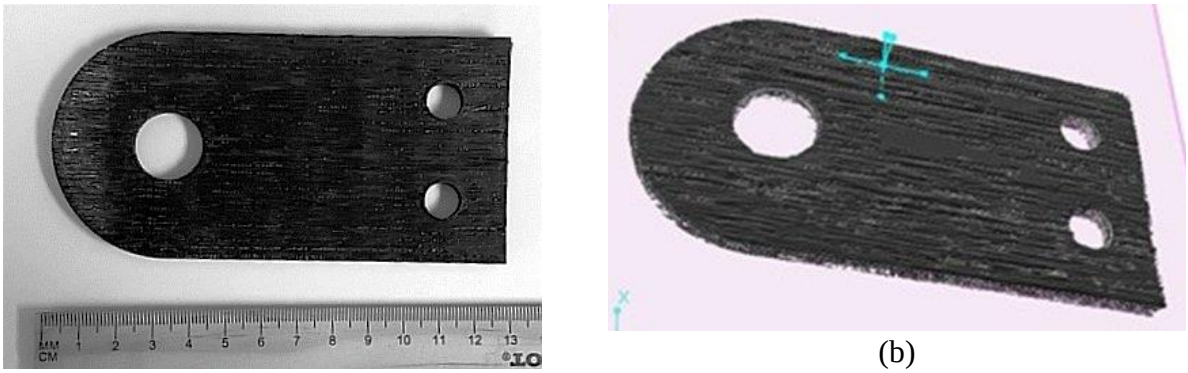

(a) (b)

Figure 5: (a) Nine-layers custom object manufactured by 3D printing (b) Micro-CT images of the custom object.

2.5. Volume Fraction Measurement

2.5.1. Experimental measurement

Burn-off tests were performed on the unidirectionally printed composite specimen (consisting of 4-layers) to determine the fiber volume fraction of the printed specimen. The burn-off test was conducted according to ASTM D3171. Five specimens were tested in the burn-off test to find the volume fraction. The specimens had an average mass of 0.52 g. Pyrolysis/burning off the resin, while keeping the reinforcement unaffected, was performed at 565 ˚C for 6 h in a nitrogen environment. To measure the mass of the resin and fibers, the weight of specimen was taken before and after the burn-off test. The volume of the resin and fiber was calculated by dividing their masses with their corresponding densities. Then the volume fraction was calculated by taking ratio of volume of fiber, and fiber-matrix together. The average volume fraction of the printed specimen was 28.84%. The standard deviation among the specimens was 2.04% in measuring the volume fraction.

2.5.2. Analytical measurement

The volume fraction of the 3D printed specimen was determined analytically by utilizing the properties of the constituent materials. The mass of the fibers within a test specimen was calculated by considering the total length of the fibers within that specimen and the linear density of the fibers. The mass of the matrix material was computed by subtracting the fiber mass from the overall mass of the test specimen. Subsequently, the analytical volume fraction of the printed specimen was calculated using a standard formula. The analytical measurement revealed a fiber volume fraction of 27.6% within the 3D printed specimen.

2.6. Void Content Measurement

To measure the void content of the specimen, a Micro-CT test was also performed on the 4-layer unidirectional specimen 3D printed specimen. The experimental scanned section has dimensions of 16.3 × 13.1 × 1.9 mm. From the Micro-CT analysis, the average void content within the specimen was 8.6%. Void content present within the specimen is strongly dependent on resin flow rate during the 3D printing process. Hence, void content within the specimen could be controlled by varying resin flow rate during the printing process.

2.7. Thermal Characterization of Resin

To characterize thermal stability of used acrylate-based photo-curable resin (Peopoly tough), thermogravimetric analysis (TGA) was performed using TGA 550 instrument. Thermal initiator mixed resin was used to print a rectangular solid resin specimen using UV laser irradiation, and post cure was done as mentioned to mimic the actual printing process without incorporating carbon fiber. Printed specimen was broken down into small pieces to fit into the standard TGA pan. Three specimens were tested in TGA to verify reproducibly. The specimen was heated from room temperature to 700°C at a heating rate of 20°C per minute. Weight loss of the specimen was

captured by the TGA instrument. Purge gas (Nitrogen) flow rate to the specimen was 60 ml/min. Figure 6 is the obtained TGA curve showing the weight loss of the specimen with respect to the temperature. Onset of weight loss starts around 280°C. However, no significant weight loss was observed until 320°C. By 480°C, the remaining weight was around 5% only. Most of the resin was decomposed within this temperature range. The cured epoxy also has a very similar decomposition temperature (320-360°C) [43]. Hence, used acrylate-based photo-curable resin have similar thermal stability like epoxy resins.

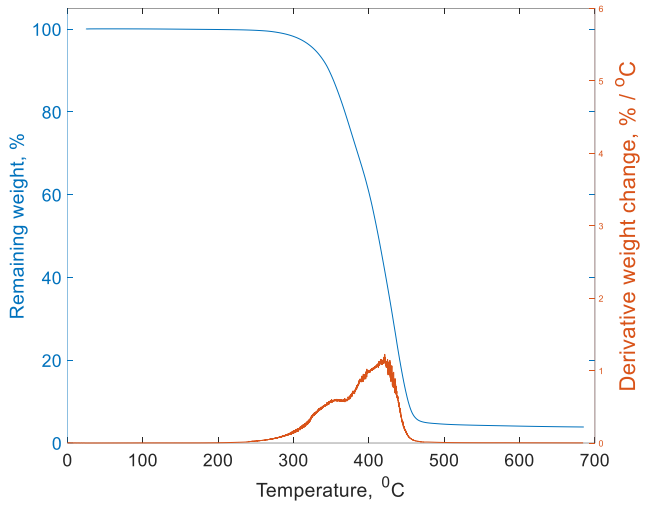

Figure 6: Thermogravimetric analysis of cured Peo-poly resin.

2.8. Tensile Test

To determine the tensile properties of CCFR 3D printed thermosets composites, four-layer unidirectional composites were fabricated. Tensile tests were conducted using an Instron Load frame equipped with a 30 kN load cell. After each printing layer, the edge of the printed layer was subjected to laser cutting as discussed in previous sections. The specimen had a length of approximately 160 mm and a width of about 12 mm. A 30 mm long glass fiber tab was inserted at each end of the specimen to ensure proper load transfer during tensile testing. Five specimens were tested to determine average tensile strength. Figure 7 (a) illustrates a representative tensile test curve for the specimen. The developed stress within the specimen increases linearly with the

applied strain throughout the entire testing duration until failure, which is typical for fiber reinforced composites. The average tensile strength was measured to be 671 MPa, with a standard deviation of 49 MPa; the average tensile modulus was measured to be 59 GPa, with a standard deviation of 3.5 GPa; the strain before failure was measured to be 1%, with a standard deviation of 0.1%.

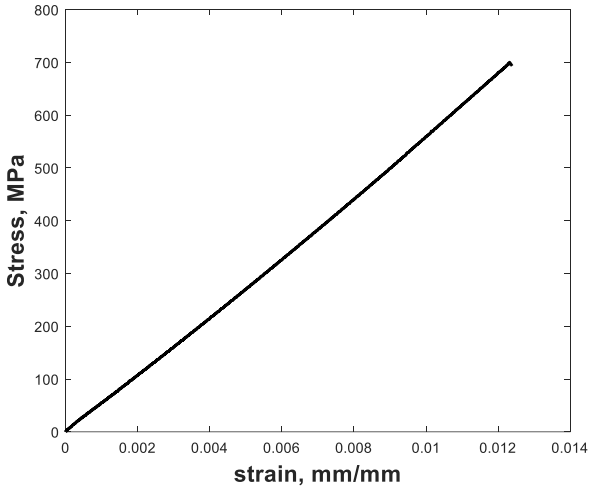

(a)

(b)

Figure 7: (a)Representative tensile test curve of 3D printed continuous carbon fiber reinforced composites, (b) Fractured specimen under tensile test.

The modified rule of mixture (ROM) model was employed for the analytical prediction of the strength of the printed composites. The modified ROM model can be expressed by Equation (1) as follows:

$$\sigma_c = \sigma_f' V_f + \sigma_m (1 - V_f) \quad (1)$$

In this equation, σ_c represents the predicted strength of the 3D printed specimen, σ_f' is the strength of the fiber at the failure strain of the composites, σ_m is the strength of the matrix material (45 MPa), and V_f is the fiber volume fraction of the printed specimen (28%).

According to the manufacturer's data sheet, carbon fiber has a strength of 4100 MPa with a failure strain of 1.7%. Since the 3D printed specimens failed at a failure strain of 1%, the

corresponding strength at a 1% failure strain is calculated to be 2410 MPa. Therefore, the predicted tensile strength using Equation (1) is estimated to be 707 MPa. This predicted strength demonstrates a reasonable agreement with the experimentally measured strength.

Moreover, the tensile modulus of the 3D printed specimen was also analytically estimated by employing ROM formula as follow:

$$E_c = E_f V_f + E_m(1 - V_f) \quad (2)$$

In the Equation (2), E_c represents the elastic modulus of the 3D printed specimens, E_f represents the elastic modulus of the fiber (240 GPa), E_m represents the elastic modulus of the matrix materials (1.5 GPa), V_f represents the fiber volume fraction of the printed specimen (28%). Using Equation (2), the estimated analytical modulus of the 3D printed specimen is estimated to be 68 GPa. This analytically estimated modulus falls within the close vicinity of the experimentally measured modulus of the specimens.

Figure 7 (b) displays the specimen's failure during the tensile test and Figure 8 displays SEM images of the fracture surface from the failed specimen under tensile loading. The SEM images clearly indicate that the primary failure modes are fiber pull-out, with short fiber lengths after being pulled out and the presence of resin on the pulled-out fibers, signifying a moderately strong bond between the fibers and the resin.

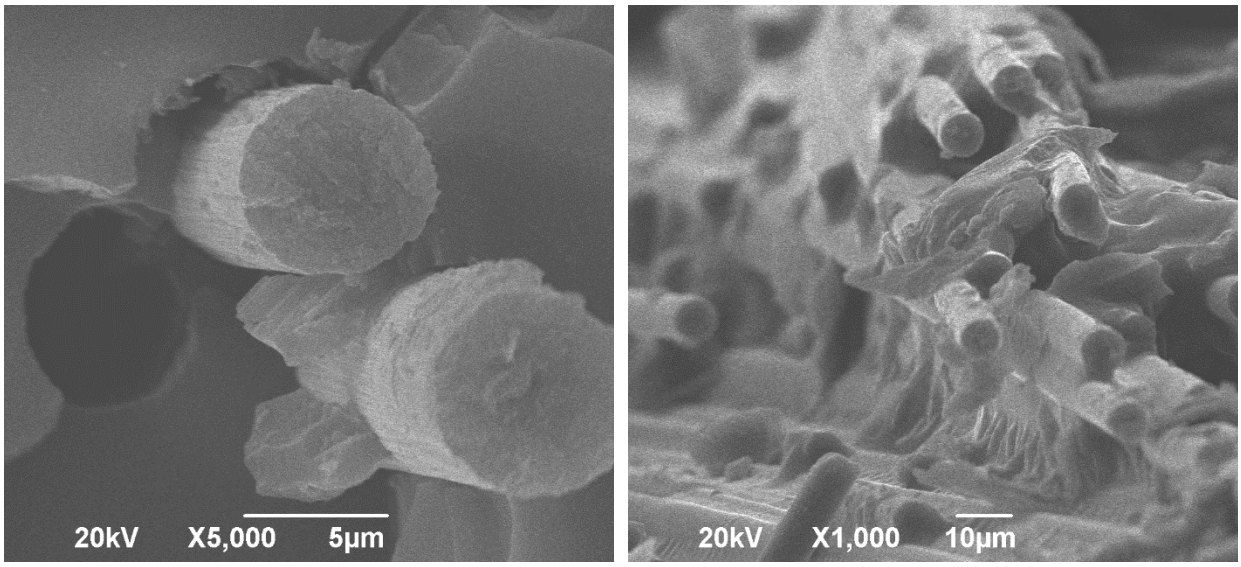

Figure 8: SEM images of the fracture surface under tensile test.

Table 1 presents a comparison of the mechanical strength between conventionally manufactured composites and the 3D printed composites featured in this study. Both sets of composites exhibit similar volume fractions, approximately 30%. Conventionally manufactured composites display a tensile strength of 826 MPa, while the 3D printed composites in this current study exhibit a strength of 686 MPa. The tensile modulus for the 3D printed composites in this study is 58.48 GPa, whereas conventionally manufactured composites have a tensile modulus of 78.7 GPa. In terms of failure strain, both 3D printed composites and conventionally manufactured composites exhibit nearly identical values. Consequently, it can be inferred that conventionally manufactured and 3D printed composites exhibit similar mechanical strength.

Table 1: Comparison of mechanical strength of 3D printed composites and conventionally manufactured composites.

	Volume Fraction (%)	Tensile Strength (MPa)	Tensile Modulus (GPa)	Strain to Failure (mm/mm)
3D printed (our study)	28%	671	59	0.01
Conventional manufacturing (Literature, epoxy resin)[44]	30%	826	78.7	0.01

2.9. Measurement of Poisson Ratio

To measure the Poisson's ratio of the 3D printed specimen, images of the test specimen were captured at certain time intervals during the tensile test. Digital Image Correlation (DIC) analysis was performed on the captured images using GOM Correlate (2019) software to obtain measurements of the Poisson's ratio. As shown in Figure 9(a), four small dots were marked on the specimen using enamel paint before performing the tensile test: two along the longitudinal direction and the other two along the transverse direction. A total of 32 image frames were captured during the tensile test of the specimen using a 24-megapixel Sony camera. Each image had a size 6000 × 4000 pixels. The camera was rigidly mounted before capturing the images to ensure stability between them. Although the time gap between consecutive images was not exactly the same, efforts were made to keep it as consistent as possible. The last image was captured just before the failure of the specimen. As depicted in Figure 9 (c)-(d), two virtual extensometers were created on the specimen using GOM Correlate software to capture the displacement of the dots. Longitudinal and transverse strain were measured using GOM correlate software. Strain in each frame was calculated by comparing it with the initially captured frame. Figure 9 (e)-(f) illustrates the longitudinal and transverse strain plotted with respect to the image frame number. The longitudinal strain measured just before the specimen's failure was +1.16%, which closely matches the strain measured using the MTS extensometer discussed in the previous section. Furthermore, the transverse strain measured before the specimen's failure was -0.38%. The Poisson ratio is determined by the ratio of transverse strain to longitudinal strain. Hence, the measured ratio of the specimen is 0.33.

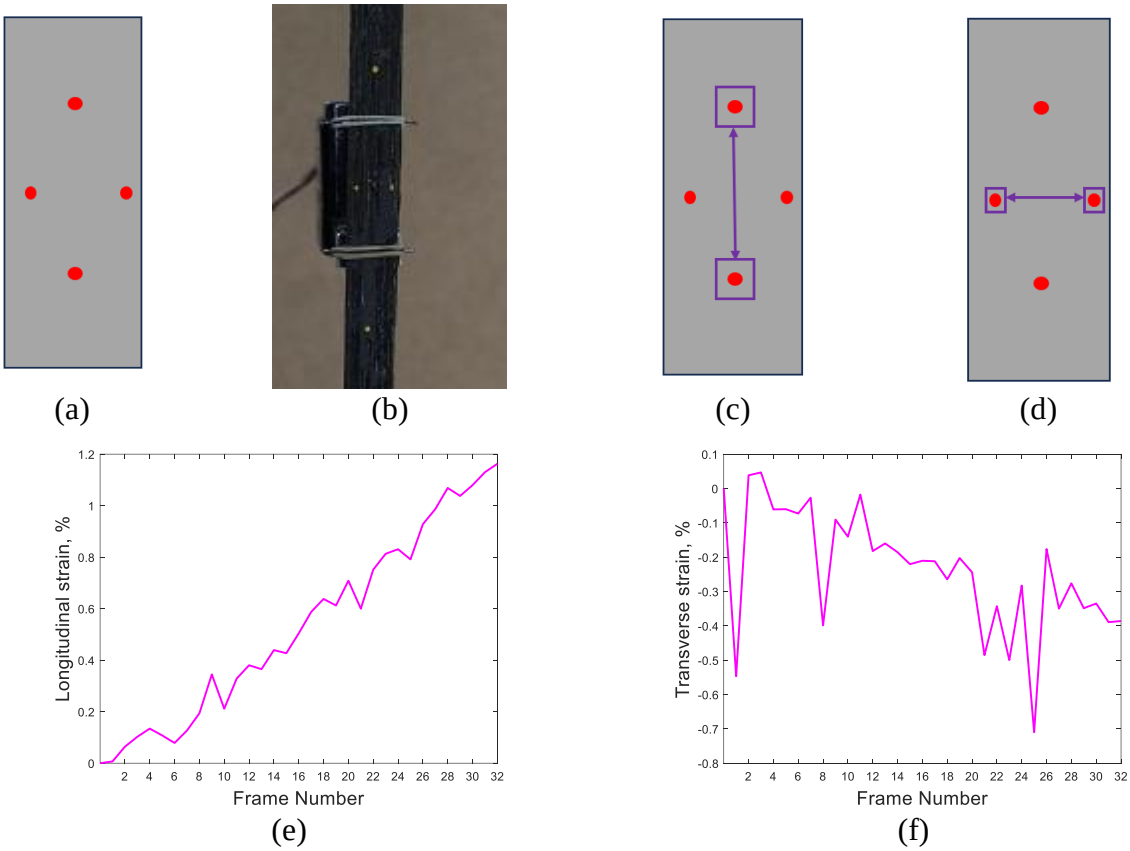

Figure 9: DIC to measure longitudinal and transverse strain during tensile test (a) schematic of four dots on the specimen, (b) real-life image of the test specimen (c) schematic of longitudinal virtual extensometer (d) schematic of transverse virtual extensometer (e) longitudinal strain vs. frame number plot (f) transverse strain vs. frame number plot.

2.10. Shear Properties Measurements

The in-plane shear properties of the 3D printed CCFR thermoset composite were evaluated using ASTM D3518. According to ASTM D3581, the shear properties of a composite can be evaluated by performing a tensile test on a composite specimen with a balanced and symmetric ±45˚ lay-up. Four layers of balanced and symmetric laminated composites were printed with a ±45˚ lay-up to measure the shear properties of the 3D printed specimen. The fiber lay-up was as follows: [+45/-45/-45/+45].

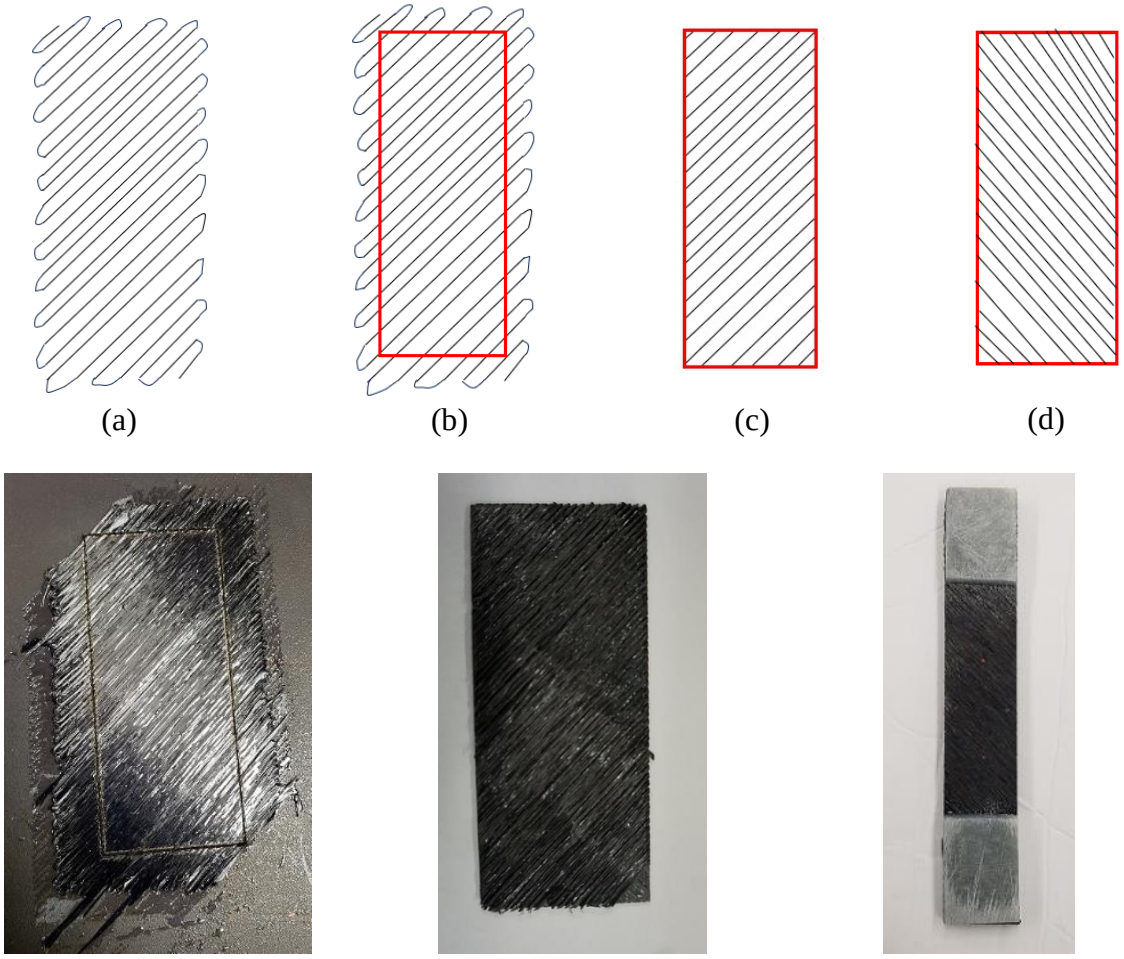

Figure 10: 3D printing of ± 45˚ lay-up specimen for shear properties evaluation, (a) schematic of + 45˚ fiber lay-up, (b) path for CO2 laser cutting (marked with red line), (c) schematic of +45˚ lay-up after laser cutting and removing superficial edges,(d) schematic of -45˚ lay-up after laser cutting, (e) +45˚ printed layer followed by laser cutting, (f) 4-layer printed specimen, (g) test specimen.

Figure 10 illustrates the printing process for a composite specimen with a ± 45˚ fiber lay-up. Figure 10 (a) shows the schematic of the toolpath for +45˚ fiber lay-up printing. The edges of the printed layers contain uneven fiber loops. Hence, CO2 laser cutting was employed after each layer of 3D printing to eliminate the uneven fiber loops. Figure 10(b) represents the trajectory for the laser cutting. Figure 10(c) depicts the schematic of + 45˚ printed lay-up after eliminating the uneven fiber loops from the edges of the printed lay-up. Similarly, Figure 10(d) depicts the schematic of -45˚ printed lay-up.

Figure 10(e) displays an actual image of the 3D printed +45˚ fiber lay-up followed by laser cutting. Figure 10(f) demonstrates the four-layer specimen with a [+45/-45/-45/+45] fiber orientation, which was thermally cured before conducting shear property measurements. Figure 10(g) presents the prepared shear test specimen with glass fiber tabs inserted on both sides. The specimen had a width of 24 mm.

To determine shear properties, the tensile test was performed on the prepared ± 45˚ fiber lay-up specimen with a crosshead displacement rate of 1 mm/min. A total of four specimens were tested to measure shear properties. A 25.4 mm extensometer was utilized during the tensile test to measure the longitudinal strain. In accordance with ASTM D3518, the developed shear stress was calculated using the following Equation:

$$\tau_{12} = \frac{F}{2A} \tag{3}$$

Where, τ_{12} is the in-plane shear stress (MPa), F represents the force developed (N), and A is the cross-sectional area of the specimen (mm^2). Figure 11 displays the representative shear stress versus longitudinal strain curve obtained from the tensile test of the ± 45˚ fiber lay-up specimen. The maximum in-plane shear stress of the 3D printed CCFR thermoset composites was determined to be 16.8 MPa, with a standard deviation of 1.46 MPa. In comparison, conventionally manufactured epoxy composites with a similar fiber volume fraction (30%) were reported to have shear strength of 20 MPa [44]. Thus, the shear strength of 3D printed CCFR thermoset composites obtained in this study is comparable to that of conventionally manufactured composites.

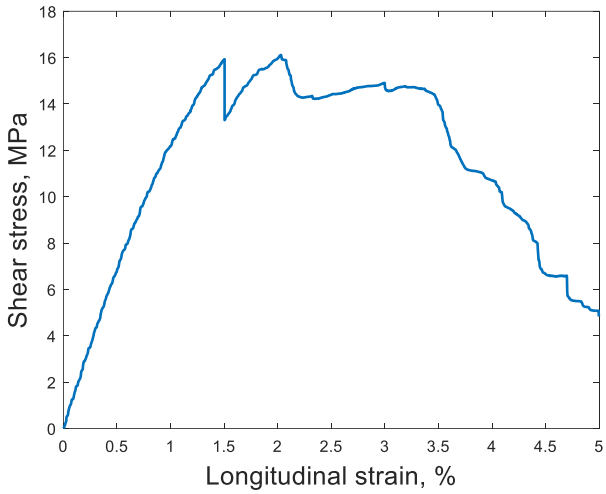

Figure 11: Representative plot of shear stress vs. longitudinal strain for 3D printed CCFR thermoset composites.

To accurately measure the maximum shear strain of 3D printed composites, it is essential to determine both the longitudinal and transverse strain at the location of maximum shear stress. The transverse strain was measured using Digital Image Correlation (DIC), as discussed in section 2.10. According to ASTM D3518, shear strain is can be defined as follow:

$$\gamma_{12} = \varepsilon_x - \varepsilon_y \tag{4}$$

Where, γ_{12} is the shear strain, ε_x is the longitudinal strain, ε_y is the transverse strain. Maximum shear strain (γ_{12}^m)could defined, based on ASTM D3518, as follow:

$$\gamma_{12}^m = \min \begin{cases} 5\ \% \\ \gamma_{12}\ at\ maximum\ shear\ stress \end{cases} \tag{5}$$

To measure the transverse strain during the tensile test of the $\pm$ 45˚ fiber lay-up specimen, DIC analysis was implemented on the time series images captured during the test, as previously discussed in section 2.10. As depicted in Figure 9 (a), four dotted marks were placed on the test specimen. Nineteen picture frames were captured during the tensile test, although not all images were captured at exactly equal time intervals. Those images were processed using GOM correlate software to measure strains. Two virtual extensometers were created on the specimen to track the

elongation between the marked dots, as shown in Figure 9 (c) and (d). One virtual extensometer was for measuring longitudinal strain, and the other for transverse strain. Longitudinal and transverse strains were measured using virtual extensometer through GOM correlate software.

Figure 12 displays the longitudinal and transverse strain plotted against image frame number. Furthermore, the longitudinal strain was also measured using a 1-inch MTS extensometer during the test, which was plotted on Figure 11. Both the extensometer and DIC analysis demonstrated similar amounts of longitudinal strain over the duration of test, which validates the accuracy of the DIC analysis. By comparing the longitudinal strain measured by the extensometer and DIC analysis, it becomes possible to establish the relationship between shear stress (τ_{12}), longitudinal strain(ε_x), and transverse strain (ε_y).

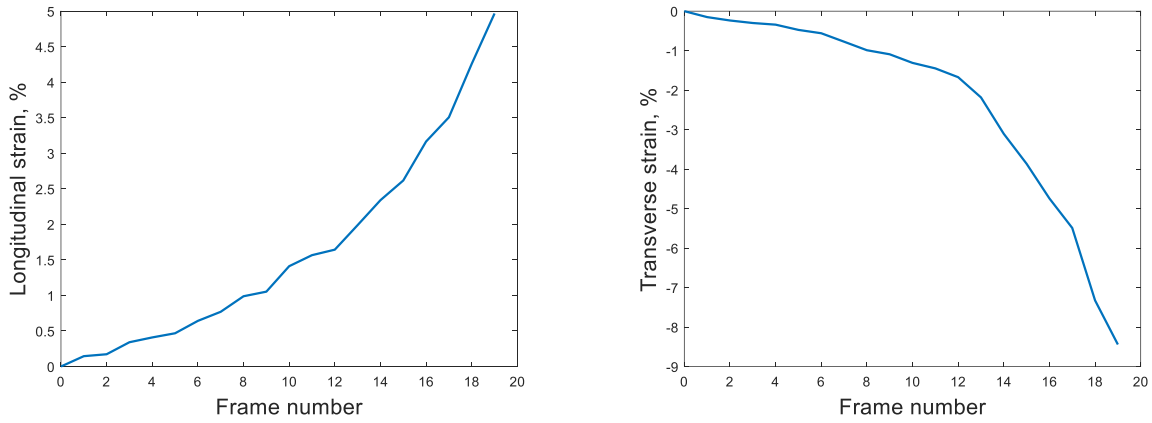

(a) (b)

Figure 12: Longitudinal and transverse strain with respect to nineteen picture frames captured during tensile test of specimen having ± 45˚ fiber lay-up.

Subsequently, shear strain (γ_{12}) can be calculated using Equation (4). Figure 13 illustrates the shear stress versus shear strain plot. From Figure 13, the shear strain at the location of maximum shear stress was calculated to be 4.17%. The shear modulus (G_{12}) can be calculated by measuring the initial slope of the shear stress versus shear strain plot. The measured shear modulus(G_{12}) for these 3D printed composites is 0.73 GPa.

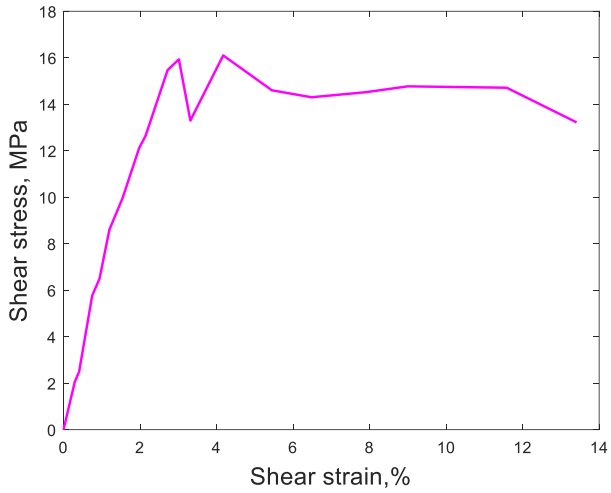

Figure 13: Plot of shear stress versus shear strain.

2.11. Conclusion

This study has reached a significant milestone by successfully demonstrating the hybrid manufacturing process of custom objects through the integration of an additive and subtractive process to fabricate CCFR thermoset composites. Mechanical characterization of the 3D printed composites in this study reveals that they exhibit comparable mechanical strength to conventionally manufactured composites. 3D printed composites achieved a fiber volume fraction of 28%, with a measured tensile strength of 671 MPa and a tensile modulus of 59 GPa. The printed composites exhibit a Poisson ratio of 0.33. The calculated shear strength and modulus were 16.8 MPa and 0.73 GPa, respectively. Properly adjusting the process parameters of this proposed 3D printing technique presents a significant opportunity to replace expensive conventional manufacturing processes for composites with cost-effective and design-flexible 3D printing.

CHAPTER 3: MECHANICAL CHARACTERIZATION AND PRODUCTION OF COMPLEX SHAPES USING CONTINUOUS CARBON FIBER REINFORCED THERMOSET RESIN BASED 3D PRINTING

3.1. Introduction

Three-dimensional (3D) printing has been experiencing significant growth in manufacturing industries as the creation of higher performance materials has improved. It has advantages over traditional manufacturing processes because of reduction in development time, cost. Additionally, it brings unparalleled design flexibility and capability to manufacture complex geometries which are not possible to manufacture through conventional machining. This is an inexpensive, custom, and mold-less manufacturing process where the parts are manufactured from a computer-based 3D model (CAD design) without having any geometric limitations. The main novelty in 3D printing lies in adding materials instead of removing it. Polymeric materials are the most commonly used materials for 3D printing.

Polymeric material used for 3D printing can be classified into two types: thermoplastics and thermosets. Thermoplastics (ABS, PLA, PA, and a few others) are most commonly used for fused deposition modeling (FDM) 3D printing because of their re-melting capabilities. Material extrusion based FDM is currently considered the most widely used technology because of its low cost, convenience, and simplicity. In this printing process, semi-solid filaments are deposited in a layer-by-layer fashion to construct a specimen. Due to the limitation of the constituent thermoplastic filament's properties, FDM printed items show poor mechanical strength [7]. Hence, those FDM printed items are primarily used as prototype products or toys.

Conversely, thermosets are commonly used as structural materials due to their better mechanical properties, chemical properties, and thermal stability. Thermoset polymer materials

are irreversibly hardened upon heating or UV or visible light laser irradiation. The most commonly used thermoset printing process is stereolithographic (SLA) printing using vat photopolymerization. SLA printing processes use high energy lasers to selectively cure photocurable thermoset resin in a layer-by-layer fashion, and thus manufacture complex objects. Typically, acrylate based thermoset resin with appropriate photo-initiator is used for SLA 3D printing. Photo-initiators generate reactive species upon light exposure to initiate free radical polymerization of resin [45].

Furthermore, an extrusion-based 3D printing of thermoset resin has also been demonstrated using direct ink writing (DIW) based 3D printing process. DIW printing process does not require curing immediately after deposition, but feedstocks must produce sufficient yield stress in order to maintain shape after deposition [46]. A DIW based process also successfully demonstrated printing of 3D structures using pressure driven deposition of viscoelastic ink, like: thermoset resin and elastomer [46, 47]. Precursor ink used for DIW based printing requires proper rheological behavior. Therefore, this DIW based printing process suffers from a limitation of nozzle clogging. However, UV assisted extrusion-based DIW printing shows a potential of printing with otherwise unprintable ink [48].

To further enhance mechanical properties of 3D printed thermoset plastics, different reinforcements (i.e., carbon black, filler, chopped fibers) have been mixed with thermoset resin to 3D print [3-6, 49]. The tensile strength of those short fiber reinforced 3D printed thermoset composites were reported below 100 MPa. Short fiber reinforcement increases the stiffness of the part, but the increase in strength is still limited as fiber pull-out occurs before fiber breakage [50]. Therefore, short fiber reinforced 3D printed composites still show inferior mechanical strength as compared to conventional fiber reinforced composites.

In order to get higher mechanical strength, continuous fiber reinforcement was incorporated in extrusion-based 3D printing of both thermoplastic and thermoset resins. Extrusion-based 3D printing shows great potential in 3D printing of continuous fiber reinforced composites. 3D printing of continuous fiber reinforced thermoplastic composites is well established over literature [9, 28, 39, 41, 50, 51]. Furthermore, MarkForged commercialized the MarkOne printer to 3D print continuous glass, aramid, and carbon fiber reinforced thermoplastic composites [52]. However, continuous fiber reinforced thermoplastic suffers from significant air void formation during printing [51, 53]. Moreover, due to high melt viscosity of thermoplastic matrix, impregnation of continuous fiber filament with thermoplastics is very challenging [54]. Hence, incomplete/partial wet out of fiber tow with the thermoplastic resin generates a weak interface between continuous fiber and thermoplastic resin [55].

Conversely, thermoset resins exhibit excellent wet-out of fibers during 3D printing with continuous fibers because of being a low viscosity liquid at room temperature. Moreover, in-situ (in-nozzle) impregnation process of 3D printing of continuous fiber has been shown to have good wetting ability of fibers [7].

Continuous carbon fiber reinforced (CCFR) thermoset polymers have wide application in automobiles, aerospace, sports equipment, etc. due to their light weight, higher thermal stability, high strength and modulus along fiber direction [56]. In fact, fiber reinforced thermosetting composites are used for high performance applications because their low viscosity enables higher fiber volume fraction, and the cured nature of the resins reduces tendency for creep under load relative to thermoplastic composites. Furthermore, continuous carbon fiber reinforcement in thermoset polymer composites also shows a great potential in developing high performance energy storage systems [57].

3D printing of CCFR thermoset composites was successfully demonstrated using frontal, self- propagating, and rapid exothermic curing reaction based reactive resin systems [10, 11, 15, 19, 56, 58, 59]. Additionally, Dong et al. exhibited 3D printing of CCFR composites using a thermic lance with a phenolic thermoset resin [14].

Research on photo-cure assisted 3D printing of CCFR thermoset composites is still limited. Abdullah et al. demonstrated CCFR 3D printing using UV light assistance with an acrylate-based thermoset resin [16]. However, the reported maximum tensile strength of the printed specimen was limited to 100 MPa. Atik et al. also reported 3D printing of CCFR thermoset composites using UV laser assistance [17]. However, in their study, they used pre-impregnated carbon fiber with a filament count of 1K (1000 filament per tows). The use of carbon fiber with a low filament count led to an increased susceptibility of the fiber to tearing during the 3D printing process.

Furthermore, there is limited literature on the demonstration of custom shapes 3D printing using continuous fiber-reinforced thermoset composites. Some studies have shown examples of 3D printing hexagonal and grid structures using thermosetting epoxy resin, but the epoxy resin used in those processes was solid at room temperature [58, 60-62]. Consequently, similar to FDM, 3D printing was carried out by melting the resin upon heating within the print nozzle. However, finding examples of grid structure 3D printing using thermoset resins that are liquid at room temperature remains challenging in the literature, despite the fact that most commercially available thermoset resins are in liquid form at room temperature. The use of liquid resins can provide better fiber impregnation with the resin, resulting in improved fiber-matrix adhesion and enhanced structural stability.

The objective of this study was to establish the CCFR 3D printing process to produce complex shapes using photocurable thermoset resin, and mechanically characterize the printed

specimens. In this current study, dry (without resin pre-impregnation) 3K carbon fiber was used, which eliminated the problem of fiber breakage during the process of 3D printing.

3.2. Experimental Methods

3.2.1. Materials

Teijin 3K continuous carbon fiber served as a reinforcement material for the 3D printing process. The carbon fiber was sourced from Teijin Carbon America, Inc (Rockwood, TN, USA). Each individual fiber strand consisted of 3000 filaments, with each filament having a diameter of 7 μm. These fibers were characterized by a linear density of 200 tex (tex representing the weight in grams for 1000m of fibers) and a density of 1.77 g/cm^3. Furthermore, the carbon fiber boasted impressive mechanical properties, including a tensile strength of 4100 MPa and tensile modulus of 340 GPa. Additionally, the elongation at break for these carbon fibers was 1.7 %.

Commercially available photo-curable thermoset Peo-Poly Moai Tough Resin (acrylate-based) was utilized as the 3D printing ink. This resin was procured from MatterHackers (California, USA), and it can be photo-cured under light irradiation with a wavelength of 405 nm. The density of the resin is 1.15 g/cm^3. To enable thermal curing along with photo-curing, 0.5% Luperox P was mixed into the resin before 3D printing. Luperox P (tert-butyl peroxybenzoate, 98%) was purchased from Sigma Aldrich (Missouri, USA). Both photo-curing and thermal-curing of the resin printing ink occur through free radical polymerization reactions.

3.2.2. Rheology test of resin

The rheological characterization of the 3D printing ink was conducted using an ARES G2 rotational rheometer (TA Instruments, DE, USA). The rheological test involved filling the resin

between two 25 mm diameter parallel plate stainless steel fixtures with a gap of 0.5 mm between them. The test was carried out at the ambient lab temperature of 25˚C.

To determine the viscosity of the resin at different shear rates, a flow sweep test was performed. Additionally, a strain sweep test was conducted at a constant frequency of 6.28 rad/s to measure the storage and loss modulus of the print ink. Before measuring any rheological parameter, the resin was allowed to equilibrate for 5 min.

3.2.3. Printing process

A commercial gantry with moveable X, Y, and Z-axes was modified to create a custom 3D printer capable of producing CCFR thermoset composites. The printer utilized a stationary hot-rolled steel plate (300 × 300 mm) as its print bed. G-code, generated using a python program, controlled the movement of the modified gantry. The print head of this customized printer included a specially designed print nozzle, a syringe pump (brand: Aitoserlea, Wentian Du, China), and light lasers (0.8W power, 405 nm wavelength, purchased from Sunshine Electronics, Guangdong, China).

As depicted in Figure 1, a print nozzle was designed to simultaneously feed carbon fiber and thermoset resin onto the print head. Carbon fiber was pulled through the top of the nozzle, while thermoset resin was supplied from the side using a syringe pump. The resin flow rate (F) used during the printing process was 0.121 mL/min. A 14-gauge syringe needle with an inner diameter of 1.6 mm was attached to the tip of the nozzle to extrude fiber and resin together. A flexible needle tip was utilized to enable continuous printing over irregularities.

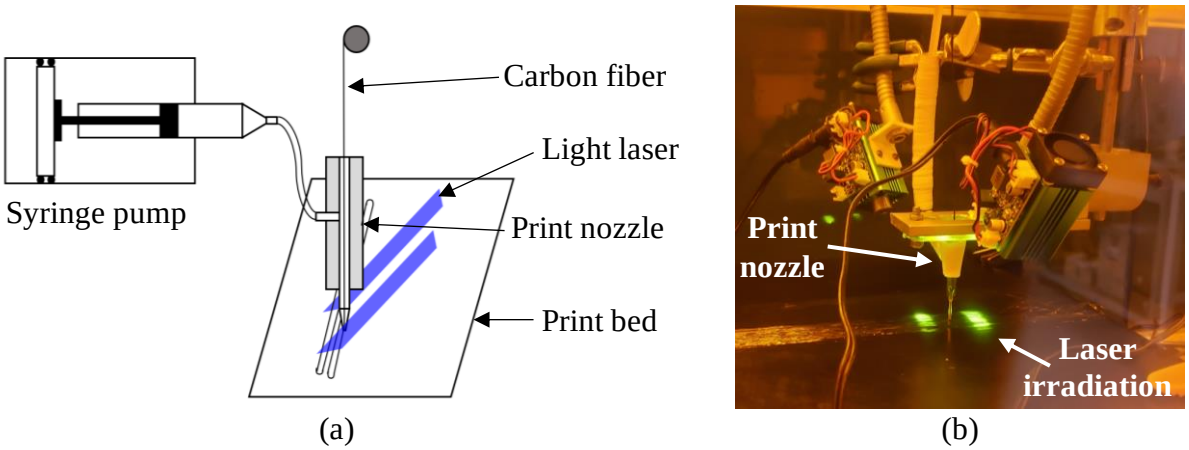

(a) (b)

Figure 14: Light-assisted 3D printing process of CCFR thermoset composites (a) schematic diagram of the printing process, (b) real-life picture of the printing set-up.

Carbon fiber impregnated with resin was deposited on the print bed through the motion of the print head. To cure the resin on the print bed, an 800 mW, 405 nm laser was employed. The laser was focused as a line at a specific distance from the print tip, as illustrated in Figure 14(b). The laser's focus distance was adjusted to prevent resin clogging at the nozzle tip. To ensure a smooth resin flow during printing, a 0.85 mm gap was maintained between the nozzle tip and the print bed (or the previous layer). The gap between two consecutive lines of fiber on the same layer is set at 1 mm. The print head speed (S) during this printing process was 120 mm/min.

A similar printing process was reported by the authors in previously published research articles [17, 63]. Similar to the previous study, the same resin was utilized in this current research. However, this research employs 3K carbon fiber tows instead of the 1K carbon fiber tows used in the previous study. The incorporation of 3K carbon fiber tow eliminates the possibility of fiber breakage due to traction forces acting on the fiber during the printing process. Unlike the previous study, this research does not involve pre-impregnating the carbon fiber with the resin. Instead, raw carbon fiber was introduced into the print nozzle to be printed with liquid photocurable thermoset resin.

Moreover, the resin flow rate and the printing speed were adjusted to print composites with higher volume fraction, reduced void content, and improved mechanical strength. The novelty of this research article lies in its elucidation of critical considerations for achieving the desired dimensional accuracy in printed objects, while also showcasing the overhanging capabilities of printed layers. Additionally, this study will illustrate algorithms designed for printing various complex shapes utilizing this particular printing process.

The amount of resin dragged along with the fiber during the printing process depends on both resin flow rate (F, ml/min) and printing speed (S, mm/min). However, using a single parameter to define the amount of resin dragged with the fiber during printing is more convenient. Therefore, in this current study, a parameter, $\frac{F}{S}$ (mL/mm) is defined, representing the amount of resin dragged per unit length of 3D printing. The parameter $\frac{F}{S}$ takes into consideration the effects of both the resin flow rate (F) and the print speed (S). The value of $\frac{F}{S}$ used during the current printing process was 1.008 mL/m.

Figure 15 (a) compares the nozzle's programmed printing path generated by the G-code with its actual printed trajectory. As depicted in Figure 15 (c), the 3D printed object was slightly shorter than the intended programmed path. This deviation arose from the light sources being focused at a 10 mm distance from the print nozzle, as illustrate in Figure 15 (c). Consequently, the realized printed specimen measured approximately 10 mm (3/8 inch = 9.5 mm) less than the programmed path (illustrated in Figure 15 (c)). In theory, the difference between the actual printed object and programmed path should have equaled the nozzle-to-laser irradiation distance. However, the discrepancy was slightly reduced due to the fiber's turning loop at the corners.

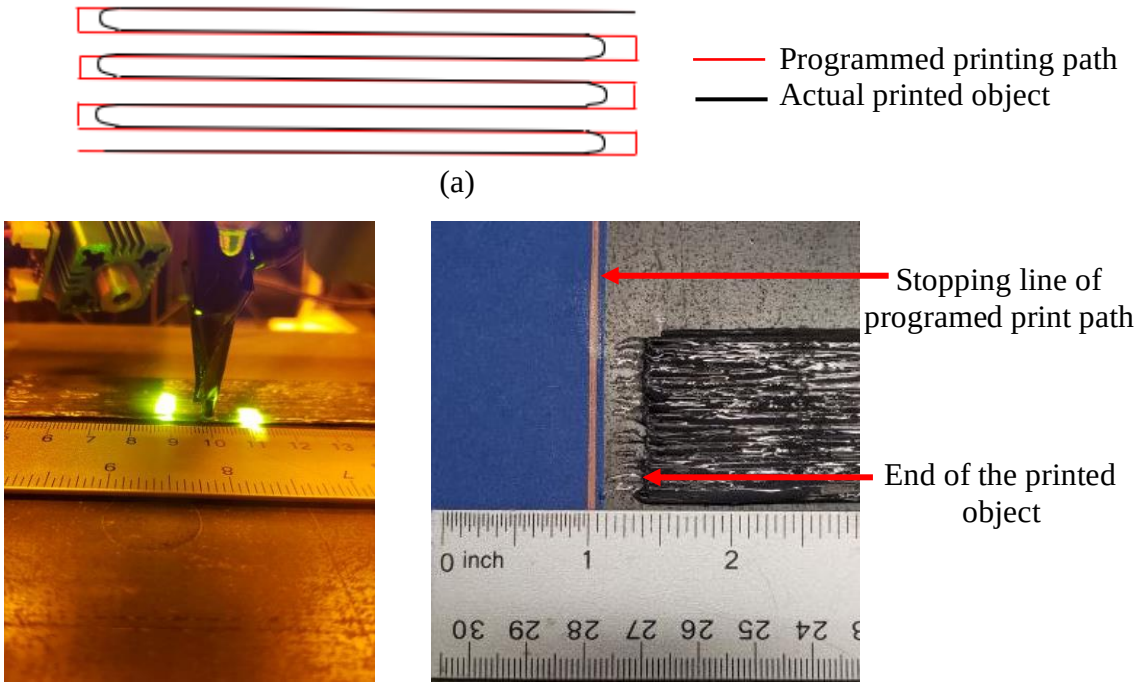

Figure 15: Dimensional accuracy analysis: (a) schematic comparison between programmed printing path and actual printed object; (b) distance between nozzle tip and laser irradiation; (c) discrepancy between programmed printing path and actual printed object.

To achieve complete curing of the photo-irradiation assisted 3D printed CCFR composite, a thermal curing process was conducted in a convection oven at a temperature of 180˚C for 8 h. Photo irradiation partially solidifies the resin, while thermal curing establishes a highly crosslinked polymer network [19, 64]. Moreover, this dual-cure system mitigates the degree of dimensional shrinkage in the resin during the printing process [65].

3.2.4. Fiber volume fraction measurement

To measure the volume fraction of 3D printed composites, constituent content (fiber and matrix) within the composites was measured using ASTM D 3171. According to ASTM D3171, the polymer matrix of the printed specimen was carbonized under nitrogen environment, while leaving reinforcement unaffected. Thus, this procedure enabled the calculation of fiber and matrix contents. Five specimens were tested. The average mass of each specimen was 0.9813 g. Crucibles

with specimens were placed in a nitrogen-purging furnace (Model, RD4-KHE24, Warrington, PA, USA) at 565˚C for 5 h.

The volume fraction of the continuous carbon fiber reinforced 3D printed thermoset composited was also evaluated by analytical approach using the materials properties. The mass of fiber within a specimen was calculated using the Equation (6):

$$m_f = \frac{LWn \times tex}{10^6 \times l} \quad (6)$$

where, m_f is the mass of fibers (g), L is the length of specimen (mm), W is the width of the specimen (mm), n is the number of carbon fiber layers printed, tex is the fibers properties (mass of 1000 m of fiber in g), l is the space between two consecutives fiber line (hatch spacing, mm). The mass of the fiber (m_f) is divided with fiber density (ρ_f) to get the volume of the fiber (v_f). Mass of the matrix material (m_m) was calculated by subtracting fiber mass (m_f) from the total mass of the specimen (m). Afterward, the volume of matrix material (v_m) was calculated by dividing matrix mass (m_m) with matrix density (ρ_m). Hence, overall fiber volume fraction (V_f) was calculated by taking the ratio of fiber volume (v_f) to the total volume ($v_f + v_m$).

3.2.5. Tensile testing

To determine the tensile strength of 3D printed composites, four-layer unidirectional specimens were printed using the printing process discussed in Section 3.2.3. The printed composites were cut into widths of 10 mm for tensile testing. Tabs were attached at both ends of the specimen to ensure better load transfer and reduce stress concentrations at the grip. The tensile tests of the printed specimens were performed following ASTM standard (ASTM D 3039 [66]). The test rate was 1 mm/min. A 25.4 mm extensometer was attached to the specimen to measure

failure strain of the specimen. Five specimens were tested under tensile load to calculate average tensile strength. The average thickness of the printed specimens was 3.2 mm.

3.2.6. Interlaminar shear testing

To measure the interlaminar shear strength (ILSS) of printed composites, seven-layer unidirectional flat specimens were 3D printed using the discussed printing mechanism. Short beam shear (SBS) testing was performed according to ASTM D 2344 to measure the ILSS of the printed specimens. Five specimens were tested to determine the average SBS strength. The thickness of the specimens was 5.1 mm.

As per the standard, the length and width used for the specimen were six and two times the thickness (30.6 mm and 10.2 mm, respectively), and the loading span used was four times the thickness (20.4 mm). The specimen was loaded in three-point bending, and the test rate used was 1 mm/min. The maximum load (P_m) during the test was calculated from the load- displacement curve. The short beam shear strength (F^{sbs}) was calculated using Equation (7), where b and h are the width and thickness of the specimen.

$$F^{sbs} = 0.75 \times \frac{P_m}{b \times h} \tag{7}$$

3.3. Results and Discussion

3.3.1. Rheological characterization

Figure 16 depicts the rheological characterization of the print ink at different shear rates. As shown in Figure 16(a), the viscosity of the print ink remains constant regardless of the shear rate, with a value of 0.94 Pa·s. Furthermore, the shear stress demonstrates a linear increase with shear rate, indicating that the print ink exhibits rheological behavior similar to that of a Newtonian fluid. However, in DIW-based printing processes, the print ink utilized typically exhibits shear

thinning behavior. This shear thinning behavior is achieved by incorporating rheology modifiers, such as silica or clay, into the thermoset resin. DIW-based print ink typically exhibit viscosities of around 500 and 40 Pa·s at the shear rates of 10 and 100 (1/s), respectively [46].

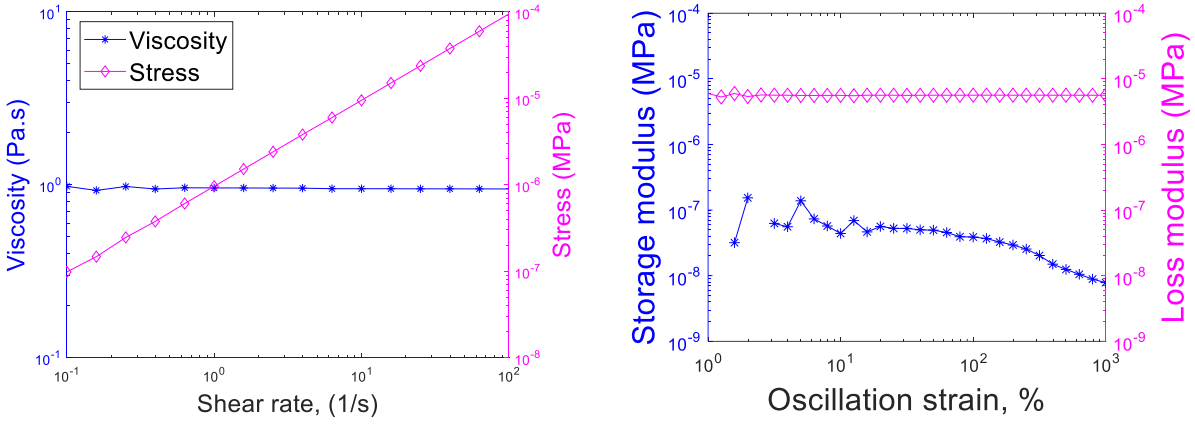

(a) (b)

Figure 16: Rheological characterization of print ink (a) viscosity at different shear rates, (b) storage and loss modulus at different oscillation strains.

Figure 16(b) illustrates the storage and loss modulus of the print ink at various oscillation strains. The loss modulus is observed to have higher values compared to the storage modulus. A viscoelastic ink that has the capability to retain shapes after being printed usually exhibits a higher storage modulus than loss modulus. However, in the case of the print ink used in this research, the loss modulus is higher than the storage modulus, indicating that the print ink lacks this shape retaining capability. The addition of a rheological modifier can increase the value of the storage modulus compared to the loss modulus. It is important to note that the inclusion of rheological modifiers can cause nozzle clogging during the printing process. However, the light-assisted 3D printing process has the potential to produce dimensionally accurate parts using low-viscosity, commercially available liquid thermoset resin, making it suitable for creating complex objects without nozzle clogging.

3.3.2. Volume fraction

The average fiber volume fraction of the printed specimen from the burn-off test was calculated as 18.29%, with a standard deviation of 0.38%. On the other hand, the calculated fiber volume fraction of the 3D printed specimen using the analytical approach was 15.5%. There is a discrepancy present between the volume fraction measured by the burn-off approach (ASTM D 3171) and the analytical approach. The degree of fiber straightness [61] during the printing process is an important factor to consider when explaining these differences. Due to lack of fiber straightness, there might be more fiber present within the specimen than what was calculated analytically.

3.3.3. Overhanging capabilities

Figure 3 represents the overhanging capabilities of the printed layer using this printing process. The resin-impregnated fiber hardened immediately after being exposed to the laser light and was able to retain its shape. Figure 17 also shows the printed carbon fiber layer extending beyond the edge of the print bed. The printed layers beyond the edge of the print bed were also able to retain their shapes. This unique characteristic of this printing technique would be very helpful in creating complex shapes and structures using this printing process.

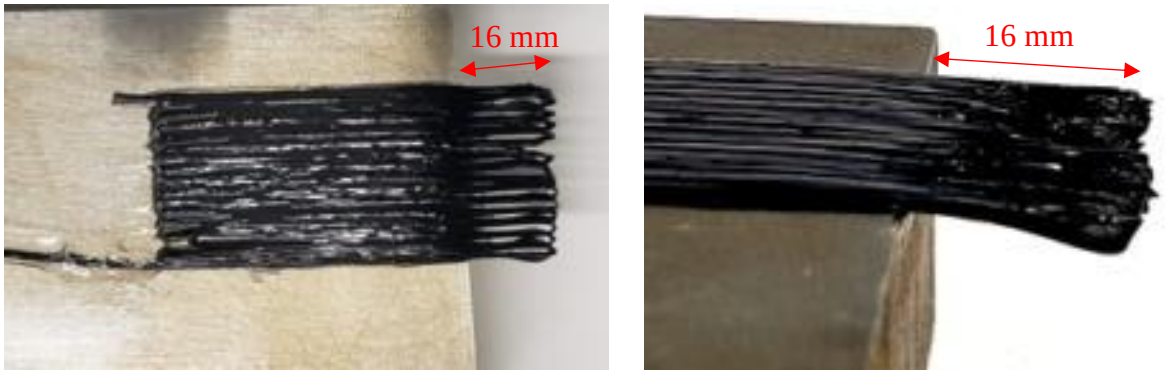

(a) (b)

Figure 17: Overhanging capabilities of 3D printed layers using the current printing process, (a) top view, (b) side view.

3.3.4. Surface profile and roughness

To quantify the smoothness of the printed object, the surface profile and line roughness of a single 3D printed layer were measured using a Keyence digital microscope (Keyence, Model: VHX - 7000, Osaka, Japan). Figure 18(a) shows the 3D surface view of a single printed layer, and Figure 18(b) shows the 2D profile of the printed layer. The average layer height of a single layer is approximately 0.8 mm. To quantify the roughness of the printed layer, a line roughness parameter - arithmetic mean roughness (R_a) - is defined as follows: -

$$R_a = \frac{1}{l}\int_0^l |Z(x)|\, dx \tag{8}$$

Where l is the length of the line drawn, and $|Z|$ is the absolute value of profile height from the mean surface. Figure 18(c) show the lines drawn on a printed layer to measure line roughness. The line for roughness measurement was drawn along the transverse direction of the printing. The printed layer was coated with thin black pigment to avoid optical measurement errors due to transparent resin. Five measurements of R_a were taken at the different locations on the printed layer.

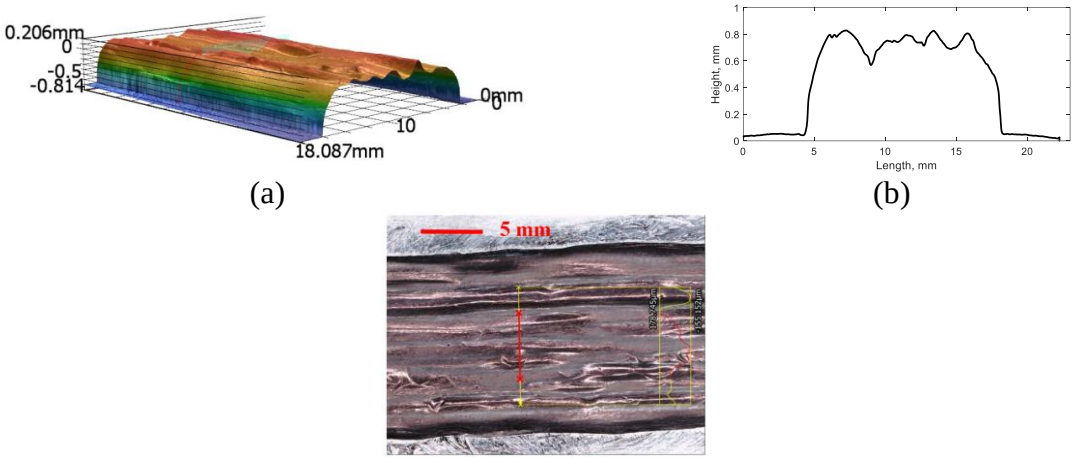

(a) (b)

(c)

Figure 18: Surface profile measurement of a single 3D printed layer: (a) 3D view of the printed layer, (b) 2D profile of the printed layer, (c) line drawn transversely on the printed layer to measure roughness.

The calculated R_a was 14.4 µm, with a standard deviation of 1.8 µm between measurements. During this measurement, the cut-off wavelength (λ_c) was set to 2.5 mm since the roughness feature repeated after every 1 mm. A value of λ_c at 2.5 mm indicates that surface profile wavelengths above 2.5 mm will not be considered as surface roughness but rather as waviness of the specimen or build-plate.

The roughness of the FDM 3D printed thermoplastic object varied between 15-60 µm [67]. Due to this superior surface roughness, these 3D printed composites have the potential to meet the surface roughness requirements as advanced structural elements.

3.3.5. Tensile strength

The average tensile strength of the CCFR 3D printed specimen was 389.7 MPa, and the average tensile modulus was 41.93 GPa. Figure 19 illustrates the representative tensile test curve for 4-layer unidirectional CCFR thermoset composites. It is evident from the tensile test curve that the specimens did not exhibit significant yielding or necking until failure, which is very typical of carbon fiber composites. The standard deviation for tensile strength was 22.26 MPa, and the standard deviation for tensile modulus was 3.65 GPa. The failure stain of the specimen (ε_f) is 0.01 mm/mm (1%).

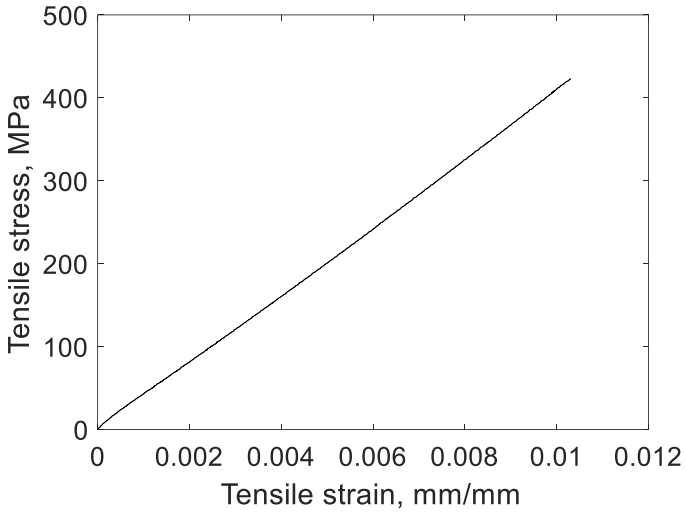

Figure 19: Representative tensile test curve for continuous carbon fiber reinforced 3D printed thermoset composite.

Theoretical tensile strength and modulus of the printed specimen were predicted using the rule of mixture (ROM) and the constituent properties provided in the manufacturer's data sheet. Equation (9) and (10) present the formulas utilized for calculating theoretical strength:

$$\sigma_c = \sigma_f' V_f + \sigma_m(1 - V_f) \tag{9}$$

$$E_c = E_f V_f + E_m(1 - V_f) \tag{10}$$

Here, σ_c and E_c represent the strength and modulus of the printed specimen. V_f denotes the fiber volume fraction of the printed specimen (18.3 %), σ_m signifies the tensile strength of the matrix material (45 MPa), E_f represents the modulus of the fiber (E_f = 240 GPa), and E_m indicates the modulus of the matrix material (E_m= 1.5 GPa). σ_f' denotes the strength of the carbon fiber at the failure strain of the printed specimen.

According to the manufacturer's data sheet, the strength of the continuous carbon fiber (Teijin, 3K) is 4100 MPa with a failure strain of 1.7%. However, the failure strain obtained from the printed specimen is 1%, potentially due to fraying of the fiber at the nozzle tip during printing. Employing the unitary method, the strength of the carbon fiber corresponding to a 1% failure strain

is calculated as σ_f' = 2412 MPa. Consequently, the calculated theoretical tensile strength and modulus of the printed specimen are 478.2 MPa and 45.1 GPa, respectively.

However, the experimentally obtained tensile strength and modulus values are 18.5% and 7% lower, respectively, compared to the corresponding theoretical values. This discrepancy is attributed to the inherent limitations associated with 3D printed specimens, such as high void content, poor interlayer adhesion, and fiber misalignment.

Table 2 presents a comparison between the presently reported tensile properties of CCFR light-cured thermoset composites and the corresponding results from existing literature. To facilitate this comparison, the tensile properties cited in the literature have been normalized for a volume fraction (V_f) of 18%. The normalization process involved utilizing linear regression, assuming zero strength at a zero percent volume fraction.

Table 2: Comparison of tensile properties between light-cured continuous fiber reinforced 3D printed composite with Literature.

	Material	Manufacturing Process	Tensile Strength (MPa)	Tensile Modulus (GPa)	ε_f (%)	V_f (%)	Strength for V_f = 18%	Modulus for V_f = 18%
Current study	Carbon fiber + acrylate resin	3D printing (UV light assisted)	389.7	41.93	1	18	389.7	41.9
Genel et al. [44]	Carbon fiber + epoxy	Conventional (manual lay-up)	826	78.7	1	30	495.6	47.2
Zhang et al. [19]	Carbon fiber +epoxy	3D printing (frontal propagation)	420	-	0.9	18	420	-
Yang et al. [61]	Carbon fiber + epoxy	3D printing (by melting engineered epoxy)	1372.4	98.2	0.8	55	441	31.6

The validity of employing linear normalization can be supported by a study conducted by Zhang et al. In their study, they fabricated composites using 3D printing techniques at two distinct volume fractions (18% and 48%). The resulting tensile strengths of these printed composites (420 MPa and 1147 MPa, respectively) exhibited a predominantly linear relationship [19]. Moreover, research conducted by Amaria et al. similarly demonstrated a linear relation between mechanical properties (specifically tensile strength and modulus) and the volume fraction of 3D printed composites [68].

Drawing from the study conducted by Genel et al., conventionally manufactured (via manual lay-up) carbon fiber-epoxy composites demonstrated a strength and modulus of 495.6 MPa, and 47.2 GPa, respectively, at a fiber volume fraction of 18% [44]. Conversely, Yang et al. pursued 3D printing of carbon fiber reinforced epoxy composites using melted engineered epoxy. Their endeavor yielded strength and modulus values of 441 MPa and 31.63 GPa, respectively, for an equivalent volume fraction of 18% [61]. Notably, this study revealed comparable tensile strength and modulus outcomes, specifically a tensile strength of 389.7 MPa and modulus of 41.9 GPa. Additionally, an anticipated observation was that acrylate-based thermosets (the resin employed in this study) would exhibit diminished strength in contrast to epoxy-based resins (utilized in the referenced literature).

Figure 20 illustrates the SEM images capturing the fracture surface of the specimen subjected to the tensile test. As depicted in Figure 20(a), it is evident that the resin impregnation into the individual fiber filaments occurred effectively. The individual fiber filaments exhibited an approximate diameter of 7 μm, and a fiber tow encompassed 3000 such fiber filaments. These fiber filaments maintained straight along the loading direction. Consequently, the SEM images

also displayed that the occurrence of bucking in the placement of fiber filaments during the printing process was minimal.

The principal mode of failure observed during tensile loading was fiber pull-out; however, predominantly isolated instances of single fiber pull-out were noted. This phenomenon of single fiber pull-out in the context of a thermoset matrix was also observed in the study conducted by Zhang et al. [61]. In contrast, the pull-out of large fiber bundles was generally observed in scenarios involving a thermoplastic matrix [61].

Furthermore, failure marks within the resin materials (indicative of matrix-dominated cohesive failure) pointed towards the gradual progression of failure through the matrix materials. This gradual nature of failure signified that the failure did not abruptly or catastrophically. This observation also provided evidence of strong adhesion between the fiber and the matrix.

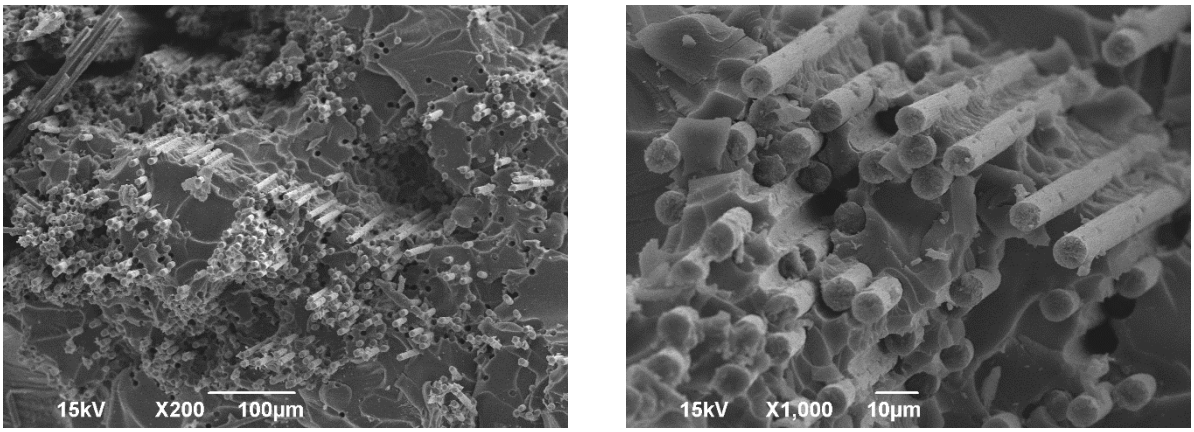

(a) (b)

Figure 20: SEM images of fracture surfaces tested under tensile load.

3.3.6. Void fraction

Figure 21 shows the micro-CT scan results of the printed specimen. Figure 21(a), (c), and (e) show the sectional planes on the printed specimen, while Figure 21(b), (d), and (f) show the corresponding sectional views indicating the void size and shapes based on the color scale bar. The voxel size (minimum resolution to detect void) for the scan was 1.8×10^{-6} mm^3. The majority

of voids, over 98%, were smaller than 1.8 $\times 10^{-4}$ mm^3. Similarly, as depicted in Figure 21(b), numerous small micro-voids were present within the specimen. Careful observation reveals that these micro-voids are primarily located within the fiber tows. Hence, it is likely that these micro-voids were created during the impregnation of resin through the individual fiber filaments.

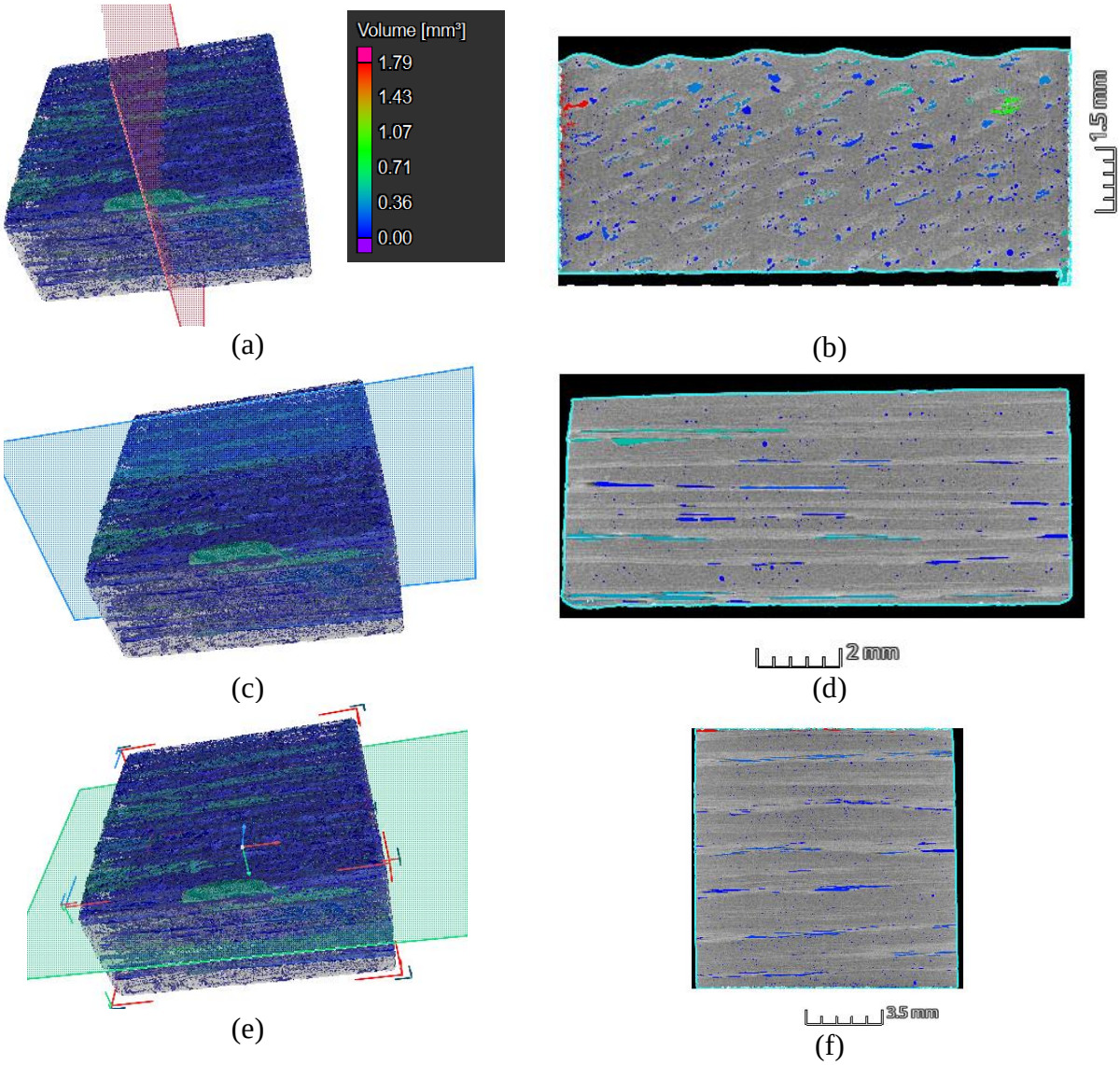

Figure 21: Micro-CT scan of printed composite specimen to measure void content, (a, c, e) section plane (b, d, f) sectional view.

Moreover, no significant voids were observed between adjacent print lines or between consecutive layers. Analysis indicated that the overall void content of the printed specimen was 5.5%. The high void content may have primarily resulted from the significant shrinkage of the

termoset resin during the thermal curing process [64]. However, this resin shrinkage did not affect the dimensional accuracy of the CCFR composites. Therefore, the thermoset resin shrinkage during thermal curing only contributed to the generation of a higher void content. Similarly, relatively high void content (7-11%) was also reported by Blok et al. [50] for the commercially available MarkForged printed CCFR thermoplastic specimens. Furthermore, measuring the fracture toughness of the printed specimens would be helpful in quantifying the effect of these voids on crack propagation. This could represent a highly promising area for future research.

3.3.7. Interlaminar shear strength

One of the most critical aspects to characterize in 3D printing technology is the bonding strength between layers and the interface between fiber and matrix. Interlaminar shear testing is a commonly used method to estimate these bonding and interface strengths [55]. The average short beam shear (SBS) strength was found to be 38 MPa, with a standard deviation of 1.7 MPa between specimens. Figure 22 illustrates the representative curve obtained from the SBS testing. It can be observed from Figure 22 that the maximum SBS strength is achieved at a flexure displacement of only 1.8 mm. This indicates that the printed specimens exhibited a higher degree of stiffness when subjected to shear loading.

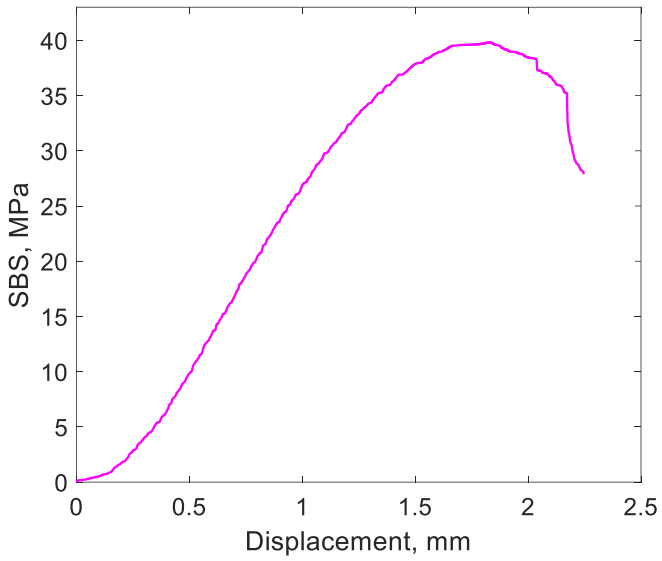

Figure 22: Representative graph of short beam shear (SBS) test for 3D printed composites.

The SBS strength for continuous carbon fiber reinforced 3D printed thermoplastic (nylon) composites was reported by Caminero [9], with a recorded strength of 31.9 MPa. Therefore, current thermoset matrix reinforced continuous carbon fiber 3D printed composites exhibited 18.8% higher SBS strength compared to their thermoplastic counterparts. Furthermore, conventionally manufactured carbon fiber-epoxy composites have SBS strength of around 70-80 MPa for a fiber volume fraction of around 58% [69]. It is generally observed that SBS strength increases with increasing fiber volume fraction [70]. Considering the volume fraction of currently 3D printed composites (18%), these show an SBS strength comparable with conventionally manufactured composites. The major failure mode of the SBS test specimens is under flexure mode. Specimens mostly fail due to compression at the top surface, but also minor damage was observed at the bottom surface due to tension.

3.4. Custom Shapes 3D Printing

Figure 23 shows the 3D printing of different shapes using the discussed 3D printed process of CCFR thermoset composites. Figure 23 shows the 3D printed square, circular, triangular, and

hexagonal shapes. The shapes had 15 layers with each layer having a height of 0.4 mm. The height of the printed shapes was 6 mm. Figure 23 (a) shows the square shape and expected/programmed edge length of the square shape was 60 mm. Actual edge length was measured using ImageJ software. A virtual scale was defined in ImageJ software based on pixel numbers. The measured actual average edge length of the square shape is 59.8 mm. The expected diameter of the printed circular shape depicted in Figure 23 (b) was 120 mm, and the actual measured diameter using ImageJ software was 116.8 mm. Figure 23 (c) exhibited the printed triangular shape. The expected base length of the triangular shape is 120 mm with having expected angles of 45˚, 45˚, and 90˚. The measured actual base length of the triangular shape using ImageJ software is 118.5 mm, having measured angle of 45 ± 0.5˚ with the base. Figure 23 (d) shows the printed hexagonal shape. Each side of the hexagonal shape would have an expected length of 60 mm, and the expected angles of the hexagon were 45˚ with the ground (X-axis). Measured actual edge length of the hexagonal shape ImageJ software was within 60 ± 1.5 mm, having an angle of 45 ± 0.5˚ with positive X-axis.

Figure 24(a) shows the position of the four-laser beam array focused at the four sides of the print nozzle. Laser beams were focused 10 mm away from the print nozzle. These focused laser beams formed a square around the nozzle tip.

Figure 24(b) shows the programmed printing path for the square shape. As the laser beam is placed 10 mm away from the printing nozzle, a section of print remained uncured just adjacent to the print nozzle. Hence, at each corner, the print nozzle moved just past the edge of the object and then back to the original edge. The overshoot of the nozzle at each edge of the square shape is shown in Figure 24(b).

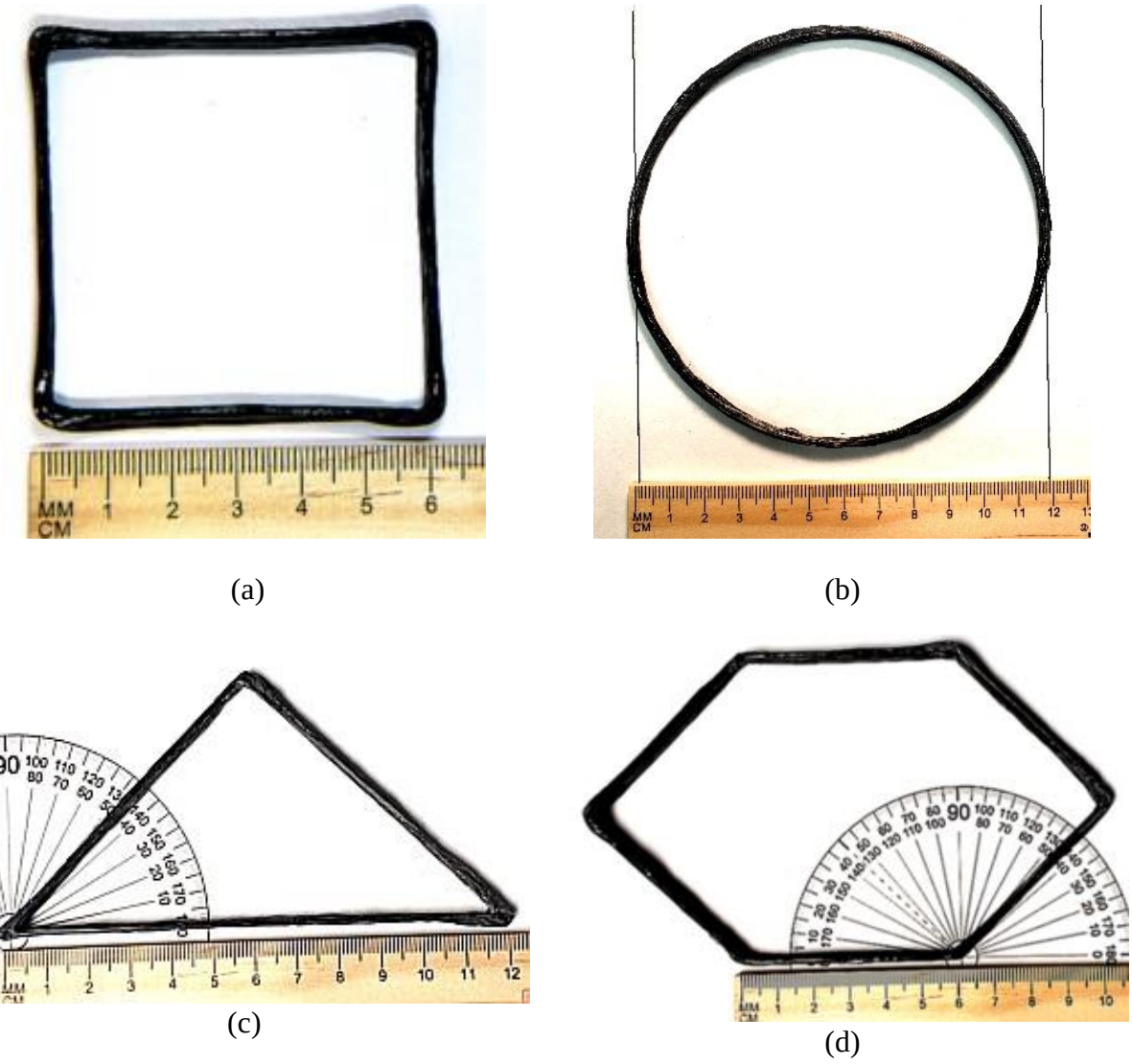

Figure 23: Custom shapes manufacturing using light-assisted 3D printing of continuous carbon fiber with thermoset resin (a) rectangular shape, (b) circular shape, (c) triangular shapes, (d) hexagon shape.

As shown in Figure 24(b), the programmed printing path was 1→2→3→4→5→6→7→8→1. The amount of overshot of the nozzle at each corner was equal to the distance between the print nozzle and the laser. A similar overshot was used while printing each shape.

Figure 24 (c) shows the programmed printing path for the triangular shape with the overshoot of the print nizzle at each corner. The angles of the printed triangle were 45˚, 45˚, and

90˚. The printing path was 1→2→3→4→5→6→1. The amount of overshoot on the angular edge (distance between point 2→3, and point 4→5) was 14.14 mm, which was equal to diagonal distance between the nozzle tip and the laser irradiation. However, the overshot on the linear edge (distance between point 6→1 was 10 mm, which was equal to horizontal/vertical distance from the nozzle tip to the laser irradiation.

Figure 24(d) exhibits the programmed printing path for the hexagonal shape. The overshoot occurred at each corner of the hexagon. The printing path was 1→2→3→4→5→6→7 →8 →9→10→11→12→1. Just as with the triangular shape, the overshoot on the angular edge was kept 14.14 mm (distance between points 4→5, 6→7, 10→11, and 12→1), while the overshoot on linear edge was kept 10 mm. (distance between points 2→3, 8→9).

Such overshot was not possible for the circular shape. However, the printed circular shape was able to maintain its shape with dimensional accuracy. The circular shape was programed for a 120 mm diameter, and the printed circular shape was able to retain the same dimensions (120 mm) as shown in Figure 23 (b).

From the printed shapes in Figure 23, it is observable that corners are not perfect in terms of accuracy, as the fiber became a little misplaced or bent along the corners or turning points. This is because focusing the laser at 10 mm away from the nozzle tip was not perfect, since the focusing was manual. Moreover, the laser beam lines are defocused (spread over an area). Having a thin laser line beam with sufficient energy that could focus on an exact location would create an object with higher accuracy at its corners.

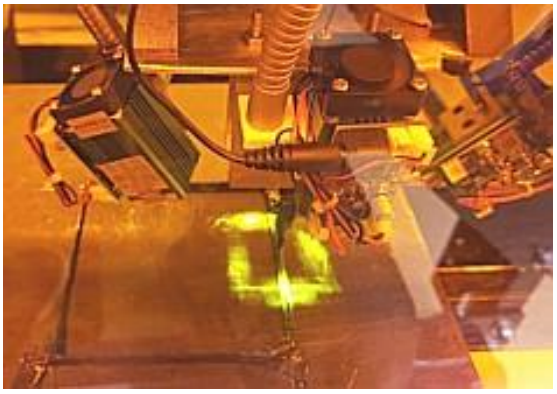

(a)

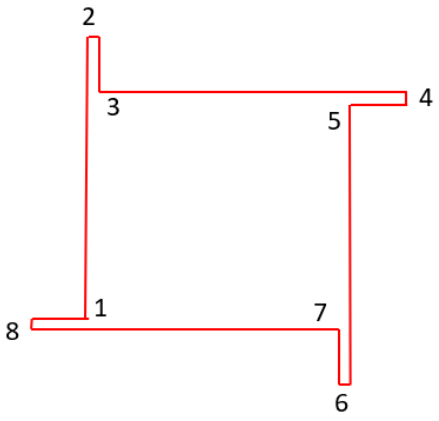

(b)

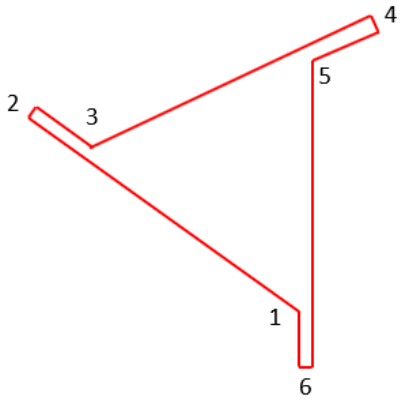

(c)

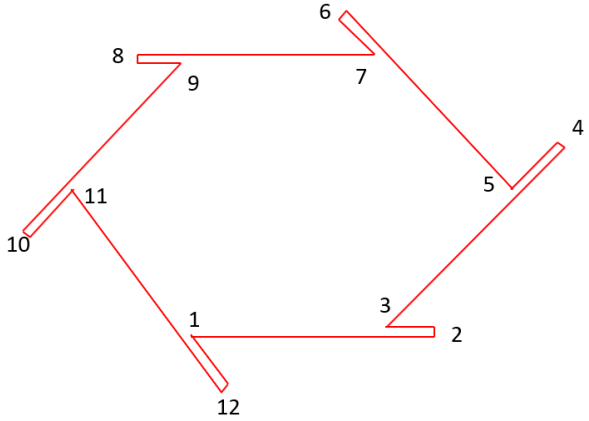

(d)

Figure 24: (a) Light- laser arrangement for printing irregular shapes, (b) programmed printing path for square shape, (c) programed printing path for triangular shape, (d) programmed printing path for hexagonal shape.

Figure 25 (a) shows the demonstration of a grid structure 3D printed using the discussed 3D printing process. Figure 25 (b) shows the exaggerated side view at each corner of the printed grid. The overhanging capabilities of the continuous fiber during this printing process is also noticeable from this exaggerated view of the printed grid. The programmed/expected length of the side for each square box in the grid was 22 mm. The actual length of the side of each square box was measured using ImageJ software. Measurement was taken on 5 × 5 square boxes (total 60 measurements). The average of the actual side length is 21.2 mm, with a standard deviation of 0.5 mm. The thickness of the overall grid structure was 5 mm.

(a) (b)

Figure 25: 3D printed grid pattern using continuous carbon fiber and thermoset resin (a) grid structure (b) enlarged side view.

Figure 26 (a-d) shows the schematic of actual printing paths for the grid structure, and Figure 26 (e) shows the schematic of printed structure. After printing each path, the print nozzle moved up by a single layer height. Together with four printing paths (a-d), it completed one single cycle of printing the grid structure. The demonstrated grid structure was created by completing three printing cycles. As discussed in the previous paragraph, the overshot in nozzle movement was required at each corner for printing the grid structure, in order to compensate for the effect of distance between the print nozzle and the laser line.

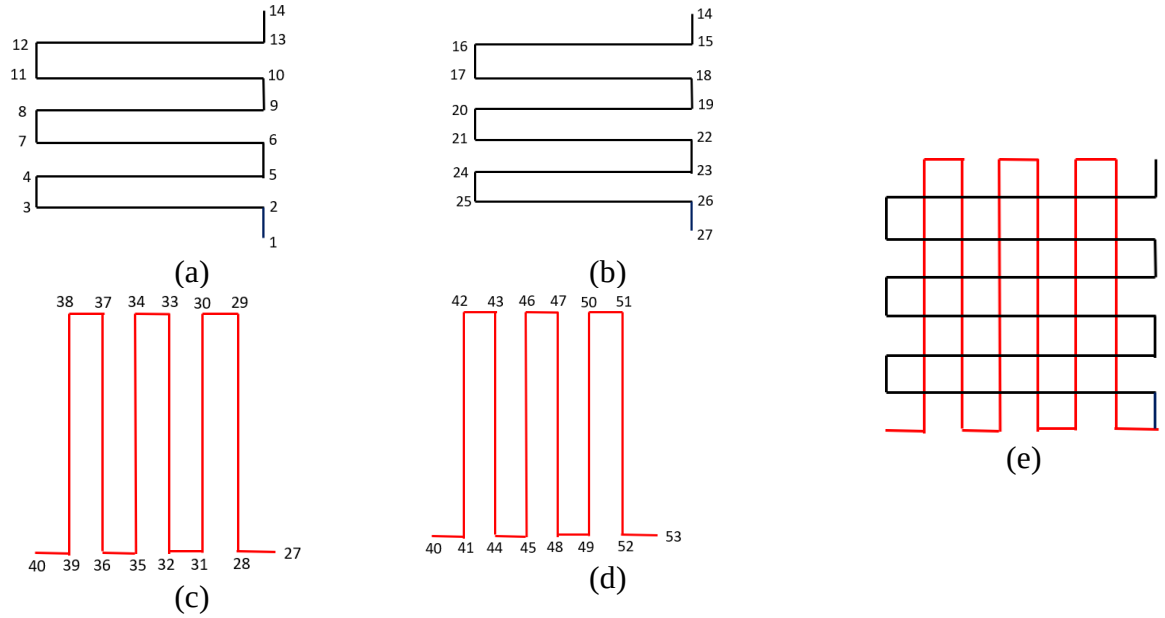

Figure 26: Schematic of printing path for grid structure. (a-d) actual printing path for one complete cycle, (e) printed structure after one cycle.

3.5. Conclusion

This study successfully demonstrated the 3D printing of CCFR thermoset composites, which have higher mechanical properties, using acrylate-based light-curable commercial SLA resin. The light assisted printing process has the ability to print with a very low viscosity resin, which eliminated the problem of clogging resin within the dispensing nozzle. The fiber volume fraction of the printed specimens was around 18%. 3D printed composites exhibited excellent mechanical properties, which were comparable with conventionally manufactured composites. Moreover, the difference between the theoretical and experimental tensile strength and modulus was 18.5% and 7%, respectively. Good wet-out of individual fiber filament with the matrix during the printing process was confirmed from SEM analysis. SEM analysis of fracture surfaces also revealed the slow propagation of failure within the matrix. The void content of the printed specimen was around 5.5%, however most of them were micro-voids, which was confirmed from micro-CT analysis. In addition, short beam shear testing revealed that the printed specimens had 18.8% higher interlaminar shear strength than CCFR thermoplastic composites. Moreover, this article also showed the 3D printing of different custom shapes and a truss structure using the demonstrated printing process. The demonstrated overhanging capabilities of the printed fiber strand will create an opportunity to print complex 3D structures using the reported printing process.

CHAPTER 4: EFFECT OF RHEOLOGICAL MODIFIER ON THE MECHANICAL PROPERTIES OF CONTINUOUS CARBON FIBER REINFORCED COMPOSITES 3D PRINTED WITH LIGHT CURABLE THERMOSET RESIN

4.1. Introduction

Additive Manufacturing, known as 3D printing, has received extensive attention as a new forming technology. Polymeric materials for 3D printing are classified into two types: Thermoplastic and Thermoset. 3D printing with thermoset polymer shows promise by addressing some of the limitations that exist with widely used thermoplastic feedstock materials. 3D printed thermoset composites offer excellent layer-to-layer bonding, high thermal and chemical stability, lower energy consumption, less void content, good surface finish, etc. [24]. However, rather than quickly cooling like thermoplastic, 3D printing of thermoset resin relies on the crosslinking reaction of the resin to solidify. 3D printing of thermoset polymer is performed via material extrusion based direct ink write process (DIW) or high-energy light assistance.

The DIW printing process relies on the deposition of continuous polymeric material or fiber filament through a wiping mechanism. Printability through the DIW printing process primarily depends on the proper rheological properties of the printing ink [71]. Proper rheological properties help the thermoset resin maintain its shape on the print bed before crosslinking occurs. The ideal DIW printing ink should have certain characteristics, such as being easy to extrude under low pressure and maintaining its shape under shear thinning. Therefore, the DIW printing ink should have proper viscosity and high elastic modulus to prevent collapse during and after printing [72].

Efforts to scale up the DIW printing process are hindered by the issue of structural stability due to the self-weight of the matrix material [73, 74]. Light- assisted DIW printing processes have

made it feasible to print large components using thermoset resin. In the light-assisted DIW printing process, violet light instantly cures the thermoset resin partially to assist with shape retention during printing [75]. The boundary of rheological properties of the resin becomes more flexible due to the incorporation of violet light as an additional curing mechanism with the DIW printing system. Mantelli et al.[76] demonstrated light-assisted DIW 3D printing of recycled carbon fiber using a dual (photo and thermal) cure thermoset resin. Because of the opacity of carbon fiber, thermoset resin loaded with carbon fiber shows low reactivity upon the irradiation of high-energy light laser. Hence, a rheology modifier was added to the thermoset resin to ensure sufficient shape retention, not only through light curing but also through rheological modification of the ink formulation.

The rheological properties of a thermoset resin can be modified by mixing filler material with the resin. Romberg et al. [73] demonstrated the effect of adding filler material on the collapse height of 3D printed thermoset structures. Gonzalez et al. [74] reported light-assisted DIW printing of complex shapes using epoxy resin modified rheologically (by mixing nano-clay).

Nano-clays have shown immense potential as filler materials to enhance the strength, stiffness, and toughness properties of polymer resin. In 3D print with thermoset resin, nano-clays are widely used as filler materials to increase the viscosity of the resin. Because of the high surface area of nano-clay, viscosity of thermoset resin leads to a large increase when mixed with nano-clay [77]. The effect of nano-clay on the rheological properties and printing behavior of thermoset resin was investigated by Hmeidat et al. [46]. Printability with direct ink write (DIW) printing process largely depends on the rheological properties of the printing ink [78].

However, 3D printing of structural members using thermoset resin is still very limited due to their limited mechanical performance [79]. To overcome the barrier of low mechanical strength,

continuous carbon fiber-reinforced (CCFR) 3D printing of thermoset composites has shown unpreceded promise [10, 19]. Light-assisted DIW is a highly promising printing process for CCFR thermoset composites [16, 17]. Increasing the feasibility of printing complex shapes using thermoset resin often requires modifying the resin's rheology by adding a rheology modifier, such as clay or SiC [47].

However, the influence of a rheology modifier in thermoset resin material on the mechanical properties of CCFR composites has not been well-established in the literature. The primary aim of this current study is to investigate the impact of filler materials on the mechanical and interlaminar strength of CCFR composites 3D printed using a light assisted DIW printing process.

4.2. Materials and Method

To compare the performance of CCFR 3D printed composites with the addition of clay to thermoset resin, two groups of specimens were 3D printed. The first group of carbon fiber reinforced specimens was 3D printed using photocurable thermoset resin mixed with a thermal initiator. However, the second group of fiber-reinforced composites was 3D printed using thermoset resin containing both clay and a thermal initiator. This section will discuss the properties of the materials used for printing and the printing process used in this research.

4.2.1. Materials

4.2.1.1. Fiber (Teijin 3K)

For 3D printing, continuous carbon fiber filament was obtained from Teijin Inc. Each fiber tow contains 3,000 filaments (3 K) with a diameter of 7 μm. The linear density of the fiber was

200 tex. The density of the fiber was 1.77 g/cm^3. The tensile strength and modulus of the fiber are 4100 MPa and 340 GPa, respectively. The elongation of the fiber at break is 1.7 %.

4.2.1.2. Resin

The photocurable thermoset resin Peo-poly Tough was purchased from Matterhackers. This is a commercial resin used for the SLA printing process. This resin cures under 405 nm violet light. The density of the resin is 1.15 g/cm^3.

4.2.1.3. Thermal initiator

To make the photocurable thermoset resin thermally curable as well, 0.5% Luperox P (by mass) was added to the commercially available Peo-poly Tough resin. Luperox P (tert-butyl peroxybenzoate, 98%) was purchased from Sigma Aldrich (Missouri, USA).

4.2.1.4. Clay

Garamite -7305 (Organophilic phyllosilicate) is used as a filler material to modify the rheology of the resin material. It was supplied by BYK USA Inc. (Texas, USA). It has a specific weight of 1.5 – 1.7 g/cm^3. It is used as a thermoset additive, with the recommended level being 0.5 - 5% of the total formulation.

The thermoset resin, thermal initiator, and clay were added together using a speed mixer (FlackTek speed mixer) at 2000 rpm for 5 min. Afterward, the mixed print ink was placed in a vacuum chamber for 30 mins to remove any generated air bubbles.

4.2.2. Printing process

A customized 3D printer was developed to facilitate the printing of CCFR thermoset composites using violet light assisted DIW printing technology. This involved the adaptation of a commercial gantry system capable of movement along the X and Y-axes. The motion of the gantry

was meticulously controlled through the manipulation of motor rotations via the Arduino intergraded development environment (IDE).

The print bed, which consisted of a hot rolled steel plate, was assembled through effective clamping. Figure 14 (a) provides a comprehensive overview of the schematic diagram associated with the printing process, while Figure 14 (b) showcases the experimental set-up meticulously arranged for the printing endeavor. Within this set-up, a distinct custom print nozzle was affixed to the print head.

The Continuous supply of carbon fiber was channeled from the upper part of the nozzle, while the resin was introduced into the print nozzle through the application of a syringe pump. The rate of resin flow was meticulously set at 0.121 mL/min. During this phase, a consistent infusion of resin into the continuous carbon fiber transpired the print nozzle.

Two distinct violet light lasers (with a power output of 0.8 W and a wavelength of 405 nm) were aligned to form lines at both the front and rear facets of the print nozzle. The laser beams were concentrated on the print bed at a specific distance (approximately 20 mm) from the tip of the nozzle. Due to the motion of the print head, the continuous fiber was drawn out from the nozzle.

Upon the placement of resin impregnated fiber onto the print bed, the laser beams were employed to solidify resin on the print bed. The pace of the printing operation was set to 120 mm/min. The gap between two adjacent fiber tows (hatch spacing) was upheld 1mm. During printing, the print nozzle was consistently maintained at a distance of 0.8 mm above from the print bed or the previously printed layer. After printing, printed specimen was thermally post cured within a convection oven at a temperature 180˚C for 8 h.

4.3. Mechanical Characterization

4.3.1. Rheological characterization

To quantify the increase in rheological properties of photocurable Peo-poly resin due to addition of clay, viscosity of the resins was measured using rotational type ARES G2 rheometer (Manufacturer: TA Instruments, New Castle, DE). A 25-mm diameter parallel plates (made of stainless steel) configuration with 0.5 mm gap in-between was used to compare the change in viscosity due to the addition of 2% clay with Peo-Poly resin. All rheological properties, i.e., viscosity, are compared at room temperature (25˚C).

Figure 27 compares the effects of clay addition on the rheological properties of Peo-poly Tough thermoset resin at various shear rates. In Figure 27 (a), the viscosity of Peo-poly Tough resin is depicted, while Figure 27 (b) illustrates the viscosity of Peo-poly Tough resin with 2% clay added. Peo-ploy Tough resin exhibits a rheological behavior similar to that of a Newtonian fluid, where viscosity remains constant regardless of shear rate. However, the introduction of 2% clay into the thermoset resin introduces shear-thinning behavior to the Peo-poly Tough resin. This is evident from the decrease in viscosity of Peo-poly Tough resin with 2% clay as the shear rate increases. Such shear-thinning behavior is a desirable characteristic for print ink used in the DIW printing process.

Figure 27 (c) represents the storage and loss modulus of the Peo-poly Tough resin, while Figure 27 (d) represents the storage and loss modulus for Peo-poly Tough resin with 2% clay added into it. In the case of Peo-poly Tough resin, loss modulus showed higher value compared to storage modulus at each shear rate. Higher loss modulus compared to storage modulus represents lack of shape retaining capability after being 3D printed. The shape retaining capability increases as the differences between loss and storage modulus decreases. Consequently, self-sustaining print ink

showed higher storage modulus than the loss modulus. On the other hand, in the case of Peo-poly tough resin with 2% clay added into it, the difference between the value of storage and loss modulus decreases significantly. This represents that the shape retaining capability after being 3D printed increases due to the addition of clay for Peo-poly Tough resin.

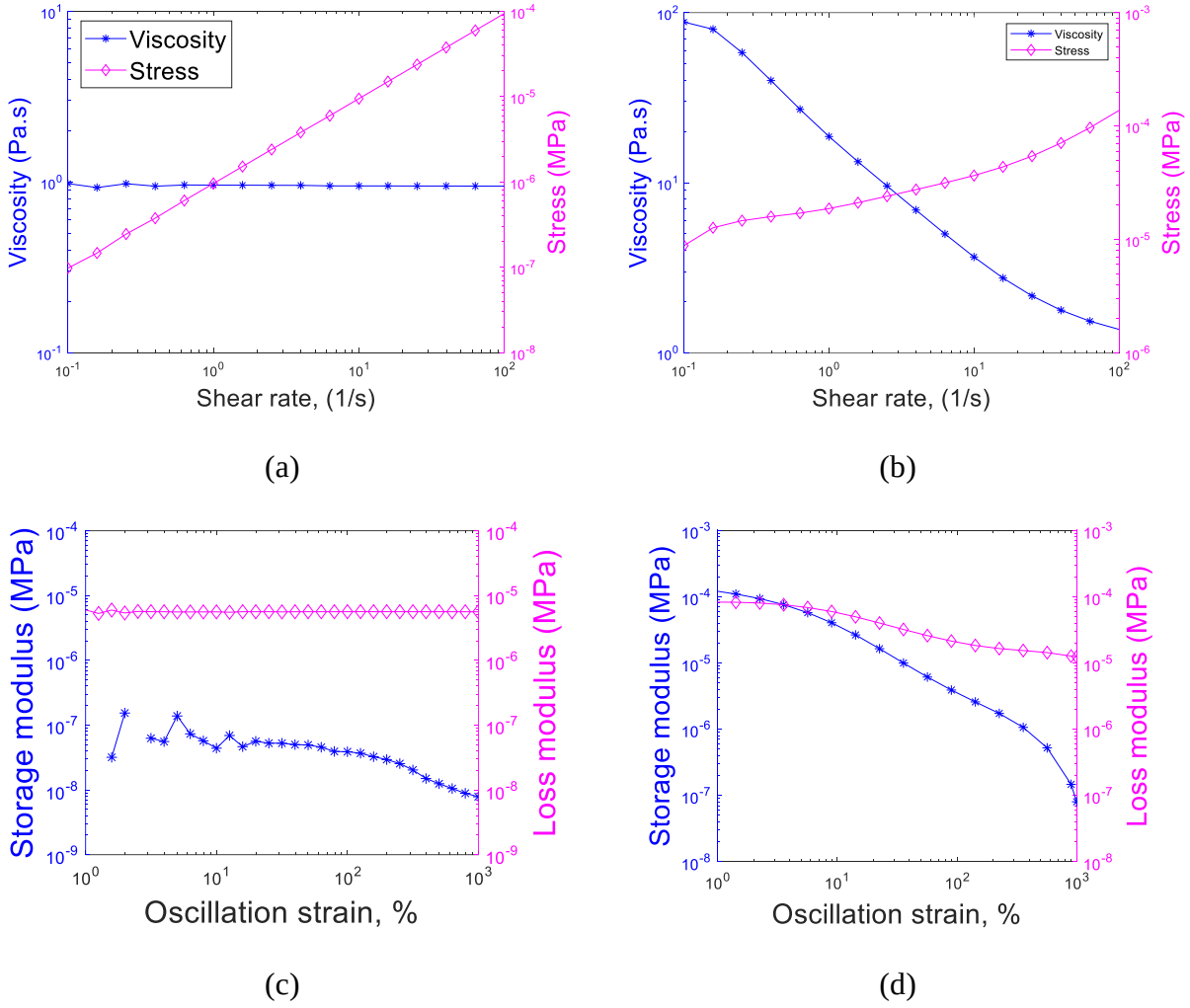

Figure 27: Comparison of rheological properties of thermoset resin with and without clay addition.

4.3.2. Volume fraction

The volume fraction of CCFR composites 3D printed using Peo-poly Tough resin, with and without clay addition, was quantified by performing burn-off of the matrix material in a nitrogen-purging high-temperature furnace. This burn-off test was conducted by following the

standard process discussed in ASTM D 3171. 3D printed specimens were heated at 565˚C for 5 h to remove all matrix materials. Thus, the mass of carbon fiber and matrix materials was separately measured to calculate the volume fraction. Five specimens were tested under burn-off for each case. The average volume fraction of the 3D printed specimens with 2% clay added to the composite is 18.9 ± 0.3%, and the average volume fraction for the specimens with no clay addition is 18.3 ± 0.4%. Therefore, the volume fractions of the specimen's 3D printed with and without clay addition are comparable to each other.

4.3.3. Void analysis

To compare the void content of the printed specimens with and without clay addition, CT scans of the specimens were performed using a Phoenix X-ray scanner (Wunstorf, Germany) with a voltage of 80 kV. Void volume analysis showed that the printed specimen without clay addition exhibits a void volume of 5.49%, while the specimen with clay mixed into the matrix material showed a void volume of 5.99%. The void contents for the specimens with and without clay addition are comparable to each other.

4.3.4. Tensile testing

To compare the effect of the addition of clay on the tensile properties of CCFR thermoset composites, CCFR specimens were 3D printed using thermoset resin with and without clay addition. Two sets of specimens, with and without clay addition, were tested under tensile load using 30kN Instron load frame by following ASTM D 3039. Five specimens were tested from each set. The test rate was 1mm/min. Figure 28 compares the effect of clay addition on the tensile strength of the 3D printed CCFR thermoset composites. The average tensile strength for the specimens with no clay content is 380.58 MPa, and the corresponding standard deviation for

tensile strength is 27 MPa. However, the tensile strength for the CCFR thermoset specimens having 2% clay content is 367.86 MPa, with a standard deviation in tensile strength of 40.29 MPa.

Moreover, Figure 29 illustrates the comparison of the tensile modulus of CCFR composites 3D printed using thermoset resin mixed with clay and those without clay addition. The average tensile modulus for the specimens with no clay content is 41.91 GPa, with a standard deviation in tensile modulus of 3.26 GPa. The tensile modulus for the specimens with 2% clay content is 37.93 GPa, accompanied by a standard deviation in modulus of 2.75 GPa. Consequently, both the tensile strength and tensile modulus of CCFR composites exhibited slight decreases with the addition of clay to the thermoset resin.

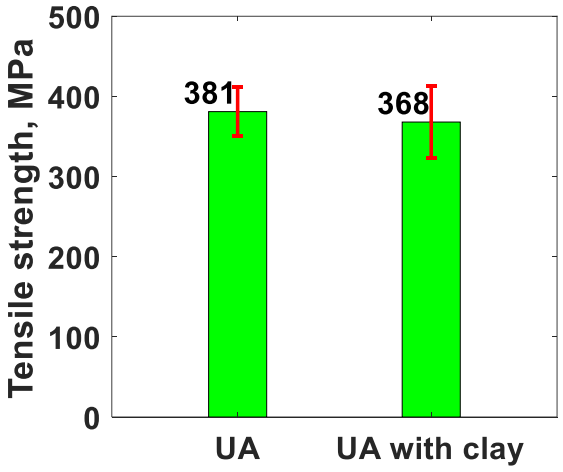

Figure 28: Tensile strength comparison of CCFR thermoset composites with (2%) clay vs. without clay.

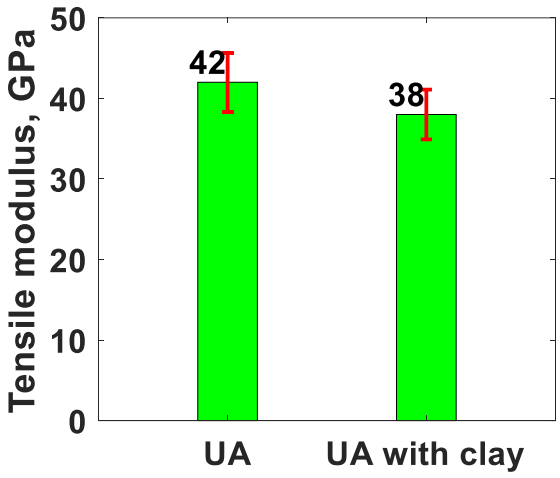

Figure 29: Tensile modulus comparison of CCFR thermoset composites with (2%) clay vs. without clay.

4.3.5. Short beam shear test

To examine the effect of clay addition on short beam shear (SBS) strength, two groups of CCFR thermoset specimens with seven-layers were 3D printed. One group was 3D printed by adding 2% clay to the liquid resin, while another group was 3D printed without the addition of clay. Each group consisted of five specimens. SBS strength was measured by applying a 3- point bending stress to the specimen following the ASTM 2344 standard. SBS strength represents the interlaminar shear strength (ILSS) of the printed specimens.

According to ASTM 2344, the recommended length for the specimen is six times the thickness, and the recommended width is two times the thickness. The thickness of the printed specimens was 5.1 mm. Test specimens were cut to the recommended length and width as per the standard. The loading span during the test was four times the thickness, and the test rate was 1 mm/min. SBS strength was calculated using Equation (11).

$$S = 0.75 \times \frac{F_m}{b \times h} \tag{11}$$

Where, S represents the SBS strength, F_m denotes the magnitude of the maximum load recorded during bending test, b is the width of the specimen, and h is the height of the specimen. Figure 30 illustrates the comparison of the influence of clay addition on the SBS strength of CCFR specimen's 3D printed with thermoset resin.

The average SBS for specimens with no clay addition is 37.9 MPa, and the corresponding standard deviation between specimens is 1.6 MPa. However, for the specimen with 2% clay addition, the average SBS is 41.7 MPa, with a corresponding standard deviation of 1.4 MPa. Therefore, due to the addition of 2% clay to the thermoset resin, the SBS strength increased by 9.9%. Moreover, in traditional manufacturing processes, an increase in the interlaminar fracture toughness due to the addition of clay to the matrix material was reported in the literature by Xu [80]. The presence of inorganic filler material in the matrix material enhances the interfacial bonding between the fibers and the matrix [81].

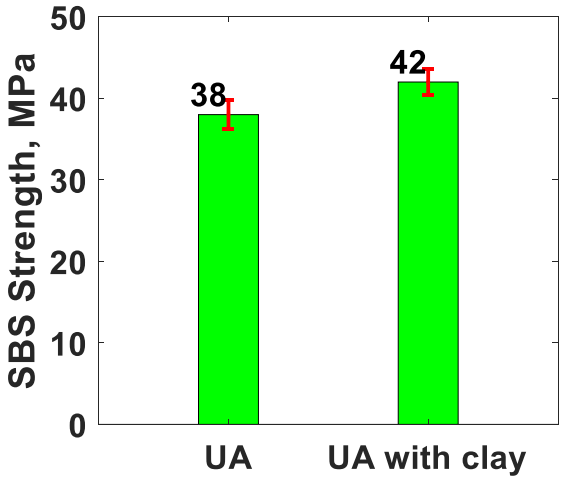

Figure 30: Comparison of SBS strength in CCFR thermoset composites with and without 2% clay addition.

4.4. Statistical Analysis

Statistical two-sample t-test [82] for equal variance were performed to determine whether the means of tensile strength, tensile modulus, and SBS strength differ significantly due to the

addition of clay. In the cases of tensile strength, tensile modulus, and SBS strength, the variance was comparable between the specimen groups with and without clay addition. The Null hypothesis assumes that the compared groups have equal means, while the Alternative hypothesis assumes that means are different from each other at given significance level.

The two-sample t- test was performed using the Statistical and Machine Learning Toolbox of MATLAB. The built-in function 'ttest2' was used to compare the means between two groups of specimens. The function 'ttest2' returns '0' if the means between groups are not significantly different (Null hypothesis accepted) and '1' otherwise (Alternative hypothesis accepted). The two-sample t-test revealed that the mean tensile strength between specimen sets with and without clay addition is not significantly different from each other at a 5% significance level. Similarly, the t-test showed that the mean tensile modulus also does not differ significantly because of the addition of clay during the 3D printing process, at a similar level of significance. However, at a 5% significance level, the means of SBS strength are significantly different between the groups of specimens printed with and without clay addition.

4.5. Conclusion

In this study, the effect of filler material on the strength of 3D printed CCFR composites was investigated. This study demonstrated an increase in the rheology of print ink due to the incorporation of filler materials. Moreover, print ink starts exhibiting shear thinning behaviors because of the addition of filler materials. Printed composites with and without clay addition exhibited almost equal volume fractions and void content. However, 3D printing with higher viscosity resin demonstrated better print surface quality and smoother performance during the 180˚ turning of the fibers. Due to the addition of filler material (2%), decreases in tensile strength and modulus were statistically insignificant, however short beam shear strength, or interlaminar shear

strength, increased significantly. A light-assisted printing process with relatively higher viscosity resin might require less laser power, as the resin will have a higher elastic modulus. The knowledge obtained from this study will be helpful in designing an optimum viscosity range of thermoset resin for light-assisted printing processes.

CHAPTER 5: LIGHT-ASSISTED 3D PRINTING OF CONTINUOUS CARBON FIBER REINFORCED COMPOSITES WITH ACRYLATED EPOXY RESIN

5.1. Introduction

Fiber reinforced polymer composites (FRPC) offer significant advantages in various industries due to their high specific strength, toughness, light-weight nature, and design flexibility. There are two main types of FRPC: thermoplastic-based and thermosets-based. As manufacturing transitions from manual to automated processes like automatic fiber placement (AFP) and automatic tape-laying (ATL), high cost and limited design freedom become challenges. 3D printing has emerged as a revolutionary solution to overcome these limitations.

Fiber reinforced thermoplastic composites have been successfully 3D printed using two methods: melting the fiber loaded thermoplastic filament [52, 83] or impregnating continuous fibers with molten thermoplastic filaments [8, 28, 84]. The melting of thermoplastic filament can be achieved by utilizing a heater at the print nozzle or by generating high temperatures through high energy laser irradiation [85]. The resulting molten fiber-loaded resins are then deposited on the print bed, following a similar process to FDM. However, 3D printing of continuous carbon fiber reinforced (CCFR) thermoplastic composites presents challenges, such as substantial air void formation, high resin viscosity, low volume fraction, and inadequate impregnation of the filament [61].

In contrast, thermoset resins offer benefits such as low viscosity and good wettability of fibers. Moreover, composites with a thermoset matrix exhibit higher mechanical strength, thermal stability, and chemical resistance. As a result, there is a significant demand for thermoset-based composite due to their exceptional thermal stability and corrosion resistance, with the global demand projected to reach to $31.7 billion by 2026 [75].

Stereolithography (SLA) is the most popular photocuring based thermoset 3D printing technology, attracting significant attention from industries due to its fast UV laser curing within seconds and operation at room temperature. SLA utilizes a layer-by-layer photo polymerization process, offering high precision printing. The commonly used thermoset resins for SLA printing are acrylates and urethanes.

In photo-curing based 3D printing, the resin primarily comprises photo-initiators and monomers. When high-energy light irradiates the resin, the photo-initiator is activated and initiates linear and cross-link polymerization of the resin by reacting with the monomers [86]. This technology is relevant due to its high printing speed and precision. However, the application of photo-curing based 3D printing is limited by the performance of photocurable thermoset polymers [87].

To enhance the mechanical performance of photo-curable thermosets, the researchers have widely employed the reinforcement of thermoset resin is with short fibers [4-6]. Nawafleh et al. [3] reported on 3D printing using a direct ink write (DIW) based process with short carbon fiber reinforced epoxy resin. However, this process faces challenges, such as nozzle clogging due to the high resin viscosity. To address this issue, Nawafleh et al. [3] attached a vibration shaker to the nozzle and extruder to reduce clogging during printing. Moreover, DIW based printing has limitations in creating tall structures. As successive layers of ink are printed, the lower layers become unable to withstand the weight of the material above, leading to structural instability [73].

However, light- assisted 3D printing is less likely to encounter issues in printing tall structures due to its ability to instantly cure the resin while printing. Invernizzi et al. [88] successfully demonstrated UV-light assisted 3D printing of complex structures using short fiber reinforcement (Glass and carbon fiber). Printing ink was formulated by mixing acrylate-based

photo curable resin with thermally curable resin. They used dual curing mechanisms for their resin system: photo-curing and thermal curing. Dual curing system ensures complete crosslinking within the thermoset resin to impart better mechanical performances. However, the reported tensile strength of the printed specimen was less than 50 MPa. Hence, Continuous fiber reinforcement is an ultimate solution to increase the strength of fiber reinforced thermoset composites.

3D printing of thermoset resin with continuous fiber reinforcement was found more challenging in terms of controlling printing process, however they exhibit superior mechanical strength due to their better stress-transfer capability between fiber and matrix. Acrylate resin based light-curable resin was adopted for 3D printing of continuous fiber reinforced composites by Abdullah at el [16]. Effect of ink viscosities, nozzle size, print speed on volume fraction of printed filament was investigated. However, the attained maximum tensile stress was limited to 100 MPa.

CCFR phenolic (thermoset) resin-based composites was successfully 3D printed by using high temperature thermic lance (220˚C - 300˚C) acting on the carbon fiber prepreg [14]. Pre-impregnated fiber was heated sufficiently using thermic lance to cure instantly during the printing process. However, the demonstrated process was suffering from dimensional inaccuracy at right angle turning.

Direct ink writing (DIW) based 3D printing of continuous carbon fiber reinforced epoxy composites was first demonstrated by Hao et al. [10]. Later on, Ming et al. [11] investigated the influence of different process parameter on the 3D printing of continuous carbon fiber reinforced thermoset (epoxy) composites. The epoxy resin used in this study was solid at room temperature, was heated on extruder (like FDM) before being 3D printed. In addition, 3D printing of continuous carbon fiber reinforced epoxy composites was demonstrated by Wang et al. [58]. They successfully 3D printed a triangular corrugated structure using FDM approach. However, the

epoxy resin used over this study was solid at room temperature (Softening temperature = 75˚C). As like FDM, resin was heated at print nozzle up-to around 100˚C to yield a low-viscosity ink to 3D print. 3D printing of continuous carbon fiber reinforced composites using solid epoxy was also exhibited on several other research article [60-62]. Moreover, thermally initiated frontal curing propagation based 3D printing of CCFR epoxy based thermoset composites was reported by Zhang et al. [19]. Furthermore, He et al. [15] developed a printer head to induce shear stress on fiber using viscous print ink to assist fiber extrusion while printing CCFR thermoset composites. Reported 3D printing of CCFR composites with epoxy resin were used solid epoxy and was being melted with a heater while printing. 3D printing of continuous carbon fiber reinforced liquid epoxy composites was demonstrated by Shi et al. [56]. They used thermal gradient to enable curing of resin during the printing process.

In light-assisted 3D printing, acrylated epoxy resin is utilized as print-ink instead of pure epoxy resin. Pure epoxy resin is not possible to use with light-based printing technologies because of the lack of photo-curable groups in epoxy resin. The acrylated epoxy resin is a blend of epoxy and acrylate monomers. The epoxy-acrylate is a dual cure resin, exhibits both photo and thermal curing [89]. The acrylate portions of the resin exhibit photo-curable properties in the presence of an appropriate photo initiator. On the other hand, the epoxy portion of the resin can undergo complete cross-linking upon thermal curing and contributes to bring unique mechanical properties [90].

CCFR composites 3D printed using liquid acrylated epoxy resin are rare in literature. Based on the author's knowledge, this article is first time demonstrating light-assisted 3D printing of CCFR composites with acrylated epoxy resin, which are liquid at room temperature. Liquid phase of acrylated epoxy resin provides better impregnation of resin within the fiber and ensures less

possibility of nozzle clogging while printing. Moreover, this study mechanically characterizes the CCFR composites 3D printed with acrylated epoxy resin and proposed an algorithm to 3D print scalable truss structures.

5.2. Materials

Teijin 3K continuous carbon fiber is used as a fiber for 3D printing of continuous carbon fiber reinforced composites over this current study. The density of the fiber was 1.77 g/cm^3. The liquid thermoset resin material used for this 3D printing process was Bisphenol-A acrylated epoxy resin (BAE). The commercial name of this resin is AgiSyn 1010-A60, and the resin was gifted by Convestro LLC (Pittsburgh, PA, USA). This resin contains both epoxy and acrylate functional group. Acrylate group will enable the possibility of making this resin photo-curable with appropriate photo-initiator, and epoxy group bring some unique properties associated with this functional group.

In order to make the resin curable under high energy light, a photo-initiator is mixed with the acrylated epoxy resin. Diphenyl (2,4,6-trimethylbenzoyl) phosphine oxide (97%) is used as a photo-initiator (PI), which is a Type-I PI. 2% photo-initiator (by mass) was mixed with the resin using a speed mixer (FlackTek speed mixer) running at 3000 rpm for 4 minutes. Curing reaction acrylated epoxy and PI is a free-radical photo polymerization process. Upon high energy light irradiation, the photo-initiator generates free-radicals. Those free radicals consecutively attach with polymer monomer to form polymer chain. Thus, polymerization happens. Acrylates portion of the acrylated epoxy resin get partially polymerized upon light irradiation. However, the complete polymerization of acrylates happens upon post-curing by heating [89].

The dual cure resin used in this current study was post-cured by heating to form complete crosslinking of polymer chains. In order to make the resin thermally curable as well, 2% K-PURE

CXC-1612 (by mass) was also mixed with the acrylated epoxy resin as a thermal initiator (TI). This is a cationic thermal initiator. Thermal post-processing crosslinked the epoxide group via cationic polymerization.

5.3. Printing Process

A commercial gantry was modified to make custom 3D printer to print CCFR acrylated epoxy composites. A custom nozzle was designed to feed continuous carbon fiber and resin simultaneously. A syringe pump is used to feed resin at a set flowrate. Carbon fiber and liquid resin get impregnated with each other within the nozzle.

A 300 × 300 mm hot-rolled steel plate was used as a print bed. Mold release agent (Frekote) was pasted on the print bed before starting printing, to ensure easy removal of printed specimen. 405 nm 0.8 W UV lasers were focused on a certain distance of 10 mm from the nozzle tip. Laser beam irradiation was positioned such a that reflection of the laser beam do not fall on the print nozzle tip (Figure). The laser beam was focused as a line of laser beam irradiation. UV laser irradiation is being used to cure the resin dragged with the carbon fiber during the printing process. A print nozzle was used that can bend over the small irregularities to continue printing by overcoming small obstruction.

The post-processing of the printed specimen was performed by heating inside a convection oven for 8 h at 180˚C. This thermal post-curing formed a complete crosslinked structure of the acrylated epoxy resin.

5.4. Mechanical Characterization

5.4.1. Rheology test

Rheological characterization of the print ink was performed using AERS G2 Rheometer. Viscoelastic print ink was loaded between two circular parallel plate fixtures. Parallel plates are

made of steel and have a diameter of 25 mm. The gap between the parallel plates was kept at 0.5 mm. To measure viscosity of the print ink, a flow sweep test was performed for the shear rate from 0.1 to 100 1/s. Before taking the measurements of viscosity, the sample was equilibrated for 2 min. All rheological tests were performed at constant temperature of 25˚C. To measure the storage and loss modulus of the print ink strain sweep test was conducted. Strain was varied from 1% to 1000% at a constant angular frequency of 6.28 rad/s.

5.4.2. Poisson's ratio measurement

In order to measure Poisson's ratio, a video extensometer was used to measure longitudinal and transverse strain of the specimen during the tensile test. CCFR specimen was painted with while paint to get rid of light reflection from the carbon fiber. As shown in the Figure 31, some black dots were inserted on the specimen along the longitudinal and transverse direction. Two virtual extensometers, along longitudinal and transverse direction, were inserted on the specimen and the movement of the dots was tracked using video extensometer to measure strain.

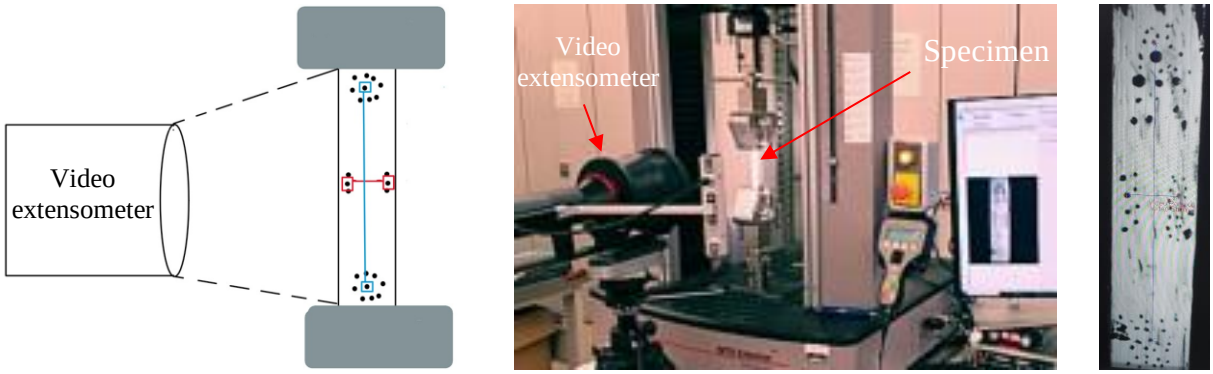

(a) (b) (c)

Figure 31: (a) Schematic of measuring longitudinal and transverse strain using video extensometer, (b) actual experimental set-up, (b) actual painted specimen with black dots to measure longitudinal and transverse strain.

5.5. Results and Discussion

5.5.1. FTIR analysis of the resin

Figure 32 displays the results of FTIR analysis performed on the acrylated epoxy resin. Based on manufacturer data sheet, this resin contains 60% Agisyn 1010 and 40% of TPGDA. The resins exhibited characteristics peaks at a wavenumber of 1723 cm^{-1}, which is indicative of the acrylate group.

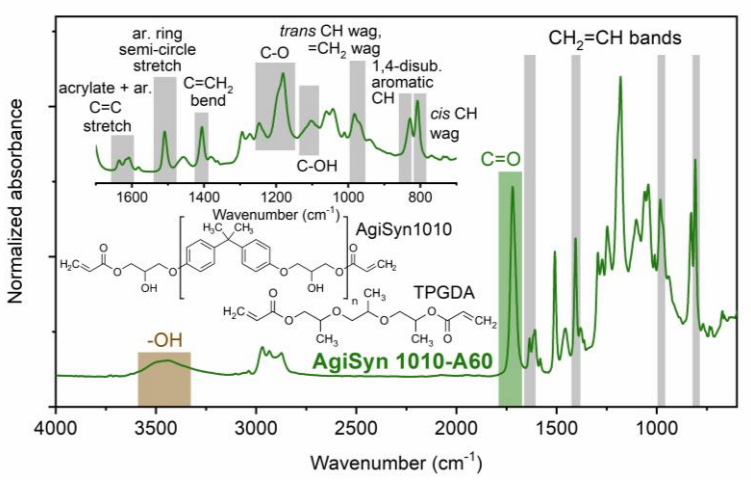

Figure 32: Result of FTIR analysis of acrylated epoxy resin (AgiSyn 1010-A60)

5.5.2. Rheology of resin

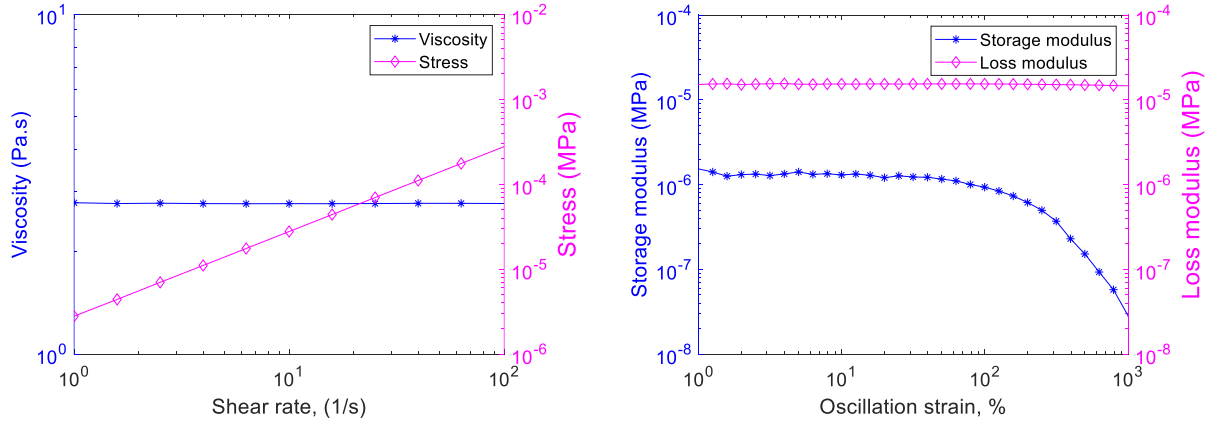

Figure 33: Rheological characterization of print ink (acrylated epoxy resin).

Figure 33 (a) illustrates the rheological characterization of the print ink, which exhibits rheological behavior akin to that of a Newtonian fluid. The viscosity of the print ink remains constant regardless of changes in shear rate, measuring at a steady 2.77 Pa.s. As a result, the behavior of the print ink remains consistent regardless of print speed variations. Additionally, the shear stress of the ink increases linearly with the shear rate, aligning with the Newtonian fluid characteristics. This kind of Newtonian behavior has been previously documented in literature for pure thermoset resins. Furthermore, it is possible to introduce shear thinning behavior into the print ink by incorporating a rheology modifier, such as clay.

Moving to Figure 33(b), we examine the storage and loss modulus of the print ink. The storage modulus reflects the ink's capacity to store elastic energy and resist deformation under applied stress, indicating its ability to maintain its shape. Conversely, the loss modulus gauges the ink's ability to flow. When the storage modulus exceeds the loss modulus, the ink can retain its shape post-printing. Conversely, when the loss modulus surpasses the storage modulus, the ink will naturally flow post-printing. Figure 33(b) demonstrates that the utilized print ink exhibits a higher loss modulus than storage modulus. Consequently, the ink has a limited capability to maintain its shape after 3D printing, tending to flow naturally. However, with the assistance of light during printing, these thermoset inks become printable with CCF reinforcement.

Comparatively, the commercially available Peo-poly tough resin displays a viscosity of 0.94 Pa.s. In contrast, the currently used acrylated epoxy resin displays a significantly higher viscosity, measuring 2.77 Pa.s. This viscosity is over 200% greater than that of the Peo-poly tough resin. Nevertheless, both resins exhibit Newtonian characteristics, maintaining consistent viscosity across different shear rates.

5.5.3. TGA test of resin

TGA tests on the acrylated epoxy matrix material assessed thermal stability using a TGA 550 instrument at a 20˚C/min heating rate and a 60 ml/min purge gas flow rate. The result is shown in Figure 34 .

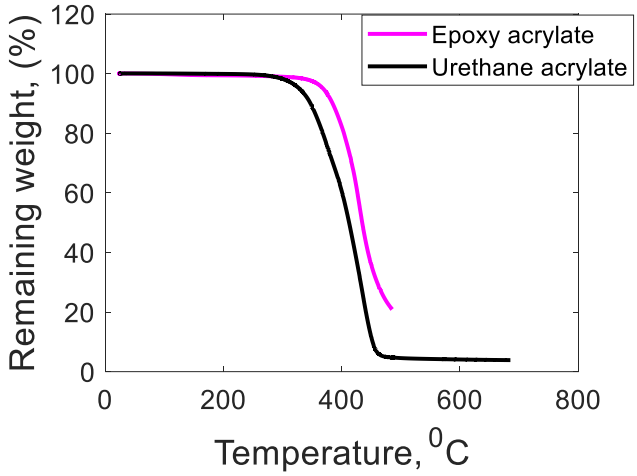

Figure 34: TGA test curve for acrylated epoxy matrix material.

The weight loss attributed to thermal degradation initiates around 350˚C, with a notable weight reduction occurring as the temperature exceeds 400˚C. In contrast, the acrylate-based peo-poly resin displays an onset temperature of approximately 280˚C, maintaining stability until 320˚C. Consequently, the acrylated epoxy based photocurable resin exhibits superior thermal stability in comparison to the acrylate-based Peo-poly resin.

5.5.4. Density measurement

The density of the composite specimen was measured by using Archimedes principle. To measure the density of the specimen, weight of the specimen was measured both in air, and while submerged in water. The density of the specimen (ρ) could be calculated by using the formula shown in following equation:

$$\rho = \frac{A}{A - B} \times \rho_w \tag{12}$$

Where, A is the weight of the specimen in air, B is the weight of the specimen while submerged in water, and ρ_w is the density of the water. Using Archimedes principles, the average measured density of the CCFR 3D printed specimen (ρ_c) was 1.3 g/cm^3. The density of the matrix material was also evaluated using Archimedes principle. The calculated average density of the matrix material was 1.19 g/cm^3.

5.5.5. Volume fraction

The volume fraction of 3D printed carbon fiber reinforced epoxy composites was determined using a burn-off test method. In this test, a specimen was subjected to heating within a nitrogen-purged furnace at 565˚C for a duration of 5 h. This process led to the combustion of the polymer matrix while preserving the integrity of the reinforcing fibers. A total of five specimens were examined to ascertain the fiber volume fraction within the printed composites. The mass of each specimen utilized for the burn-off test averaged around 0.8g.

The calculated average fiber volume fraction for the printed composites was found to be 17.9%, with a corresponding standard deviation of 0.72% among the specimens. Previously, the specimens were 3D printed with same parameter using acrylate based peo-poly resin, and obtained volume fraction was 18.3 %. Hence, the obtained volume fraction is comparable with each other.

The volume fraction of the 3D printed specimen was also determined using an analytical approach. In the analytical approach, the mass of the fiber and matrix within the specimen was calculated using properties of the raw materials. The length and mass of the fiber present within the specimen was calculated using following equations:

$$L_f = \frac{LWN}{1000b} \tag{13}$$

$$m_f = \frac{tex}{1000} \times L_f \tag{14}$$

Where L_f is the length of the fiber present within the specimen (m), L is the length of the specimen along the fiber direction (mm), W of the specimen (mm), N is the number of layers printed within the specimen, b in the gap between two consecutive fiber lines in a single layer (mm), m_f is the mass of the fiber present within the specimen (g), and tex is the properties of the fibers.

Consequently, the mass of the matrix material (m_m) present within the specimen was measured by subtracting fiber mass from the mass of the printed specimen. Then, the density of the fiber and matrix material was used to calculate volume fraction of the printed specimen analytically. The calculated volume fraction using this analytical approach was 20.3%.

The density of the 3D printed composites was also calculated by using rule of mixture (ROM) as follow-

$$\rho_{c,rom} = \rho_f V_f + \rho_m (1 - V_f) \tag{15}$$

The calculated density of the composite's using ROM was 1.29 g/cm^3, which is comparable with density measured by Archimedes principle.

5.5.6. Surface profile and line roughness

The average line roughness of a single layer of 3D printing with acrylated epoxy resin was measured using a Keyence microscope. The average line roughness (R_a) was 34.16 µm. The line roughness was measured using a cut-off length of 2.5 mm. The average line roughness for a single layer 3D printed with peo-poly tough resin was 14.4 µm. Therefore, the line roughness is higher for printing with acrylated epoxy resin.

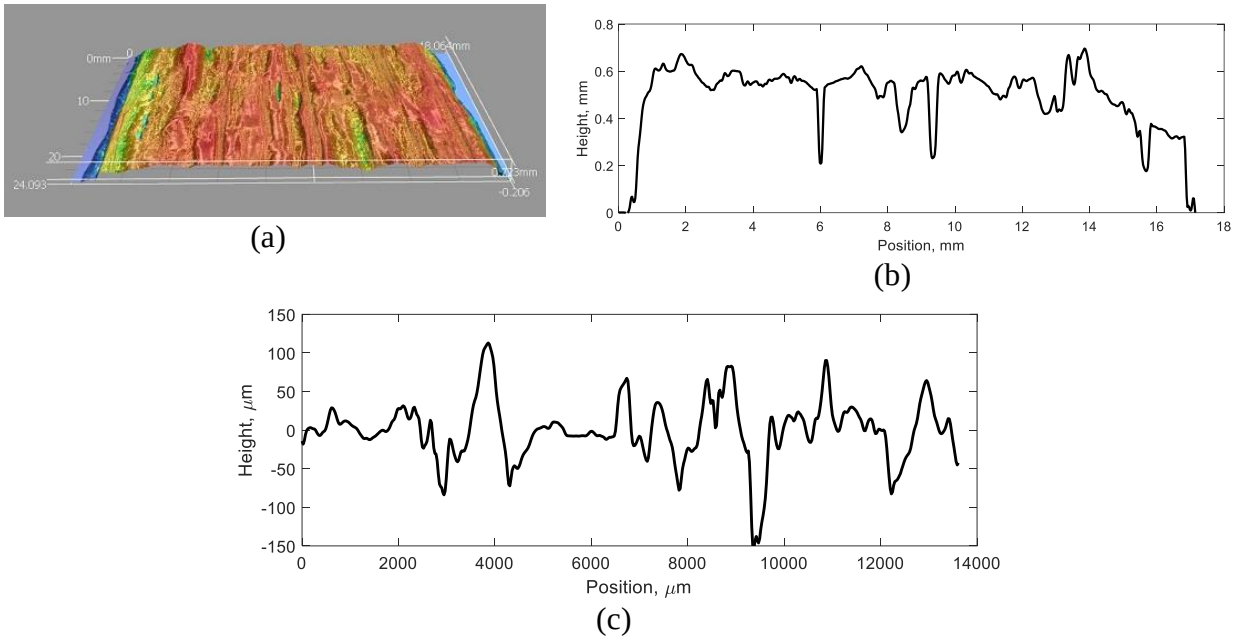

(a) (b) (c)

Figure 35: Measurement of roughness of a printed single layer: (a) 3D profile, (b) surface profile, (c) roughness profile.

5.5.7. Tensile strength

Four-layer unidirectional composites were 3D printed using the discussed 3D printing approach. Printed coupons were cut into test specimens using a ceramic cutter. A tab was inserted at both ends of the specimen to ensure better load transfer. The tensile test was performed according to the ASTM standard. Width of the specimen was approximately 10 mm. Test rate was 1 mm/min. A video extensometer was used to measure the longitudinal and transverse strain. Five specimens were tested under tensile loading. Average tensile strength was 432.54 MPa, with a Standard deviation between the tensile strengths is 24.22 MPa. The average tensile modulus was 59.03 GPa, with a standard deviation between tensile modulus is 6.10 GPa. Figure 36 shows the representative tensile test plot for the printed composites showing the plot of stress versus longitudinal strain. The failure strain is around 1%.

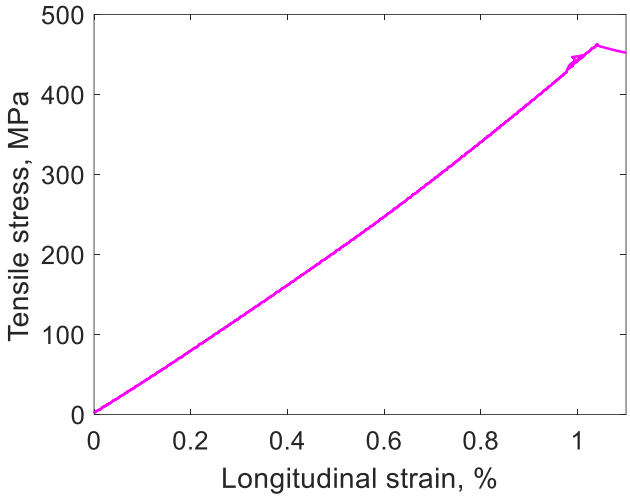

Figure 36: Representative tensile test plot for 3D printed CCFR acrylated epoxy resin composites.

To determine the Poisson's ratio, the tensile tests were conducted by employing an MTS AVX video extensometer. This enabled the simultaneous capture of both longitudinal and transverse strains. As the tensile load was applied, the transverse dimension of the specimen exhibited a reduction, while the longitudinal dimensions increased. In Figure 37(b), the relationship between transverse strain and longitudinal strain is depicted. By calculating the ratio of transverse strain to longitudinal strain within the linear elastic range, the Poisson's ratio was calculated. The calculated Poisson's ratio was found to be 0.43.

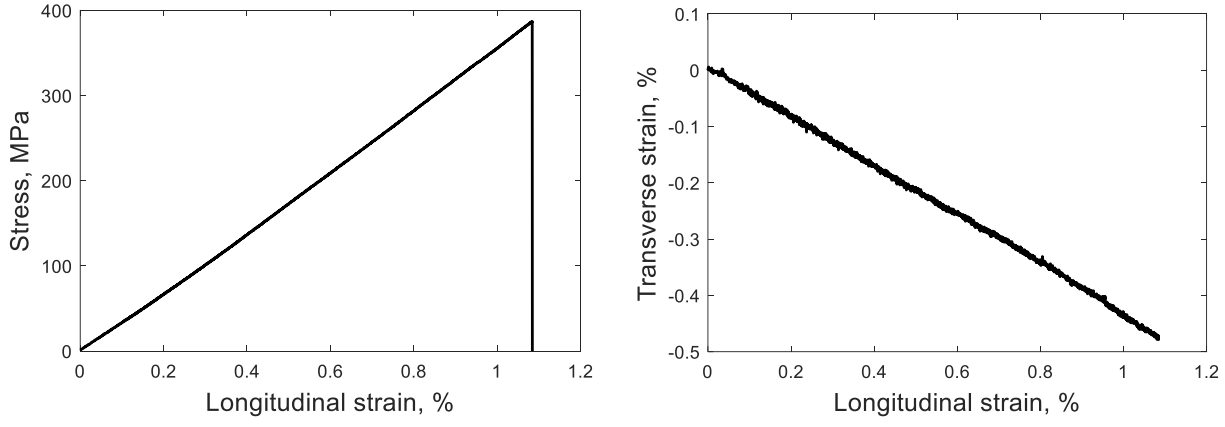

(a) (b)

Figure 37: Representative curve for tensile test with video extensometer, (a) plot for stress versus longitudinal strain, (b) plot for transverse strain versus longitudinal strain.

The tensile strength of Teijin continuous carbon fiber is 4100 MPa, and the elongation until failure for those fibers is 1.7 %. However, the carbon fiber reinforced 3D printed epoxy composites failed at a strain of around 1%. Hence, the strength of carbon fiber at 1% strain could be calculated as 2410 MPa.

Figure 38 showed the representative tensile test curve for resin material. The ultimate tensile strength of the specimen made with matrix material was 36.1 MPa, and the tensile modulus was 2.56 GPa. The failure strain of the resin specimen was 2.1 %. However, 3D printed CCFR composite specimen failed at strain 0f 1%. Therefore, from the tensile test curve, the calculated strength of matrix material at the failure strain of composite was 20 MPa.

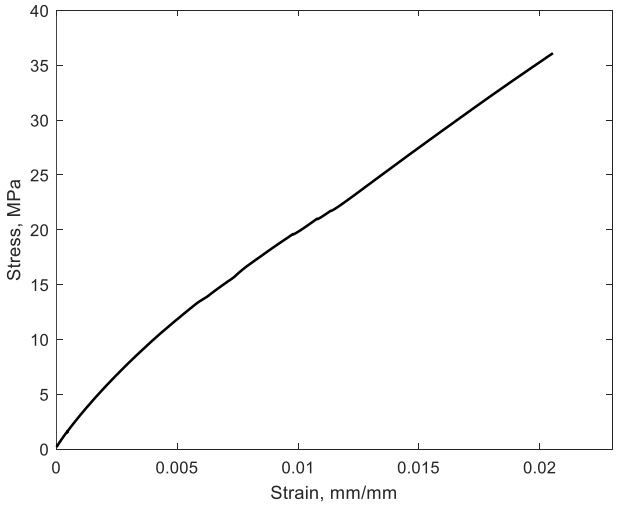

Figure 38: Representative tensile test curve for acrylated epoxy resin specimen.

Using the rule of mixture (ROM), strength for composites having volume fraction of 17.9% could be calculated as 430.18 MPa. Hence, experimentally obtained mechanical strength showed a close match with theorical strength predicted from ROM.

The average tensile properties for the 3D printed CCFR acrylate-based peo-poly resin composites were measured at 389.7 MPa. Consequently, the CCFR acrylated epoxy resin specimen

demonstrated an 11% increase in tensile strength compared to the commercially available acrylate-based CCFR peo-poly resin composites.

Figure 39 depicts SEM images of the fracture surface of the CCFR acrylated epoxy specimen subjected to tensile loading. The SEM images reveal that the primary failure mode during tensile loading is fiber pull-out. Mostly, individual fiber filaments were observed to have pulled out. Evidence of failure mark is visible within the matrix material. Additionally, a portion of the matrix material remains attached to the fiber filaments, indicating a strong bond between the fiber and matrix.

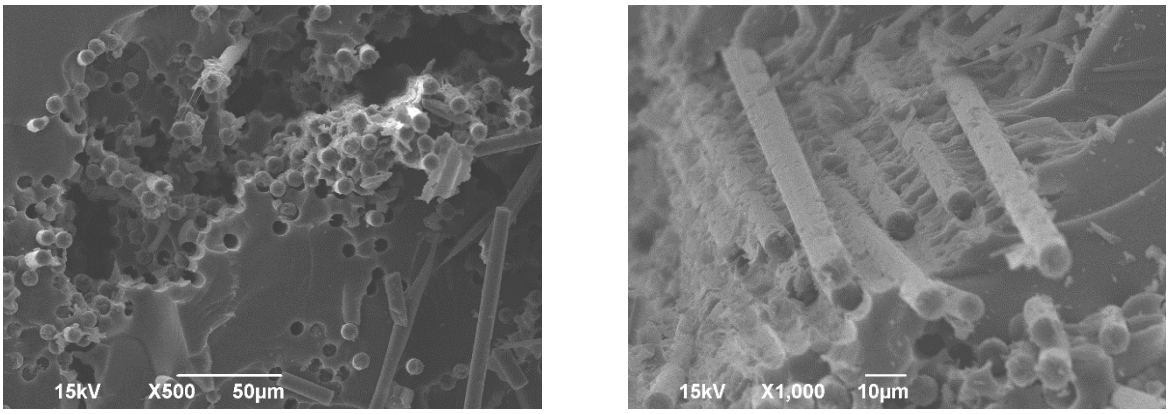

(a) (b)

Figure 39: SEM images of the fracture surface of the tensile-loaded CCFR acrylated epoxy specimen.

5.5.8. Short beam shear strength

Short beam shear (SBS) test was performed to define interlaminar shear strength of the 3D printed objects. The SBS tests were performed according to ASTM D 2344. The thickness of the specimen was 4.1 mm. According to the ASTM standard, the dimensions of the sample were such that its length and width equated to six and two times its thickness. Additionally, the span under which the load was applied was four times the thickness. 3D printed composite beam was loaded in three-point bending with a crosshead movement of 1 mm/min. Load-displacement curve was used to determine the maximum load (P_m) achieved during the test. The Equation (3) was

employed to calculate the SBS strength (F^{sbs}), with 'b' representing the width and 'h' representing the thickness of the specimen. Five specimens were tested to define the SBS strength of CCFR epoxy composites. Figure 40 presents the representative strength versus displacement curve for SBS test. The average SBS strength of 3D printed CCFR epoxy composites are 43.4 MPa, and the standard deviation between those SBS strengths was 2.1 MPa. The overall vertical deflection of the specimen to reach maximum SBS strength was approximately 1.1 mm. Average short beam shear strength for CCFR Peo-poly resin-based composites was 37.95 MPa. CCFR acrylated epoxy composites showed a 14.2% increase in the SBS strength.

$$F^{sbs} = 0.75 \times \frac{P_m}{b \times h} \tag{16}$$

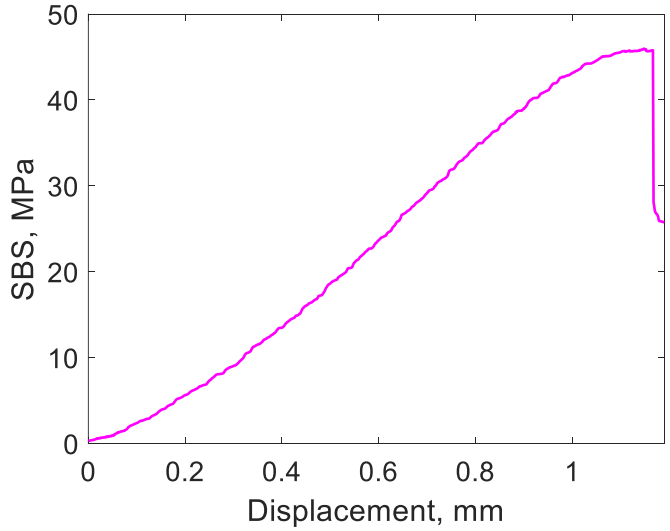

Figure 40: Representative curve for short beam shear (SBS) test of 3D printed CCFR epoxy composites.

5.5.9. Cross-sections of printed specimen

To examine the distribution of fiber and matrix within the 3D printed specimen, the specimen was affixed onto epoxy resin using a mounting press (Techpress 3, produced by Allied High-Tech Products Inc). The 3D printed specimen was carefully positioned within epoxy powder (black glass-filled) during the mounting process. The following parameters were employed to

ensure successful epoxy mounting: temperature of 200˚C, pressure set to 3800 psi, and a curing time of 5 min.

The attached 3D printed specimen underwent polishing using the Metpress 3 polishing system. The polishing process involved using a series of grit papers in the following sequence: 60, 120, 240, 400, 600, 800, and 1200 grit. Each grit size was polished for a duration of 10 minutes, applying a pressing pressure of 18 N and a rotation speed of 120 rpm.

Subsequently, the specimen underwent further polishing steps. It was first polished using a diamond cloth with a one µm polycrystalline diamond suspension and a polishing lubricant known as "green lube." Following that, the specimen received a final polishing treatment using colloidal silica suspension with a particle size of 0.04 µm, and a water droplet was used as the polishing medium.

Following the conclusion of the polishing stages, the cross-sectional aspect of the specimen was subjected to scrutiny via an optical microscope. Figure 41 depicts the distribution of fiber and matrix within the 3D printed specimen from the transverse direction, where distinctive white dots signify individual fiber filaments with a diameter of 7 µm each. These fiber filaments are grouped into bundles, with each bundle encompassing a total of 3,000 individual fiber filaments. These fibers are arranged within the specimen in an oval configuration. Conversely, the black region is likely indicative of voids present within the specimen.

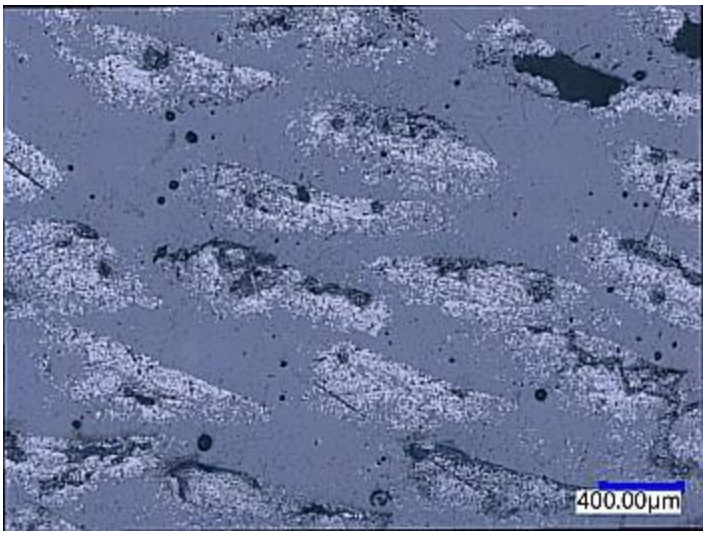

Figure 41: Cross-section of the 3D printed specimen.

5.5.10. Void analysis

The void analysis of the printed specimen was conducted using Micro-CT scanning. Figure 42 displays sectional images of the specimen derived from the micro-CT analysis. The Micro-CT test revealed that the predominant voids within the specimen were micro-voids. The majority of the larger voids were located within the fiber tows. However, micro-voids were observed in both the fiber and matrix regions. The total void content of the specimen was measured at 6.9%.

Comparing the overall void content of the printed CCFR composites with acrylated epoxy resin to the Peo-poly based resin, it is evident that the former has a higher void content. This can be attributed to the higher viscosity of the acrylated epoxy resin, which leads to less effective penetration within the fiber filaments during the printing process. Consequently, the printed specimen using acrylated epoxy resin exhibits a higher void content compared to that printed using Peo-poly resin.

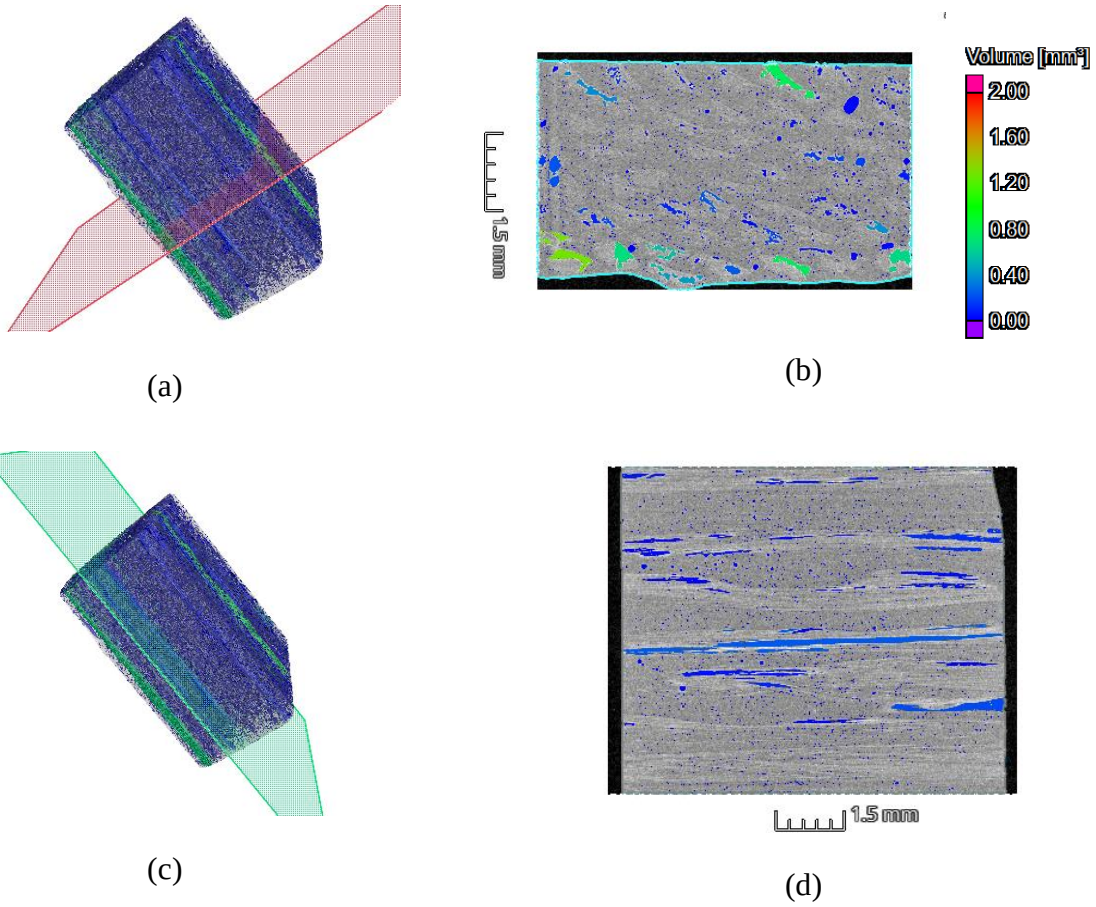

Figure 42: Images from micro-CT analysis of the CCFR 3D printed acrylated epoxy specimen, (a) section plane perpendicular to the fiber direction and (b) corresponding sectional view, (c) section plane parallel to the fiber direction and (d) corresponding sectional view.

5.6. Truss Structures 3D Printing

The goal of this section is to propose an optimized printing path for printing truss structure using continuous fiber reinforcement. 3D printing continuous fiber with liquid thermoset resin does not include a jumping feature in the printing path; the path must remain continuous. Cheng [91] demonstrated a continuous printing path for honeycomb structure. However, the continuous path is not possible to design for cellular or truss structures. Hence, a periodic superposition method is required to print cellular or truss structures [92]. This is achieved by completing a specific sequence of printing paths, forming what is known as a 'print cycle.' The print cycle then repeats to create the entire truss structure.

Wang et al. [58] introduced an algorithm for printing truss structures in which the first and second layers of fiber were printed simultaneously by adjusting the layer height as required. However, the number of passes of the fiber at each corner of the truss was not consistent after each cycle of truss printing. This inconsistency in fiber pass at the corners results in varying layer heights at different corners of the truss. No previously proposed algorithm in the literature ensures an equal number of carbon fiber passes at each corner of the truss structure, leading to uneven layer heights at various corners after each layer of truss printing. Unequal heights at different corners of the printed structure can lead to a loss of contact between the print nozzle and the previously printed layer. Furthermore, this uneven height at various corners of the truss is posing a significant challenge when scaling up truss structure production.

This research is proposing a toolpath consisting of four sequential printing paths, collectively referred to as a "print cycle" for completing the truss structure. During each printing path, continuous fibers are directed toward each corner of the truss, ensuring that the height of the printed structure remains consistent at every corner. After finishing a printing path, the print nozzle moves up by an amount equal to the layer height to continue the next paths.

Figure 43 (a-d) illustrates the four consecutive printing paths used in constructing the truss structure. In Figure 43 (e), these four consecutive paths are superimposed to create a schematic representation of a complete cycle to print truss structure. It is noticeable from the Figure that each member in the printed truss structure does not contain an equal number of fibers. Figure 43 (f) depicts the original image of printed truss structure. The printed truss structure lacked sharpness at the corners because the laser light used during printing was diffused within the region. Utilizing thinner and more coherent laser light may enhance the corner quality of the printed truss.

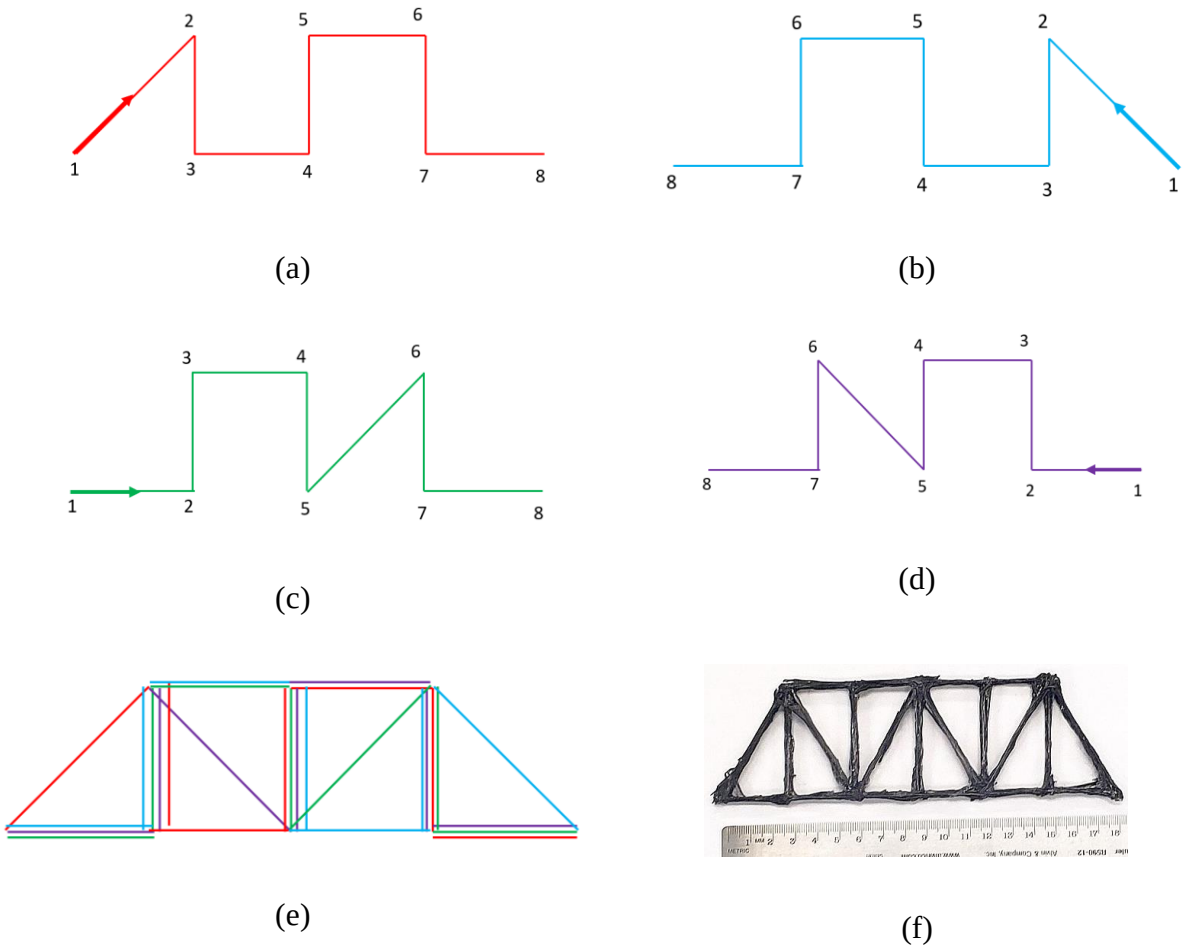

Figure 43: Printing path for truss structure, (a) first printing path, (b) second printing path, (c) third printing path, (d) forth printing path, (e) schematic of combined truss structure, (f) original printed truss.

5.7. Conclusions

To the author's best knowledge, this study for the first time demonstrated the light- assisted 3D printing of CCFR thermoset composites using liquid acrylated epoxy resin. Printed CCFR specimens with acrylated epoxy resin showed 11% and 40%, respectively, higher tensile strength and tensile modulus compared to the printed specimen with urethane acrylate resin. In addition, acrylated epoxy resin based CCFR composites showed 14% more SBS strength compared to urethane acrylate resin-based composites. Moreover, this study demonstrated an algorithm of printing scalable truss structure by ensuring equal layer height after each cycle of printing.

CHAPTER 6: MEASUREMENT OF OPTIMUM LASER ENERGY REQUIRED TO 3D PRINT CONTINUOUS FIBER REINFORCED COMPOSITES USING PHOTO-CURABLE THERMOSET RESIN

6.1. Introduction

Conventional manufacturing of polymeric materials provides limited design flexibility and requires costly molds. In contrast, 3D printing is well-suited for creating complex shapes without the need for expensive tools or molds [93]. 3D printing of polymeric materials can be categorized into two types: thermosets and thermoplastics. Thermoplastic materials (polypropylene, ABS) are solid at room temperature. Thermoplastic filaments are melted by heated extruders and deposited layer by layer to 3D print various shapes [94]. On the other hand, thermoset resins are liquid at room temperature. Therefore, 3D printing with thermoset resin requires an instant solidification mechanism during the printing process [24]. 3D printing using thermoset resin has demonstrated higher precision [95]. Light-assisted 3D printing of thermoset resin can be classified into two major types: Stereolithography (SLA) [96] and digital light processing (DLP) [97] . SLA 3D printing cures the resin point by point, while DLP printing cures an entire layer of resin at once.

Light-assisted 3D printing of thermoset resin utilizes light energy to solidify liquid resin during the printing process. The photopolymer used in this printing process mainly consists of monomers and photo initiators. Photopolymerization can be broadly classified into two categories: radical and cationic photo-polymerization. In radical photo-polymerization, reactive free radicals are generated from the photo-initiator upon light irradiation with specific wavelength and intensity. These free radicals then attach consecutively to monomer molecules, forming a solid polymeric chain network. The propagation of polymeric chains stops through a termination reaction. In contrast, in cationic polymerization, the photo-initiator is converted into a strong acid species upon

light irradiation, which initiates polymerization [98]. Free-radical polymerization offers advantages over cationic polymerization due to its fast-curing response, however it exhibits larger volumetric shrinkage.

3D printed parts using pure thermoset resin via SLA printing have shown poor mechanical strength [99]. To address this issue and enhance mechanical properties, significant attention has been given to research on short fiber-reinforced 3D printing of thermoset composites. Fiber reinforced thermoset composites are typically 3D printed using an extrusion-based printing process, either with high energy light assistance [4] or without it [3]. Printing of thermoset resin without light assistance is known as direct ink writing (DIW), which requires crucial resin preparation to retain its shape after being extruded onto the print bed [47]. However, the requirement of resin preparation is more flexible in the case of light-assisted printing [16, 17, 88]. This is because, to retain shape, thermoset resins are instantly solidified by high-energy light irradiation during printing.

Short fiber reinforcement only marginally enhances the mechanical properties [6]. Thus, continuous fiber reinforcement emerges as the ultimate solution for achieving excellent mechanical strength [10, 19]. Continuous carbon fiber reinforced (CCFR) polymer matrix composites exhibit superior mechanical strength, and demands for CCFR thermoset polymer matrix composites are increasing rapidly [45]. Nevertheless, the manufacturing of CCFR thermoset polymer matrix composites through 3D printing remains a significant challenge. Light-assisted 3D printing of CCFR thermoset composites has garnered considerable attention [15, 57, 63]. The main hurdle lies in the opacity of carbon fiber, which obstructs the adequate solidification of the thermoset resin during printing with continuous carbon fiber (CCF) reinforcement.

However, literature focusing on estimating the required amount of light energy to continue 3D printing of thermoset resin with CCFR is scarce and difficult to find.

The overall objective of this study is to experimentally measure and compare the minimum light energy required to continue 3D printing with CCF reinforcement. The study involved experimental measurements and comparisons of the energy required to print with two different photo-curable resins: a commercially available acrylate resin, and an acrylated epoxy resin.

6.2. Materials and Methods

6.2.1. Materials

To measure the minimum laser power requirement for 3D printing with CCFR, continuous carbon fiber was 3D printed with two distinct types of thermoset resin: Peo-poly Tough resin and Bisphenol-A acrylated epoxy resin (BAE) resin. The properties of the continuous carbon fiber and thermoset resins used for this current study will be discussed in this section.

Teijin 3K continuous carbon fiber was collected from Teijin Carbon America, Inc. (Rockwood, TN). Each carbon fiber tow contained 3000 individual filaments, with each filament having a diameter of 7 μm. The weight and density of the carbon fiber filament were 200 tex and 1.77 gm/cm^3, respectively. The tensile strength and modulus of the carbon fiber was 4100 MPa and 240 GPa, respectively.

Peo-poly Tough resin was purchased from MatterHackers (California, USA). This is a commercially available SLA resin, specifically designed for curing under 405 nm light irradiation. It has a strength of 45 MPa, a modulus of 1500 MPa, and a viscosity of 0.94 Pa·s.

Bisphenol-A acrylated epoxy (BAE) resin was collected from Covestro (Pittsburgh, PA). The commercial name of this resin is Agisyn 1010-A60. This BEA resin is designed for making energy curable system (ultraviolet/electron beam). The viscosity of the resin is 1800-2500 mPa.s

at a temperature of 25˚C. To make the resin curable under 405 nm light, a photo-initiator (Diphenyl (2,4,6-trimethylbenzoyl) phosphine oxide (97%), (TPO)) was mixed with the resin. This is a type-I free radical photo-initiator. Type-I photo-initiator undergoes intramolecular bond cleavage to produce free radicals for polymerization to occur. This photo-initiator was purchased from Sigma-Aldrich (St. Louis, MO). The mixing ratio (by mass) of the resin and the photo-initiator was 100:2. The resin and the photo-initiator were mixed using a speed mixer (FlackTek speed mixer) running at 2000 rpm for 2 minutes.

6.2.2. Printing method

Figure 44 illustrates the light assisted 3D printing process for thermoset resin with continuous carbon fiber reinforcement. A commercial gantry (moveable along X and Y axis) was modified to create a custom 3D printer. The gantry's movement along the X and Y axes was facilitated by controlling the rotation of the motor using motor controllers and Arduino set-up. A custom print nozzle was manufactured to feed continuous carbon fiber and thermoset resin simultaneously. The continuous carbon fiber was impregnated with liquid thermoset resin within the print nozzle. The resin was fed into the print nozzle at a constant flowrate of 0.121 mL/min achieved by using a syringe pump.

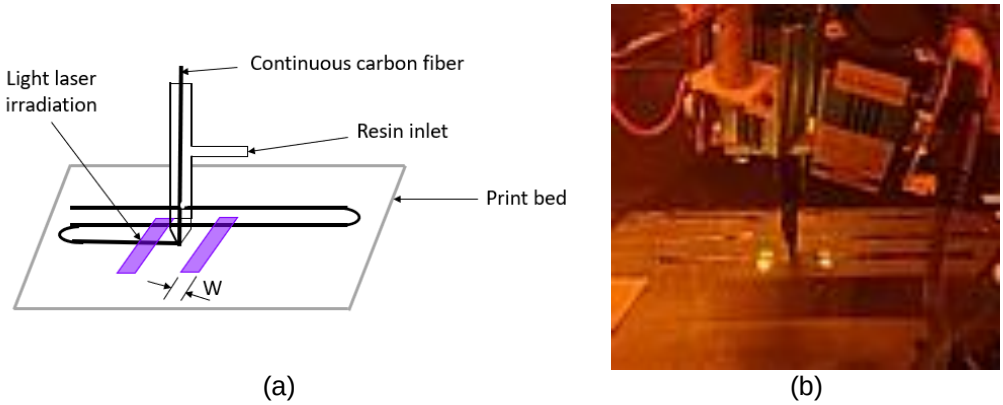

(a) (b)

Figure 44: Photograph of the printing process (a) schematic diagram, (b) actual printing process.

The continuous carbon fiber was pulled by the print nozzle due to the motion of the gantry or print head. The printing speed was set at 120 mm/min, and a hot-rolled steel plate (305 mm × 305 mm) served as the print bed, coated with mold release agent (Frekote) before starting the printing process. A 0.5 mm gap was maintained between the print nozzle and the print bed during printing to ensure smooth flow of resin impregnated carbon fiber.

As shown in Figure 44, two high-energy 405 nm wavelength pulsed light lasers were irradiated on the print bed at the front and back of the print nozzle. The laser beam was focused 10 mm away from the print nozzle tip to prevent the solidification of the resin within the print nozzle. The laser beam's shape was rectangular with dimensions of (L×W) 20 × 5 mm. The pulsed light laser was utilized to instantly solidify the resin after deposition on the print bed with continuous carbon fiber.

Figure 45 compares the programmed printing path with the actual/expected printed path. The actual/expected printed specimen's length (B) should be smaller than the length of programmed printing path (A). The printed specimen was shorted by length C at each side of the specimen, where length C equaled the distance between the nozzle tip and the laser irradiation during printing. A successful printing outcome was achieved if continuous carbon fiber could print 180˚ turns with precision and maintain the expected dimensional accuracy. The gap between the two consecutive fiber lines was set to 1 mm.

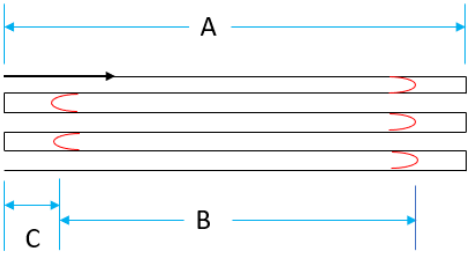

Figure 45: Comparison between programmed printing path and actual printed path.

6.2.3. Laser power measurement

A pulsed light laser was utilized in this study to perform 3D printing. The average power output of the pulsed laser was determined using a laser power measurement device (VLP-2000), as illustrated in Figure 46. The dot size of light employed for laser power measurement was 15 mm^2, which exceeds the minimum recommended dot size for the measurement device at 3.1 mm^2. The laser irradiation dot was precisely focused on the detector hole, and the detector was connected to a display to digitally exhibit the laser power (mW). Consequently, the average power output of the laser was accurately measured.

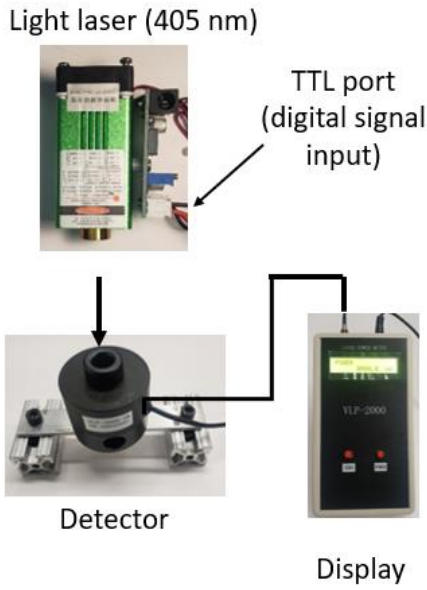

Figure 46: Laser power measurement system.

The power output of the pulsed-light laser was controlled through pulse width modulation (PWM). By altering the input digital signal into the laser, the pulse width could be adjusted. This was achieved using transistor-transistor logic (TTL) port, which facilitated digital signal input to the laser. The pulse width of the light laser varied proportionally with the digital signal input received at the TTL port. The digital signal width ratio (ON/OFF ratio) within the TTL port played

a crucial role in controlling the pulse width of the light laser, consequently leading to changes in its power output.

Figure 47 presents a schematic displaying an input digital signal with ON and OFF duty cycle width ratios 1/1 (Figure 47 (a)) and 1/2 (Figure 47(b)), respectively. These duty cycle width ratios (ON/OFF ratio) were modified by programming an Arduino connected at the TTL port of the light laser. By adjusting the time-length of the ON and OFF duty cycles, the average power output of the pulsed light laser could be effectively changed.

To determine the minimum energy requirement for printing, 3D printing experiments were conducted for each resin using different laser power settings achieved by varying the ON and OFF signal width ratios in the TTL port of the laser. The average power output of the laser under different ON/OFF ratios was calculated using the laser power measurement device (VLP-2000).

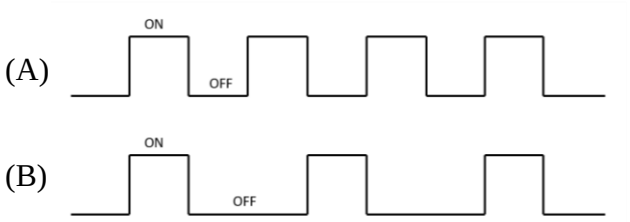

Figure 47: TTL signal for laser to vary power output of the laser, (a) ON/OFF ratio = 1/1, (b) ON/OFF ratio = 1/2.

The amount of applied surface energy (SE) required to print with CCF reinforcement, which is independent of print speed, can be defined by Equation (17).

$$SE = \frac{60\ W}{F} \times P_A \tag{17}$$

Where, SE represents the work per unit area required for curing the resin to continue printing with CCF reinforcement (mJ/mm^2), W is the width of the laser beam irradiation during printing (Shown in Figure 44 (A), W = 5 mm), F is the printing speed (120 mm/min), P_A is the power of the incident laser beam per unit area (mW/mm^2). The value of P_A was calculated by

dividing the laser power (mW) from VLP -2000 at a specific power setting by the area of the laser irradiation on the print bed.

6.3. Results and Discussion

Table 3 presents the outcomes of CCFR printing with Peo-poly Tough resin at various laser power settings. Printing at different power settings was conducted by modifying the digital signal band-width ratio at the TTL port of light laser. The ON/OFF band-width ratio of the digital signal was adjusted to the following values: 10/1, 3/1, 1/1, 1/3, 1/5, and 1/10. Figure 48 displays the images of the printed specimen layer at the mentioned laser power settings. The vertical lines on Figure 48 indicate the expected length of the printed specimen.

Table 3: Results for CCFR 3D printing of Peo-poly Tough resin at different laser power setting

TTL ON/OFF ratio	Laser power, P_A (mW/mm^2)	Applied surface energy, SE (mJ/mm^2)	Printing process
$\frac{10}{1}$	4.5	11.3	Perfectly successful
$\frac{3}{1}$	3.45	8.6	Perfectly successful
$\frac{1}{1}$	2.03	5.1	Perfectly successful
$\frac{1}{3}$	0.93	2.3	Successful
$\frac{1}{5}$	0.58	1.5	Successful
$\frac{1}{10}$	0.31	0.8	Unsuccessful

Successful prints were achieved until the TTL port signal ON/OFF ratio dropped to 1/5. However, printing was unsuccessful when using a TTL ON/OFF ratio of 1/10. The corresponding

power and applied surface energy (SE) from the laser are also provided in Table 3. Specimen printed with a light SE of up to 5.1 mJ/mm^2 exhibited higher dimensional accuracy, as expected. When the SE dropped below this level, dimensionally inaccurate specimens were produced. Specimens printed with SE values of 2.3 and 1.5 mJ/mm^2 displayed minor dimensional inaccuracy (less than 5 mm) but exhibited reasonable precision at 180˚ turns. Theoretically, the maximum possible dimensional error with precision should be less than the width of the laser beam irradiation (W = 5 mm). However, specimens printed with a SE of 0.8 mJ/mm^2 encountered issues, such as peeling up at the corners and creating fiber loops, leading to unsuccessful prints.

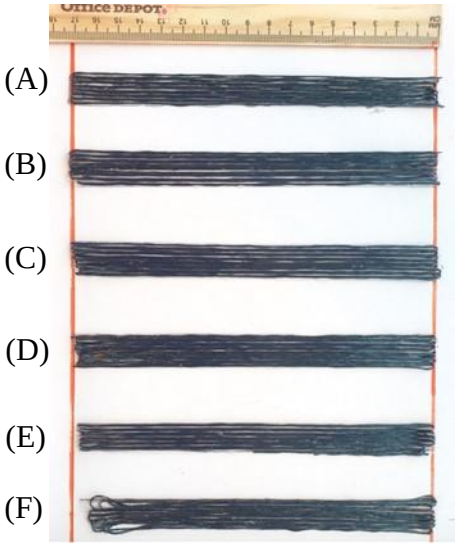

Figure 48: Printed carbon fiber layer with Peo-poly Tough resin at varying laser power, with TTL on/off ratio: (a) 10/1, (b) 3/1, (c) 1/1, (d) 1/3, (e) 1/5, (f) 1/10.

Table 4 shows the results for CCFR 3D printing with different laser power setting for BEA resin. The laser power was varied by changing the width ratio (ON/OFF ratio) of the pulse in the TTL port of the laser. Figure 49 shows the printed layers using the various laser power setting mentioned in Table 4. Printing was successful until the ON/OFF ratio of the TTL signal dropped below 1/10. However, printing was unsuccessful when having TTL ON/OFF ratio of 1/15.

The specimen's 3D printed with a light SE of 2.3 mJ/mm^2 or above ensured very high dimensional accuracy and precise turning (180˚) at the corner. The accuracy of the printing at

180˚ turning was within an acceptable range until light SE dropped below 0.8 mJ/mm^2. On the other hand, printing with a light SE of 0.5 mJ/mm^2 exhibited large dimensional inaccuracy, and fiber partially peeled out of the bed, creating fiber loops at the corner. Consequently, printing was considered a failure at the light SE of 0.5 mJ/mm^2. Therefore, the minimum light SE requirement of BEA resin to 3D print successfully with continuous fiber reinforcement was determined to be 0.8 mJ/mm^2.

Table 4: Results for CCFR 3D printing of BEA resin at different laser power setting

TTL ON/OFF ratio	Laser power, P_A (mW/mm^2)	Applied surface energy, SE (mJ/mm^2)	Printing process
$\frac{10}{1}$	4.5	11.3	Perfectly successful
$\frac{3}{1}$	3.45	8.6	Perfectly successful
$\frac{1}{1}$	2.03	5.1	Perfectly successful
$\frac{1}{3}$	0.93	2.3	Successful
$\frac{1}{5}$	0.58	1.5	Successful
$\frac{1}{10}$	0.31	0.8	Critically successful
$\frac{1}{15}$	0.20	0.5	Unsuccessful

Photocurable thermoset resin contains polymer monomers and photo-initiators. Under light energy irradiation, the photo-initiator decomposes, leading to the generation of free radicals. These free radicals initiate polymerization reactions, irreversibly crosslinking and solidifying the polymer monomer. The rate of free radical generation is directly proportional to the energy of the incident light photons. Therefore, the incident light must possess enough energy to create sufficient

free-radical polymerization in the polymer monomer, allowing the CCF to retain its shape after being 3D printed.

This study presents an experimental process to quantify the minimum light SE required for successful 3D printing with CCF reinforcement. The minimum light SE required for Peo-poly Tough resin and BEA was measured, and found to be comparable, although BEA resin requires slightly less SE compared to the Peo-poly Tough resin. Consequently, it can be concluded that BEA resin is capable of achieving sufficient free radical polymerization to print with CCF reinforcement using light photons with slightly less energy than those needed for the Peo-poly Tough resin.

Understanding the optimal laser energy requirement for 3D printing with CCF is crucial for developing energy-efficient and scalable manufacturing processes for CCFR 3D printed composites. Moreover, this knowledge may prove beneficial in controlling the portion of light curing in a dual cure (heat and light) based printing systems.

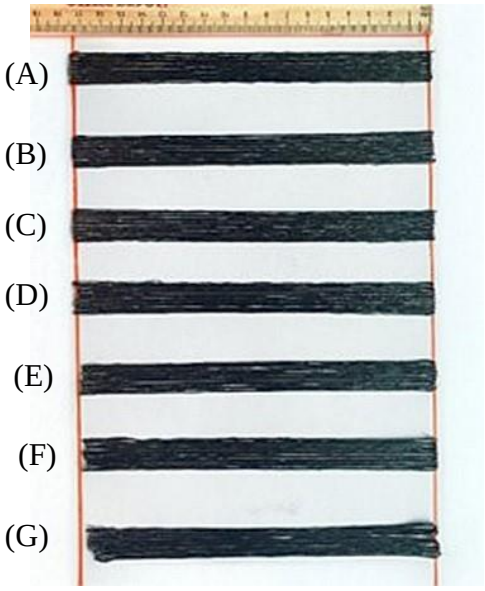

Figure 49: Printed layer with CCF and BEA resin using varying laser power at TTL on/off ratio: (a) 10/1, (b) 3/1, (c) 1/1, (d) 1/3, (e) 1/5, (f) 1/10, (g) 1/15.

6.4. Conclusion

In this research article, the minimum light energy required for 3D printing with continuous fiber reinforcement was experimentally evaluated for two types of thermoset resin. The study estimated the light energy required for 3D printing with Peo-poly Tough and bisphenol acrylated epoxy resin (BAE) resin. The results indicate that Peo-poly resin requires a higher light energy level for 3D printing with CCF reinforcement compared to BEA resin. Specifically, the minimum light energy required for 3D printing with CCF reinforcement for Peo-poly Tough resin and BEA is 1.5 and 0.8 mJ/mm^2, respectively. These experimental findings will enable the 3D printing of CCFR thermoset composites by utilizing optimized laser power, thereby providing a method for developing an energy-efficient printing process.

CHAPTER 7: CONCLUSION

This research establishes the light-assisted 3D printing technologies for CCFR thermoset composites. Both urethane acrylate based and acrylated epoxy resin with low viscosity were utilized to print successfully with continuous fibers reinforcement. 3D Printed composites achieved 28% fiber volume fraction, and corresponding tensile strength and modulus of 671 MPa and 59 GPa, respectively. Mechanical characterization of those 3D composites showed comparable strength and stiffness to conventionally manufactured composites. The resin flow rate was varied during printing to produce composites with tailored mechanical strength, surface finish, and void content. For a similar fiber volume fraction, acrylated epoxy resin composites exhibited higher mechanical strength compared to urethane acrylate composites. This dissertation furthermore demonstrated different algorithms to 3D print complex structures. A laser cutter incorporated 3D printing technique was demonstrated to print shapes with interior features, such as holes. This eliminates the problem of fiber loops creations at the corner of the printed object. This study demonstrated the algorithms of printing different shapes, such as rectangle, triangle, circle, hexagon, grid structure, by using overshoots at the printing. An algorithms of printing truss structures was also demonstrated with ensuring equal height after each layer or cycle of truss printing. Moreover, a study was conducted to investigate the effect of rheological modifier on the mechanical strength of the 3D printed composites. Furthermore, research was conducted to measure the minimum light energy required to print with continuous fibers reinforcement using both acrylate-based and acrylated epoxy resin. Therefore, this research explored the optimal printability of complex structure using thermoset resin reinforced with continuous fibers.

In the era of light- assisted printing process, this research explored the printing challenges by implementing the algorithms of creating various shapes using low viscosity thermoset resin and

continuous carbon fiber reinforcement. This printing technology has the potential to eliminate the challenges associated with preparing print ink with crucial rheological properties, thereby addressing thermoset resin printing challenges, such as nozzle clogging. Further research on employing coherent laser beams with optimized laser power is of crucial importance to improve accuracy of the printed objects. Developing an FEM model to predict the strength of printed composites based on print parameters would be a beneficial future research topic. Using the output of those FEM models, it is possible to train machine learning algorithms to predict print parameters needed to manufacture composites with desired strength, surface finish, and void content. Developing an automated printing process with established methodologies and proposed printing paths would pave the way for the creation of a commercial 3D printer capable of manufacturing CCFR composites with improved mechanical strength, utilizing a low-viscosity thermoset resin system. These 3D printing technologies have the potential to align with conventional manufacturing processes in various composite industries or even replace conventional manufacturing altogether.

REFERENCES

[1] F. Ning, W. Cong, J. Qiu, J. Wei, S. Wang, Additive manufacturing of carbon fiber reinforced thermoplastic composites using fused deposition modeling, Composites Part B: Engineering 80 (2015) 369-378.

[2] H.L. Tekinalp, V. Kunc, G.M. Velez-Garcia, C.E. Duty, L.J. Love, A.K. Naskar, C.A. Blue, S. Ozcan, Highly oriented carbon fiber–polymer composites via additive manufacturing, Composites Science and Technology 105 (2014) 144-150.

[3] N. Nawafleh, E. Celik, Additive manufacturing of short fiber reinforced thermoset composites with unprecedented mechanical performance, Additive Manufacturing 33 (2020) 101109.

[4] G. Griffini, M. Invernizzi, M. Levi, G. Natale, G. Postiglione, S. Turri, 3D-printable CFR polymer composites with dual-cure sequential IPNs, Polymer 91 (2016) 174-179.

[5] J. Zhao, Q. Li, F. Jin, N. He, Digital light processing 3D printing Kevlar composites based on dual curing resin, Additive Manufacturing 41 (2021) 101962.

[6] Y. Sano, R. Matsuzaki, M. Ueda, A. Todoroki, Y. Hirano, 3D printing of discontinuous and continuous fibre composites using stereolithography, Additive Manufacturing 24 (2018) 521-527.

[7] R. Matsuzaki, M. Ueda, M. Namiki, T.-K. Jeong, H. Asahara, K. Horiguchi, T. Nakamura, A. Todoroki, Y. Hirano, Three-dimensional printing of continuous-fiber composites by in-nozzle impregnation, Scientific reports 6 (2016) 23058.

[8] J. Qiao, Y. Li, L. Li, Ultrasound-assisted 3D printing of continuous fiber-reinforced thermoplastic (FRTP) composites, Additive Manufacturing 30 (2019) 100926.

[9] M. Caminero, J. Chacón, I. García-Moreno, J. Reverte, Interlaminar bonding performance of 3D printed continuous fibre reinforced thermoplastic composites using fused deposition modelling, Polymer Testing 68 (2018) 415-423.

[10] W. Hao, Y. Liu, H. Zhou, H. Chen, D. Fang, Preparation and characterization of 3D printed continuous carbon fiber reinforced thermosetting composites, Polymer Testing 65 (2018) 29-34.

[11] Y. Ming, S. Zhang, W. Han, B. Wang, Y. Duan, H. Xiao, Investigation on process parameters of 3D printed continuous carbon fiber-reinforced thermosetting epoxy composites, Additive Manufacturing (2020) 101184.

[12] H. Zhang, D. Li, T. Huang, Q. Hu, Q. Jiang, J. Wang, Investigation of a 3D Printing Method for Continuous Carbon Fiber-Reinforced Thermosetting Epoxy Composite, Applied Composite Materials (2024) 1-18.

[13] H. Xiao, Q. He, Y. Duan, J. Wang, Y. Qi, Y. Ming, C. Zhang, Y. Zhu, Low-temperature 3D printing and curing process of continuous fiber-reinforced thermosetting polymer composites, polymer composites 44(4) (2023) 2322-2330.

[14] W. Dong, C. Bao, W. Lu, R. Liu, H. Ma, S. Li, K. Sun, Fabrication of a continuous carbon fiber-reinforced phenolic resin composites via in situ-curing 3D printing technology, Composites Communications (2023) 101497.

[15] X. He, Y. Ding, Z. Lei, S. Welch, W. Zhang, M. Dunn, K. Yu, 3D printing of continuous fiber-reinforced thermoset composites, Additive Manufacturing 40 (2021) 101921.

[16] A.M. Abdullah, Y. Ding, X. He, M. Dunn, K. Yu, Direct-write 3D printing of UV-curable composites with continuous carbon fiber, Journal of Composite Materials (2022) 00219983221127182.

[17] M.A. Rahman, M.Z. Islam, L. Gibbon, C.A. Ulven, J.J. La Scala, 3D printing of continuous carbon fiber reinforced thermoset composites using UV curable resin, Polymer Composites 42(11) (2021) 5859-5868.

[18] H. Jiang, A. Abdullah, Y. Ding, C. Chung, M.L. Dunn, K. Yu, 3D Printing of Continuous Fiber Composites Using Two-stage UV Curable Resin, Materials Horizons (2023).

[19] Z. Zhang, R. Liu, W. Li, Y. Liu, H. Luo, L. Zeng, J. Qiu, S. Wang, Direct writing of continuous carbon fibers/epoxy thermoset composites with high-strength and low energy-consumption, Additive Manufacturing 47 (2021) 102348.

[20] S. Vyavahare, S. Teraiya, D. Panghal, S. Kumar, Fused deposition modelling: a review, Rapid Prototyping Journal (2020).

[21] S. Wickramasinghe, T. Do, P. Tran, FDM-based 3D printing of polymer and associated composite: A review on mechanical properties, defects and treatments, Polymers 12(7) (2020) 1529.

[22] M. Vinyas, S. Athul, D. Harursampath, T.N. Thoi, Experimental evaluation of the mechanical and thermal properties of 3D printed PLA and its composites, Materials Research Express 6(11) (2019) 115301.

[23] Y. Cui, J. Yang, D. Lei, J. Su, 3D printing of a dual-curing resin with cationic curable vegetable oil, Industrial & Engineering Chemistry Research 59(25) (2020) 11381-11388.

[24] B. Wang, Z. Zhang, Z. Pei, J. Qiu, S. Wang, Current progress on the 3D printing of thermosets, Advanced Composites and Hybrid Materials 3(4) (2020) 462-472.

[25] M. Pagac, J. Hajnys, Q.-P. Ma, L. Jancar, J. Jansa, P. Stefek, J. Mesicek, A review of vat photopolymerization technology: Materials, applications, challenges, and future trends of 3D printing, Polymers 13(4) (2021) 598.

[26] Y. Lu, X.X. Han, A. Gleadall, L.-G. Zhao, Fracture Toughness of Three-Dimensional Stereolithography Printed Polymer Reinforced with Continuous Carbon Fibers, 3D Printing and Additive Manufacturing (2021).

[27] M. Ziaee, J.W. Johnson, M. Yourdkhani, 3D Printing of Short-Carbon-Fiber-Reinforced Thermoset Polymer Composites via Frontal Polymerization, ACS Applied Materials & Interfaces (2022).

[28] M. Heidari-Rarani, M. Rafiee-Afarani, A. Zahedi, Mechanical characterization of FDM 3D printing of continuous carbon fiber reinforced PLA composites, Composites Part B: Engineering 175 (2019) 107147.

[29] A. Todoroki, T. Oasada, Y. Mizutani, Y. Suzuki, M. Ueda, R. Matsuzaki, Y. Hirano, Tensile property evaluations of 3D printed continuous carbon fiber reinforced thermoplastic composites, Advanced Composite Materials 29(2) (2020) 147-162.

[30] Y. Huang, X. Tian, Z. Zheng, D. Li, A.V. Malakhov, A.N. Polilov, Multiscale concurrent design and 3D printing of continuous fiber reinforced thermoplastic composites with optimized fiber trajectory and topological structure, Composite Structures (2022) 115241.

[31] H. Zhao, X. Liu, W. Zhao, G. Wang, B. Liu, An Overview of Research on FDM 3D Printing Process of Continuous Fiber Reinforced Composites, Journal of Physics: Conference Series, IOP Publishing, 2019, p. 052037.

[32] G.D. Goh, V. Dikshit, A.P. Nagalingam, G.L. Goh, S. Agarwala, S.L. Sing, J. Wei, W.Y. Yeong, Characterization of mechanical properties and fracture mode of additively manufactured carbon fiber and glass fiber reinforced thermoplastics, Materials & Design 137 (2018) 79-89.

[33] Y. Duan, J. Li, W. Zhong, R.G. Maguire, G. Zhao, H. Xie, D. Li, B. Lu, Effects of compaction and UV exposure on performance of acrylate/glass-fiber composites cured layer by layer, Journal of Applied Polymer Science 123(6) (2012) 3799-3805.

[34] B. Najafloo, A.M. Rezadoust, M. Latifi, Investigation on process window of 3D printed continuous glass fiber-reinforced thermosetting composites, Polymer Composites.

[35] R. Matsuzaki, T. Nakamura, K. Sugiyama, M. Ueda, A. Todoroki, Y. Hirano, Y. Yamagata, Effects of set curvature and fiber bundle size on the printed radius of curvature by a continuous carbon fiber composite 3D printer, Additive Manufacturing 24 (2018) 93-102.

[36] H.-J.L. Dirk, C. Ward, K.D. Potter, The engineering aspects of automated prepreg layup: History, present and future, Composites Part B: Engineering 43(3) (2012) 997-1009.

[37] B.C. Kim, P.M. Weaver, K. Potter, Computer aided modelling of variable angle tow composites manufactured by continuous tow shearing, Composite Structures 129 (2015) 256-267.

[38] D. Klosterman, R. Chartoff, G. Graves, N. Osborne, B. Priore, Interfacial characteristics of composites fabricated by laminated object manufacturing, Composites Part A: Applied Science and Manufacturing 29(9-10) (1998) 1165-1174.

[39] B. Chang, P. Parandoush, X. Li, S. Ruan, C. Shen, R.A. Behnagh, Y. Liu, D. Lin, Ultrafast printing of continuous fiber-reinforced thermoplastic composites with ultrahigh mechanical performance by ultrasonic-assisted laminated object manufacturing, Polymer Composites 41(11) (2020) 4706-4715.

[40] B.G. Mekonnen, G. Bright, A. Walker, A study on state of the art technology of laminated object manufacturing (LOM), CAD/CAM, Robotics and Factories of the Future, Springer2016, pp. 207-216.

[41] P. Parandoush, C. Zhou, D. Lin, 3D printing of ultrahigh strength continuous carbon fiber composites, Advanced Engineering Materials 21(2) (2019) 1800622.

[42] G.K. Ze, A. Pramanik, A. Basak, C. Prakash, S. Shankar, N. Radhika, Challenges associated with drilling of carbon fiber reinforced polymer (CFRP) composites-A review, Composites Part C: Open Access (2023) 100356.

[43] C.S. Wu, Y.L. Liu, Y.C. Chiu, Y.S. Chiu, Thermal stability of epoxy resins containing flame retardant components: an evaluation with thermogravimetric analysis, Polymer degradation and stability 78(1) (2002) 41-48.

[44] S. Ekşı, K. Genel, Comparison of mechanical properties of unidirectional and woven carbon, glass and aramid fiber reinforced epoxy composites, composites 132(3-II) (2017) 879-882.

[45] M.B.A. Tamez, I. Taha, A review of additive manufacturing technologies and markets for thermosetting resins and their potential for carbon fiber integration, Additive Manufacturing 37 (2021) 101748.

[46] N.S. Hmeidat, J.W. Kemp, B.G. Compton, High-strength epoxy nanocomposites for 3D printing, Composites Science and Technology 160 (2018) 9-20.

[47] B.G. Compton, J.A. Lewis, 3D-printing of lightweight cellular composites, Advanced materials 26(34) (2014) 5930-5935.

[48] C.M. Clarkson, C. Wyckoff, M.J. Parvulescu, L.M. Rueschhoff, M.B. Dickerson, UV-assisted direct ink writing of Si3N4/SiC preceramic polymer suspensions, Journal of the European Ceramic Society 42(8) (2022) 3374-3382.

[49] Y. Wu, C. Li, T. Chen, R. Qiu, W. Liu, Photo-curing 3D printing of micro-scale bamboo fibers reinforced palm oil-based thermosets composites, Composites Part A: Applied Science and Manufacturing 152 (2022) 106676.

[50] L.G. Blok, M.L. Longana, H. Yu, B.K. Woods, An investigation into 3D printing of fibre reinforced thermoplastic composites, Additive Manufacturing 22 (2018) 176-186.

[51] M. Ueda, S. Kishimoto, M. Yamawaki, R. Matsuzaki, A. Todoroki, Y. Hirano, A. Le Duigou, 3D compaction printing of a continuous carbon fiber reinforced thermoplastic, Composites Part A: Applied Science and Manufacturing 137 (2020) 105985.

[52] G.W. Melenka, B.K. Cheung, J.S. Schofield, M.R. Dawson, J.P. Carey, Evaluation and prediction of the tensile properties of continuous fiber-reinforced 3D printed structures, Composite Structures 153 (2016) 866-875.

[53] G. Struzziero, M. Barbezat, A.A. Skordos, Consolidation of continuous fibre reinforced composites in additive processes: A review, Additive Manufacturing 48 (2021) 102458.

[54] D.-J. Kwon, Y.-J. Jang, H.H. Choi, K. Kim, G.-H. Kim, J. Kong, S.Y. Nam, Impacts of thermoplastics content on mechanical properties of continuous fiber-reinforced thermoplastic composites, Composites Part B: Engineering 216 (2021) 108859.

[55] C. Yang, X. Tian, T. Liu, Y. Cao, D. Li, 3D printing for continuous fiber reinforced thermoplastic composites: mechanism and performance, Rapid Prototyping Journal 23(1) (2017) 209-215.

[56] B. Shi, Y. Shang, P. Zhang, A.P. Cuadros, J. Qu, B. Sun, B. Gu, T.-W. Chou, K.K. Fu, Dynamic capillary-driven additive manufacturing of continuous carbon fiber composite, Matter 2(6) (2020) 1594-1604.

[57] A. Thakur, X. Dong, Printing with 3D continuous carbon fiber multifunctional composites via UV-assisted coextrusion deposition, Manufacturing letters 24 (2020) 1-5.

[58] B. Wang, Y. Ming, J. Zhou, H. Xiao, F. Wang, Y. Duan, Z. Kazancı, Fabrication of triangular corrugated structure using 3D printed continuous carbon fiber-reinforced thermosetting epoxy composites, Polymer Testing 106 (2022) 107469.

[59] I.D. Robertson, M. Yourdkhani, P.J. Centellas, J.E. Aw, D.G. Ivanoff, E. Goli, E.M. Lloyd, L.M. Dean, N.R. Sottos, P.H. Geubelle, Rapid energy-efficient manufacturing of polymers and composites via frontal polymerization, Nature 557(7704) (2018) 223-227.

[60] Z. Xin, Y. Ming, Y. Duan, B. Wang, Q. Yang, Compression performance and analytical model of hexagonal-core sandwich panels fabricated by 3D printed continuous carbon fiber-reinforced thermosetting epoxy composites, Materials Research Express (2022).

[61] H. Zhang, K. Zhang, A. Li, L. Wan, C. Robert, C.M.Ó. Brádaigh, D. Yang, 3D printing of continuous carbon fibre reinforced powder-based epoxy composites, Composites Communications 33 (2022) 101239.

[62] Y. Ming, Y. Duan, B. Wang, H. Xiao, X. Zhang, A novel route to fabricate high-performance 3D printed continuous fiber-reinforced thermosetting polymer composites, Materials 12(9) (2019) 1369.

[63] M.A. Rahman, E. Hall, L. Gibbon, M.Z. Islam, C.A. Ulven, J.J. La Scala, A Mechanical Performance Study of Dual Cured Thermoset Resin Systems 3D-Printed with Continuous Carbon Fiber Reinforcement, Polymers 15(6) (2023) 1384.

[64] T. Wu, P. Jiang, X. Zhang, Y. Guo, Z. Ji, X. Jia, X. Wang, F. Zhou, W. Liu, Additively manufacturing high-performance bismaleimide architectures with ultraviolet-assisted direct ink writing, Materials & Design 180 (2019) 107947.

[65] Y. Guo, J. Xu, C. Yan, Y. Chen, X. Zhang, X. Jia, Y. Liu, X. Wang, F. Zhou, Direct ink writing of high performance architectured polyimides with low dimensional shrinkage, Advanced Engineering Materials 21(5) (2019) 1801314.

[66] ASTM D3039: Standard Test Method for Tensile Properties of Polymer Matrix, ASTM.

[67] I. Buj-Corral, A. Domínguez-Fernández, R. Durán-Llucià, Influence of print orientation on surface roughness in fused deposition modeling (FDM) processes, Materials 12(23) (2019) 3834.

[68] A.P. Amaria, F.M. Pasquali, J.N. Armstrong, J. Hall, Rule of Mixtures Model to Determine Tensile Strength of 3D-Printed Kevlar-Reinforced Nylon: Thermal Gravimetric Analysis of Kevlar Filaments, Design for Tomorrow—Volume 3, Springer2021, pp. 273-283.

[69] D. Mamalis, T. Flanagan, C.M.Ó. Brádaigh, Effect of fibre straightness and sizing in carbon fibre reinforced powder epoxy composites, Composites Part A: Applied Science and Manufacturing 110 (2018) 93-105.

[70] X. Yang, L. Zhan, Y. Peng, C. Liu, R. Xiong, Interface Controlled Micro-and Macro-Mechanical Properties of Vibration Processed Carbon Fiber/Epoxy Composites, Polymers 13(16) (2021) 2764.

[71] Z. Jiang, B. Diggle, M.L. Tan, J. Viktorova, C.W. Bennett, L.A. Connal, Extrusion 3D printing of polymeric materials with advanced properties, Advanced Science 7(17) (2020) 2001379.

[72] Z. Ye, C. Chu, D. Zhang, S. Ma, J. Guo, Y. Cheng, G. Xu, Z. Li, A. Sun, Study on 3D-Direct Ink Writing based on adding silica submicron-particles to improve the rheological properties of alumina ceramic ink, Materials Today Communications 28 (2021) 102534.

[73] S.K. Romberg, M.A. Islam, C.J. Hershey, M. DeVinney, C.E. Duty, V. Kunc, B.G. Compton, Linking thermoset ink rheology to the stability of 3D-printed structures, Additive Manufacturing 37 (2021) 101621.

[74] J.E.A. Gonzalez, W.J. Wright, R. Gustinvil, E. Celik, Hybrid direct ink write 3D printing of high-performance composite structures, Rapid Prototyping Journal (ahead-of-print) (2022).

[75] C. Gao, J. Qiu, S. Wang, In-situ curing of 3D printed freestanding thermosets, Journal of Advanced Manufacturing and Processing 4(3) (2022) e10114.

[76] A. Mantelli, A. Romani, R. Suriano, M. Diani, M. Colledani, E. Sarlin, S. Turri, M. Levi, UV-assisted 3D printing of polymer composites from thermally and mechanically recycled carbon fibers, Polymers 13(5) (2021) 726.

[77] T. Mohan, M. Ramesh Kumar, R. Velmurugan, Rheology and curing characteristics of epoxy–clay nanocomposites, Polymer international 54(12) (2005) 1653-1659.

[78] S. Li, H. Zhang, Y. Han, Z. Lu, K. Miao, Z. Wang, D. Li, Thermally assisted extrusion-based 3D printing of continuous carbon fiber-reinforced SiC composites, Composites Part A: Applied Science and Manufacturing 172 (2023) 107593.

[79] J. Saini, L. Dowling, J. Kennedy, D. Trimble, Investigations of the mechanical properties on different print orientations in SLA 3D printed resin, Proceedings of the Institution of Mechanical Engineers, Part C: Journal of Mechanical Engineering Science 234(11) (2020) 2279-2293.

[80] Y. Xu, S. Van Hoa, Mechanical properties of carbon fiber reinforced epoxy/clay nanocomposites, Composites Science and Technology 68(3-4) (2008) 854-861.

[81] X. Kornmann, M. Rees, Y. Thomann, A. Necola, M. Barbezat, R. Thomann, Epoxy-layered silicate nanocomposites as matrix in glass fibre-reinforced composites, Composites Science and Technology 65(14) (2005) 2259-2268.

[82] D.S. Moore, Introduction to the Practice of Statistics, WH Freeman and company2009.

[83] Q. Hu, Y. Duan, H. Zhang, D. Liu, B. Yan, F. Peng, Manufacturing and 3D printing of continuous carbon fiber prepreg filament, Journal of materials science 53(3) (2018) 1887-1898.

[84] T. Kuncius, M. Rimašauskas, R. Rimašauskienė, Interlayer adhesion analysis of 3d-printed continuous carbon fibre-reinforced composites, Polymers 13(10) (2021) 1653.

[85] T. Yiwen, T. Yuegang, Z. Fan, Z. Jun, Laser assisted rapid 3D printing of continuous carbon fiber reinforced plastics: Simulation, characterization, and properties, Polymer Composites.

[86] I. Gibson, D. Rosen, B. Stucker, M. Khorasani, Additive manufacturing technologies, Springer2021.

[87] S.I. Macías, G. Ruano, N. Borràs, C. Alemán, E. Armelin, UV assisted photo reactive polyether-polyesteramide resin for future applications in 3D printing, Journal of Polymer Science 60(4) (2022) 688-700.

[88] M. Invernizzi, G. Natale, M. Levi, S. Turri, G. Griffini, UV-assisted 3D printing of glass and carbon fiber-reinforced dual-cure polymer composites, Materials 9(7) (2016) 583.

[89] I. Binyamin, E. Grossman, M. Gorodnitsky, D. Kam, S. Magdassi, 3D Printing Thermally Stable High-Performance Polymers Based on a Dual Curing Mechanism, Advanced Functional Materials (2023) 2214368.

[90] J.W. Kopatz, J. Unangst, A.W. Cook, L.N. Appelhans, Compositional effects on cure kinetics, mechanical properties and printability of dual-cure epoxy/acrylate resins for DIW additive manufacturing, Additive Manufacturing 46 (2021) 102159.

[91] Y. Cheng, J. Li, X. Qian, S. Rudykh, 3D printed recoverable honeycomb composites reinforced by continuous carbon fibers, Composite Structures 268 (2021) 113974.

[92] K. Dong, L. Liu, X. Huang, X. Xiao, 3D printing of continuous fiber reinforced diamond cellular structural composites and tensile properties, Composite Structures 250 (2020) 112610.

[93] M. Attaran, The rise of 3-D printing: The advantages of additive manufacturing over traditional manufacturing, Business horizons 60(5) (2017) 677-688.

[94] A. Cano-Vicent, M.M. Tambuwala, S.S. Hassan, D. Barh, A.A. Aljabali, M. Birkett, A. Arjunan, Á. Serrano-Aroca, Fused deposition modelling: Current status, methodology, applications and future prospects, Additive Manufacturing 47 (2021) 102378.

[95] H. Quan, T. Zhang, H. Xu, S. Luo, J. Nie, X. Zhu, Photo-curing 3D printing technique and its challenges, Bioactive materials 5(1) (2020) 110-115.

[96] V.V. Shinde, A.-D. Celestine, L.E. Beckingham, B.S. Beckingham, Stereolithography 3D printing of microcapsule catalyst-based self-healing composites, ACS Applied Polymer Materials 2(11) (2020) 5048-5057.

[97] X. Kuang, Z. Zhao, K. Chen, D. Fang, G. Kang, H.J. Qi, High-speed 3D printing of high-performance thermosetting polymers via two-stage curing, Macromolecular rapid communications 39(7) (2018) 1700809.

[98] X. Xu, J. Yang, W. Jonhson, Y. Wang, A. Suwardi, J. Ding, C. Guan, D. Zhang, Additive manufacturing solidification methodologies for ink formulation, Additive Manufacturing (2022) 102939.

[99] J.R.C. Dizon, A.H. Espera Jr, Q. Chen, R.C. Advincula, Mechanical characterization of 3D-printed polymers, Additive manufacturing 20 (2018) 44-67.